Ulm University Hospital

Institute of Molecular Oncology and Stem Cell Biology

Director: Prof. Dr. Alexander Kleger

Characterizing early oncogenic KRAS signaling by employing human stem cell-derived pancreatic ductal organoids as a pre-cancer model

Dissertation submitted in partial fulfillment of the requirements for the degree of

„Doctor rerum naturalium" (Dr. rer. nat.)

of the International Graduate School in Molecular Medicine Ulm

by

Chantal Allgöwer

born in Bad Urach

2025

Current dean of the Medical Faculty:	**Prof. Dr. Thomas Wirth** *Institute of Physiological Chemistry* *Ulm University*
Current chairman of the Graduate School:	**Prof. Dr. Bernd Knöll** *Institute of Neurobiochemistry* *Ulm University*

Thesis Advisory Committee:

First supervisor:	**Prof. Dr. Alexander Kleger** *Institute of Molecular Oncology and Stem Cell Biology* *Ulm University Hospital*
Second supervisor:	**Prof. Dr. Holger Barth** *Institute of Experimental and Clinical Pharmacology, Toxicology and Pharmacology of Natural Products* *Ulm University Hospital*
Third supervisor:	**Prof. Dr. Stefan Liebau** *Institute of Neuroanatomy and Developmental Biology* *Eberhard Karls University Tübingen*
External reviewer:	**Prof. Dr. Günter Schneider** *Department of General, Visceral and Pediatric Surgery* *University Medical Center Göttingen*
Day doctorate awarded:	23.04.2026

Results gained in this thesis have previously been published as follows:

Allgöwer, C., Mulaw, M. A., Nagai, J., Wiedenmann, S., Ringel, E. A., Ferrara, B., Piemonti, L., Maulana, T. I., Ferreira, L. T., Flinders, A., Teufel, C., Reichardt, L., Lopatta, P. B., Srinivasan, D., Lahusen, A., Gaisa, N. T., Beck, A., Lindenmayer, J., Melzer, M. K., Rodger, E., Heller, S., Löhr, M., Liebau, S., Loskill, P., Lin, Y.-N., Camisa, P. R., Jorgensen, C., Crippa, S., Meier, M., Hohwieler, Costa, I. G., Breunig, M., Kleger, A. An oncogenic KRAS-driven secretome involving TNFα promotes niche preparation prior to pancreatic cancer onset. *Molecular Cancer,* 2026, 25 (29). https://doi.org/10.1186/s12943-025-02541-1.

© The Author(s) 2026. This article is licensed under a Creative Commons Attribution 4.0 International License (http://creativecommons.org/licenses/by/4.0/).

Table of contents

Table of contents iii
List of abbreviations vi
List of tables and figures x
Figures x
Tables x
1. Introduction 1
1.1 The Pancreas 1
1.1.1 Anatomy and physiology of the pancreas 1
1.1.2 Pancreatic development *in vivo* and differentiation *in vitro* 3
1.2 Pancreatic cancer 5
1.2.1 Epidemiology and risk factors 5
1.2.2 Tumor evolution 7
1.2.3 Tumor microenvironment 10
1.2.4 Molecular subtypes of PDAC 14
1.2.5 KRAS mutations 17
1.2.6 Clinical management of PDAC 19
1.2.7 Pancreatic cancer models 22
1.3 Aims and objectives 25
2. Material and Methods 27
2.1 Material 27
2.1.1 Antibodies 27
2.1.2 Buffers and solutions 28
2.1.3 Cell culture media, supplements, and reagents 29
2.1.4 Chemicals 31
2.1.5 Consumables 32
2.1.6 Computational tools and packages 33
2.1.7 Cytokines, growth factors and inhibitors 34
2.1.8 Devices 35
2.1.9 Kits and ready-to-use reagents 36
2.1.10 Primers and oligos 37
2.1.11 Software 38
2.2 Cell culture methods 39
2.2.1 Cultivation of human embryonic stem cells (hESCs) 39
2.2.2 Cultivation of human pancreatic stellate cells (PaSCs) 39
2.2.3 Gene editing of hESCs and PaSCs 39

2.2.4 Generation and cultivation of pancreatic duct-like organoids (PDLOs) 40
2.2.5 T cell isolation 42
2.3 Global analysis techniques 42
2.3.1 Sample preparation and sequencing for scRNA-seq analysis 42
2.3.2 ATAC-sequencing 43
2.3.3 Mass spectrometry for proteome analysis 44
2.3.4 Data availability 44
2.4 Computational analysis 44
2.4.1 Pre-processing of the PDLO scRNA-seq data sets 44
2.4.2 *KRAS*^{G12D}-dependent grouping of cells and multilayer deep learning 45
2.4.3 Normalization, dimension reduction, and identification of differentially expressed genes (DEGs) of the PDLO scRNA-seq data sets 46
2.4.4 Gene set enrichment 47
2.4.5 Velocity analysis 48
2.4.6 Survival analysis of the TCGA-PAAD data set 48
2.4.7 Reprocessing of publicly available scRNA-seq data sets 48
2.4.8 Integration of a published PDAC scRNA-seq data set 49
2.4.9 Grouping of PDAC samples based on deep learning classifiers 49
2.4.10 Cell-cell communication analysis 50
2.5 *In vitro* assays 51
2.5.1 Co-culturing of matrix-embedded organoids and T cells ("InterOMaX") 51
2.5.2 Co-culturing of PDLOs and T cells with cancer-on-chip platform 51
2.5.3 Generating conditioned media from PDLOs 52
2.5.4 Transwell® migration assay 52
2.5.5 Multiplex flow cytometry analysis of T cells 52
2.5.6 Live imaging of PDLO-PaSC co-cultures 52
2.5.7 Indirect co-culture of PDLOs and PaSCs 53
2.5.8 Enzyme-Linked Immunosorbent Assay (ELISA) 53
2.5.9 EdU staining for cell cycle analysis 53
2.5.10 Quantitative real-time PCR 53
2.5.11 Taqman™ Copy Number Assay 54
2.5.12 Western Blot 54
2.5.13 Flow cytometry 54
2.5.14 Statistical analysis 55
3. Results 56
3.1 KRAS^{G12D}-expressing PDLOs as a pre-cancer model 56
3.1.1 Time-resolved single-cell RNA sequencing of *KRAS*^{G12D}-expressing PDLOs 56
3.1.2 Doxycycline treatment efficiently induces KRAS^{G12D} expression and canonical KRAS signaling in PDLOs 58

3.1.3 KRAS^{G12D} correlates with epithelial-to-mesenchymal transition (EMT) and alters the cell-cycle 60
3.1.4 KRAS-PDLOs show enrichment of neoplasia signatures 61
3.2 KRAS^{G12D} induces niche-preparatory signatures 64
3.2.1 KRAS-dependent grouping of cells 64
3.2.2 *KRAS^{G12D}*-expressing PDLO transcriptome is clinically relevant 65
3.2.3 KRAS^{G12D} induces ECM- and inflammation-related signaling 66
3.2.4 Deep learning identifies KRAS classifier signature 68
3.3 KRAS^{G12D} induces T cell shielding and activates PaSCs *in vitro* 71
3.3.1 KRAS^{G12D} reduced T cell infiltration and migration 71
3.3.2 KRAS^{G12D} activates human pancreatic stellate cells (PaSCs) 73
3.4 TNFα as a potential *KRAS^{G12D}*-dependent mediator of niche preparation 76
3.4.1 Cell-cell communication analysis predicts TNFα as a potential candidate for *KRAS^{G12D}*-dependent niche modelling 76
3.4.2 TNFα is upregulated in *KRAS^{G12D}*-expressing PDLOs and is involved in T cell shielding and PaSC activation 80
3.5 Single-cell RNA sequencing of PDLO co-cultures 83
3.5.1 PDLOs in mono- and bi-culture 84
3.5.2 T cells in co-culture with PDLOs 85
3.5.3 PaSCs in co-culture with PDLOs 87
3.5.4 Cell-cell communication analysis within PDLO co-cultures 89
4. Discussion 90
4.1 KRAS^{G12D} expression in PDLOs 90
4.1 *KRAS^{G12D}*-dependent senescence & EMT 93
4.2 *KRAS^{G12D}*-induced ECM- and inflammation-related gene signatures 93
4.3 *KRAS^{G12D}*-dependent effects on T cells 95
4.4 KRAS^{G12D}-dependent effects on stellate cells 97
4.5 The role of TNFα in the pre-cancer niche 98
4.6 Conclusion and outlook 100
5. Summary 101
6. References 103
7. Statutory declaration 128
8. List of publications 129
9. Acknowledgements 130

List of abbreviations

5-FU	Fluorouracil
ACh	Acetylcholine
ACTA2	Actin alpha 2, smooth muscle
ADEX	Aberrantly differentiated endocrine exocrine
ADM	Acinar-to-ductal metaplasia
ATAC-seq	Assay for Transposase-Accessible Chromatin using sequencing
ATM	Ataxia telangiectasia mutated
BMP	Bone morphogenic protein
BRCA1	Breast Cancer 1
BRCA2	Breast Cancer 2
Ca^{2+}	Calcium ion
CAF	Cancer-associated fibroblasts
cAMP	Cyclic adenosine monophosphate
CCK	Cholecystokinin
CCL5	C-C motif chemokine ligand 5
CDKN2A	Cyclin dependent kinase inhibitor 2A
CDX	Cell line-derived xenograft
CFTR	Cystic fibrosis transmembrane conductance regulator
Cl^-	Chloride ion
CLDN1	Claudin-1
CTLA4	Cytotoxic T-lymphocyte-associated protein 4
CXCL12	C-X-C motif chemokine ligand 12
CXCL2	C-X-C motif chemokine ligand 2
DDR	DNA damage repair
DE	Definitive endoderm
DEGs	Differentially expressed genes
Dox	Doxycycline
ECM	Extracellular matrix
EMT	Epithelial–mesenchymal transition
ERK	Extracellular signal-regulated kinase
ESMO	European Society for Medical Oncology
FAMMM	Familial atypical multiple mole melanoma syndrome
FBS	Fetal bovine serum
FGF	Fibroblast growth factors

FOLFIRINOX	Fluorouracil, leucovorin, irinotecan, and oxaliplatin
FOXP3	Forkhead box P3
GAP	GTPase-activating protein
GAPDH	Glyceraldehyde-3-phosphate dehydrogenase
GATA6	GATA binding protein 6
GDP	Guanosine diphosphate
GEFs	Guanine nucleotide exchange factors
GEMM	Genetically-engineered mouse models
GM-CSF	Granulocyte-macrophage colony-stimulating factor
GNAS	Guanine nucleotide binding protein alpha stimulating
GO	Gene Ontology
GSEA	Gene set enrichment analysis
GTE	Gut tube endoderm
GTP	Guanosine triphosphate
H^+	Hydrogen ion
HBOC	Hereditary breast and ovarian cancer syndrome
HCO_3^-	Bicarbonate
hESC	Human embryonic stem cells
HSL	Hormone sensitive lipase
iCAF	Inflammatory cancer-associated fibroblasts
IFNγ	Interferon γ
IGF-1	Insulin-like growth factor-1
IL1	Interleukin 1
IL2RA	Interleukin 2 receptor subunit alpha
IL6	Interleukin 6
IPMN	Intraductal papillary mucinous neoplasm
iPSCs	Induced pluripotent stem cells
JAK	Janus kinase
KPC	$Kras^{LSLG12D/+}$-$p53^{LSL.R172H/+}$ -PdxCre
KRAS	Kirsten ras oncogene homolog
KRT19	Keratin-19
log2FC	Log2 fold change
LSF	Li Fraumeni syndrome
MACS	Magnetic-activated cell sorting
MAPK	Mitogen-activated protein kinase
MCN	Mucinous cystic neoplasms
MDSCs	Myeloid-derived suppressor cells

MHC II	Major histocompatibility complex class II
miRNA	Micro RNA
MLH1	MutL homolog 1
MMP11	Matrix metalloproteinase-11
MRI	Magnetic resonance imaging
MSH2	MutS homolog 2
myCAF	Myofibroblastic cancer-associated fibroblasts
Na+	Sodium ion
NaCl	Sodium chloride
NFκB	Nuclear factor kappa B
NKX6-1	NK6 homeobox 1
NSCLC	Non-small cell lung cancer
OIS	Oncogene-induced senescence
PALB2	Partner and localizer of BRCA2
PanIN	Pancreatic intraepithelial neoplasia
PaSC	Pancreatic stellate cells
PBMCs	Peripheral blood mononuclear cells
PCA	Principal component analysis
PD-1	Programmed death-1 receptor
PDAC	Pancreatic ductal adenocarcinoma
PD-L1	Programmed death-1 ligand
PDLO	Pancreatic duct-like organoids
PDO	Patient-derived organoid
PDX	Patient-derived xenograft
PDX1	Pancreatic and duodenal homeobox 1
PE	Pancreatic endoderm
PI3K	PI 3-kinase
PJS	Peutz-Jeghers syndrome
PNETs	Pancreatic neuroendocrine tumors
PP	Pancreatic progenitor
PRSS1	Serine protease 1
QM	Quasi-mesenchymal
RNF43	Ring finger protein 43
ROS	Reactive oxygen species
scRNA-seq	Single-cell RNA sequencing
SHH	Sonic hedgehog
SLC26A6	Solute carrier family 26 member 6

SMAD	Mothers against decapentaplegic homolog
SOX9	SRY-Box transcription factor 9
STAT	Signal transducer and activator of transcription
STK11	Serine/threonine kinase 11
T2DM	Type 2 diabetes mellitus
TAMs	Tumor-associated macrophages
TCGA	The Cancer Genome Atlas
TGFβ	Transforming growth factor β
TME	Tumor microenvironment
TNFα	Tumor necrosis factor α
TP53	Tumor protein P53
Tregs	Regulatory T cells
UICC	Union for International Cancer Control
UMAP	Uniform manifold approximation and projection
VEGF	Vascular endothelial growth factor
αSMA	Alpha smooth muscle actin

List of tables and figures

Figures

Figure 1 | Anatomy of the pancreas. 2
Figure 2 | Pancreatic development in vivo and differentiation in vitro. 4
Figure 3 | Tumor evolution of PDAC.. 8
Figure 4 | The tumor microenvironment of PDAC....12
Figure 5 | Single-cell RNA sequencing of PDLOs after different timepoints of doxycycline treatment 56
Figure 6 | PDLOs are of ductal identity 57
Figure 7 | KRAS copy number and expression 58
Figure 8 | PDLOs exhibit canonical KRAS signaling after Dox treatment....59
Figure 9 | KRAS^{G12D} induces EMT and senescence in PDLOs 60
Figure 10 | The expression of PanIN-related genes gradually increases over the time of Dox treatment.... 61
Figure 11 | ATAC-sequencing of PDLOs reveals KRAS-dependent changes in chromatin dynamics.....62
Figure 12 | KRAS^{G12D} expression correlates with the gene signature of basal tumors. 63
Figure 13 | KRAS-dependent grouping of cells. 65
Figure 14 | KRAS^{G12D}-expressing PDLO transcriptome is clinically relevant 66
Figure 15 | KRAS^{G12D} induces ECM- and inflammation-related gene signatures....67
Figure 16 | Deep learning identifies classifier genes accurately predicting KRAS group identity 69
Figure 17 | Grouping of PDAC patients based on deep learning classifiers 70
Figure 18 | KRAS^{G12D}-expression in PDLOs reduces T cell infiltration and migration 72
Figure 19 | Conditioned medium from KRAS^{G12D}-expressing PDLOs does not alter T cell subtypes.....73
Figure 20 | KRAS^{G12D}-expressing PDLOs induce proliferation of PaSCs....74
Figure 21 | KRAS^{G12D}-expressing PDLOs induce CAF polarization of PaSCs.. 75
Figure 22 | Cell-cell communication analysis within the healthy niche....77
Figure 23 | Cell-cell communication analysis within the PDAC TME....78
Figure 24 | Unique ligand-receptor pairs sourced from KRAS^{G12D}-expressing PDLOs 79
Figure 25 | KRAS^{G12D}-dependent TNF signaling in PDLOs 80
Figure 26 | TNFα secretion is KRAS^{G12D}-dependent....81
Figure 27 | Single-cell RNA sequencing of PDLO co-cultures....83
Figure 28 | PDLOs in mono- and bi-culture.... 84
Figure 29 | T cells are differently distributed between treatment conditions....85
Figure 30 | T cells show overstimulated growth signaling and stress response. 86
Figure 31 | KRAS^{G12D}-expressing PDLOs induce a shift of CAF populations in PaSCs. 87
Figure 32 | Differently expressed genes of PaSCs 88
Figure 33 | Cell-cell communication analysis of PDLO bi-cultures. 89
Figure 34 | Schematic summary 102

Tables

Table 1 | Overview of different studies describing molecular subtypes of PDAC. 15
Table 2 | Overview of different PDAC models. 23
Table 3 | Stage-specific media composition for pancreatic differentiation.... 41

1. Introduction

1.1 The Pancreas

As the term “pancreas” (from Greek πάγκρεας, páŋkreas) translates to “all flesh”, it remains unclear when and by whom the pancreas was first described as a distinct organ.[1,2] Nevertheless, ancient pioneers of medicine, such as Hippocrates, Herophilus, and Galen, described a glandular organ, presumably referring to the pancreas.[1] However, its physiological relevance was by far underestimated, as the pancreas was solely described as a cushion, protecting adjacent blood vessels and supporting the architecture of the stomach.[1,3,4] Therefore, the pancreas attracted little attention over the following centuries, as it did not seem to fulfill any relevant physiological purpose.[1,3] A more detailed description of pancreatic anatomy was given by Johann Georg Wirsung in 1642, as he allegedly was the first to describe the human pancreatic duct.[1] Further centuries later, the actual function of the pancreas was, at least in parts, understood after Claude Bernard and others described that the pancreatic juice is involved in digestion.[3] Today, it is not only evident how indispensable the pancreas is for digestion and metabolism, but it is also recognized as a source of life-threatening diseases, such as diabetes and cancer.

1.1.1 Anatomy and physiology of the pancreas

The pancreas is located behind the posterior wall of the abdomen and is anatomically divided into head, neck, body, and tail (**Figure 1**).[5–7] While the head of the pancreas lies within the curve of the duodenum, the tail is oriented towards the spleen.[5–7] The majority of pancreatic tissue (>90%) consists of the exocrine compartment, namely acinar and ductal cells, which produce the pancreatic juice.[8,9] The pancreatic juice is essential for the digestive process, and various stimuli tightly orchestrate its production.

Upon stimulation with the neurotransmitter acetylcholine (ACh) and the neuropeptide cholecystokinin (CCK), acinar cells secrete a NaCl-rich fluid spiked with a broad repertoire of digestive enzymes.[10,11] The synthesis of these enzymes occurs at an extraordinarily high rate, after which the proteins are stored in zymogen granules until secretion is performed by exocytosis.[12] Some of the enzymes are produced and stored as pro-enzymes (zymogens), including, for example, trypsinogen, which does not undergo conversion to the active form (trypsin) until it

has reached the duodenum.[10,13] Besides trypsinogen, acinar cells produce additional proteases (e.g. chymotrypsinogen), carbohydrate-degrading enzymes, such as amylase, lipolytic enzymes, including lipase, and nucleases (e.g., ribonuclease).[7,10]

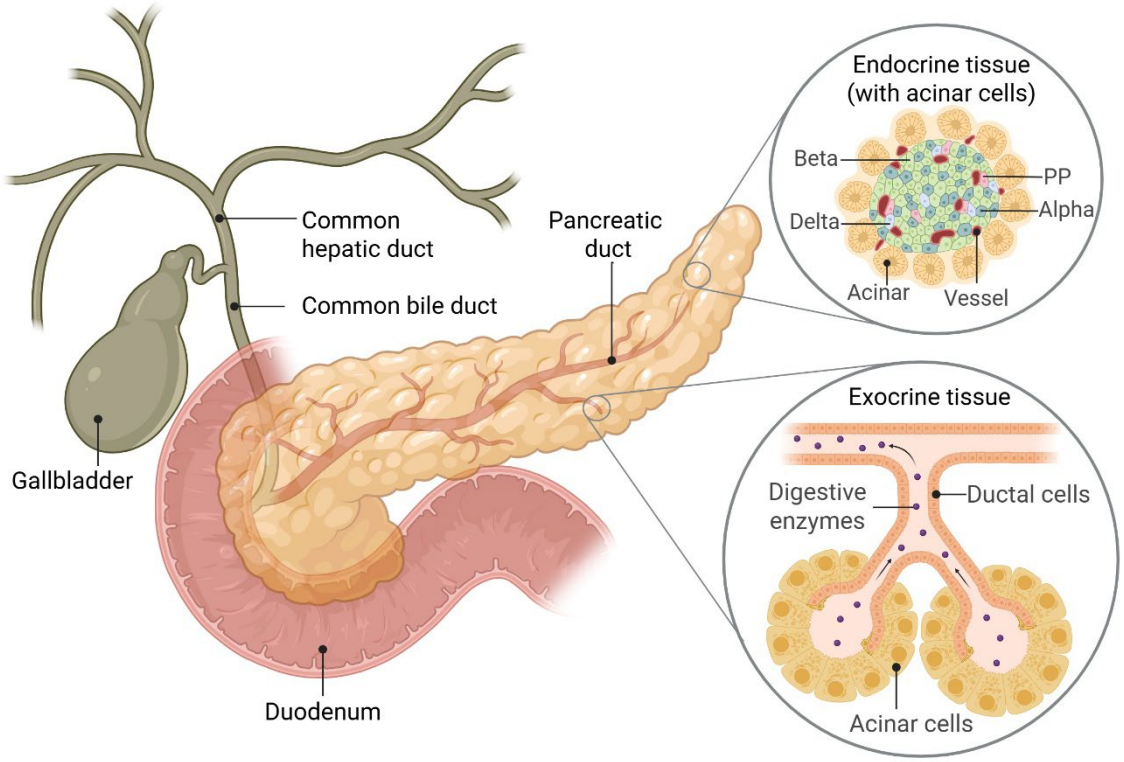

Figure 1 | Anatomy of the pancreas. The majority of the pancreas is composed of exocrine tissue, which includes acinar and ductal cells. Acinar cells secrete a NaCl-rich fluid, spiked with digestive enzymes. The acinar-derived fluid is then further modified by a HCO_3^--rich fluid, secreted by ductal cells. Ductal cells form tubes branching across the entire pancreas, allowing transfer of the pancreatic juice to the duodenum. Besides the exocrine compartment, clusters of endocrine cells are distributed across the pancreas. These pancreatic islets consist of different endocrine cell types, including alpha, beta, delta, and pancreatic polypeptide (PP) cells. Each cell type produces and secretes a specific hormone, including glucagon and insulin. By being released directly into the bloodstream, these hormones regulate blood glucose homeostasis. (Scheme was created with BioRender.com, using the template "Pancreas Anatomy")

The acinar-derived fluid is then subsequently modified by the ductal compartment of the pancreas.[14] The ductal cells form branch-like tubes running through the entire organ, thereby connecting to the common bile duct and the duodenum (Figure 1).[6] Ductal cells fulfill the primary function of secreting substantial volumes of a bicarbonate (HCO_3^-)-rich fluid.[10,14] This secretion is regulated by several factors, including the hormone secretin, as well as by the presence of ions (e.g., Cl^-, Na^+, Ca^{2+}, H^+), which are released by the acinar cells into the lumen.[10,14] HCO_3^- release is then mediated by ion channels, such as the cystic fibrosis transmembrane conductance regulator (CFTR) and the solute carrier family 26 member 6

(SLC26A6), which exchange luminal Cl^- anions with intracellular HCO_3^-, and vice versa.[15,16] The pancreatic juice is then transported through the main duct to the duodenum, where it neutralizes the gastric acid and supports the decomposition of nutrients.[10]

In addition to its crucial role in digestion, the pancreas also carries out endocrine functions. The endocrine cells are clustered in the pancreatic islets, also termed islets of Langerhans (**Figure 1**), where each of the five cell types is dedicated to producing a specific hormone.[17,18] These hormones are directly released into the bloodstream, thereby collectively regulating glucose homeostasis.[17] Alpha cells produce glucagon, while beta cells secrete insulin, which both regulate blood glucose levels antagonistically.[17,19] Hormone secretion is partially regulated by somatostatin and pancreatic polypeptide, which are sourced from delta cells and PP (pancreatic polypeptide) cells, respectively.[17,18] Less than 1% of endocrine cells are ghrelin-producing epsilon cells.[17,20]

1.1.2 Pancreatic development *in vivo* and differentiation *in vitro*

As the pancreas harbors various cell types with distinct functions, its embryological development is highly complex and needs to be precisely orchestrated. Inhibition of sonic hedgehog (SHH) signaling and activation of the Wnt pathway, along with other modulators such as fibroblast growth factors (FGFs) and bone morphogenic proteins (BMPs), tightly regulate this process.[21] Human pancreatic development begins about 30 days post-conception when the endoderm thickens and gives rise to the ventral and dorsal pancreatic bud (**Figure 2**).[22,23] During this phase, multipotent pancreatic progenitors (PP) expand, and the formation of microlumina can be observed. These microlumen further evolve into tubular structures, establishing central trunk and peripheral tip domains. Trunk cells are considered bipotent progenitors, giving rise to either the ductal or the endocrine lineage, while tip cells represent progenitors of the acinar tissue.[5,21–23]

Although mimicking the complex human pancreatic development *in vitro* is challenging, it offers valuable opportunities for disease modeling. Applying defined stage-specific cell medium recipes allows *in vitro* differentiation of pluripotent stem cells towards pancreatic identity. A great range of protocols has been established for endocrine differentiation, enabling research on diabetes.[24–29] Protocols for differentiation towards the exocrine lineage, however, remain sparse.[30–32] Among

these approaches, protocols have been established and further optimized, allowing the generation of exocrine cells derived from pluripotent stem cells (**Figure 2**).[33–36] Here, human pluripotent stem cells, such as embryonic stem cells (hESCs) or induced pluripotent stem cells (iPSCs), are initially differentiated towards PPs using stage-specific defined compounds. The resulting PPs are characterized by co-expressing the transcription factors pancreatic and duodenal homeobox 1 (*PDX1*) and NK6 Homeobox 1 (*NKX6-1*) and have the potential to give rise to all three lineages of the pancreas: ductal, acinar, and endocrine.[35]

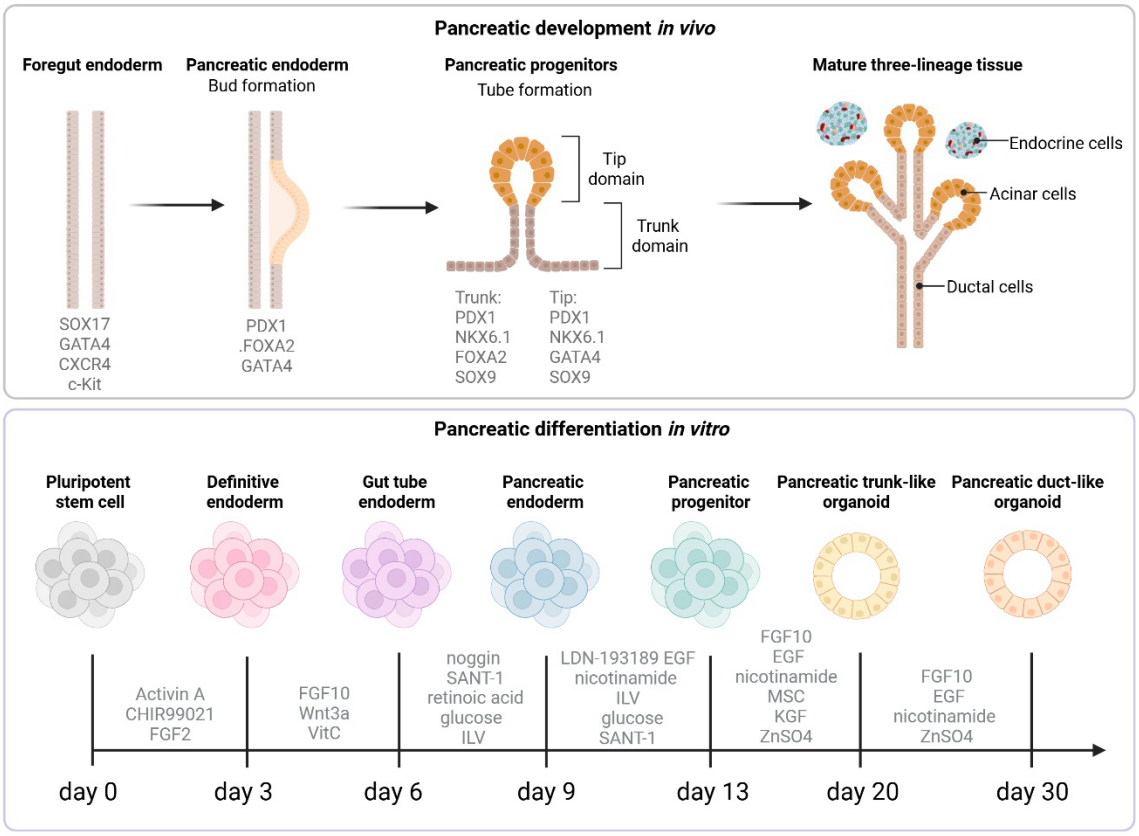

Figure 2 | Pancreatic development *in vivo* and differentiation *in vitro*. Pancreatic development begins with the budding of the foregut endoderm. Multipotent pancreatic progenitors expand and form tubular structures, thereby establishing a tip and trunk domain. Trunk cells then give rise to ductal and endocrine cells, while tip cells mature into acinar cells. To mimic this process *in vitro*, human pluripotent stem cells are initially differentiated toward the definitive endoderm (DE) stage before transforming into pancreatic endoderm (PE) via the gut tube endoderm (GTE). Further maturation leads to the generation of pancreatic progenitors (PPs). The PPs are then reseeded into ECM-mimicking materials, allowing 3D growth of ductal organoids. This differentiation process is achieved by adding defined stage-specific compounds. (Scheme is partially based on Clinical Tree[37] and created with BioRender.com using the template "Multistep cell fate decisions during pancreatic development")

Acinar differentiation, however, remains particularly challenging, as these cells are prone to undergo metaplasia, resulting in the loss of acinar features and the acquisition of ductal characteristics.[38–40] In contrast, ductal differentiation was

shown to be robust and capable of mimicking the morphology and functionality of human ducts.[34,35] This is achieved by reseeding the adherent growing PP cells into extracellular matrix (ECM)-mimicking materials, allowing three-dimensional (3D) culturing of the cells. By further adding a defined compound cocktail, the progenitors mature to duct-like cells, structured in ring-shaped organoids (**Figure 2**).[34,35]

1.2 Pancreatic cancer

Malignancies can arise from all cell types of the pancreas. The majority of cases, however, originate from the exocrine compartment, while cases sourced from the endocrine tissue, such as pancreatic neuroendocrine tumors (PNETs), are rare (< 2%).[41] Among exocrine tumors, the pancreatic ductal adenocarcinoma (PDAC) represents the most common form, accounting for more than 90 % of all pancreatic cancer cases.[41–43]

1.2.1 Epidemiology and risk factors

In 2022, the GLOBOCAN database reported 510,992 new cases of pancreatic cancer worldwide, which represents a relatively low incidence compared with other malignancies (e.g. lung cancer with 2,480,675 cases).[44–46] Despite the relatively low incidence, pancreatic cancer ranks among the leading causes of cancer-related deaths, with an estimated increased mortality of 43.6 % until the year 2035.[44–46]

A high prevalence of pancreatic cancer is observed in Europe and North America, while cases in Southeast Asia seem to be less frequent.[44–46] Overall, men are slightly more affected than women, with 5.5 cases compared to 4.0 cases per 100,000, respectively, and cases increase with age.[44–46]

Several risk factors for PDAC have been described, including intrinsic factors, such as genetic predispositions, and extrinsic factors mainly involving unfavorable lifestyle habits.[47–49]

Around 5-20 % of PDAC patients (depending on the study cohort) carry germline mutations, which are associated with various hereditary cancer syndromes.[47,50] An increased risk of about 5 % was, for example, observed in patients with hereditary breast and ovarian cancer syndrome (HBOC), where mutations in the genes Breast Cancer 1 and 2 (*BRCA1/2*) lead to deficiencies in DNA damage repair (DDR).[47,49,50] A comparable increased risk was found for patients with Lynch syndrome, which

involves mutations of DNA mismatch repair genes, such as MutL Homolog 1 (*MLH1*), as well as MutS Homolog 2 and 6 (*MSH2/6*).[50] Other germline mutations affecting DDR mechanisms, including Ataxia Telangiectasia Mutated (*ATM*) and Partner And Localizer Of BRCA2 (*PALB2*), are also associated with an increased risk of PDAC.[47,50] Moreover, hereditary cancer syndromes related to mutations of tumor suppressor genes can elevate the lifetime risk of PDAC to over 15%.[47] These include the Familial atypical multiple mole melanoma syndrome (FAMMM), where mutations in the Cyclin Dependent Kinase Inhibitor 2A (*CDKN2A*) impair cell cycle regulation, as well as the Peutz-Jeghers syndrome (PJS), which is driven by pathogenic variants of the Serine/Threonine Kinase 11 (*STK11*).[49,50] Patients suffering from the Li Fraumeni syndrome (LFS), caused by mutations of the tumor suppressor gene Tumor Protein P53 (*TP53*) exhibit an increased PDAC risk of approximately 5 %.[47,50]

Furthermore, pancreatitis has been associated with an increased risk of PDAC by more than 50 %.[47,50,51] Pancreatitis is an inflammatory disease of the exocrine pancreas that leads to fibrosis and tissue damage.[51,52] In rare cases, pancreatitis is induced by inherited mutations of the Serine Protease 1 (*PRSS1*) gene, which encodes for trypsinogen, the inactive form of trypsin produced by acinar cells.[51] Mostly, however, pancreatitis is triggered by environmental factors such as alcohol consumption and smoking.[52] While patients with acute pancreatitis only seem to have a slightly increased risk, individuals suffering from chronic pancreatitis are 9 times more likely to develop PDAC.[49] The recurrent cycles of inflammation and fibrosis leading to DNA damage might be a probable cause, resulting in the onset of PDAC.[47]

In addition, a correlation between PDAC and type 2 diabetes mellitus (T2DM) can be observed.[47–49,53] Diabetes was shown to double the risk for developing PDAC.[47,48] T2DM leads to high levels of insulin-like growth factor-1 (IGF-1), which can promote proliferation and cell survival in the exocrine cells, thereby facilitating tumor growth.[49,53] Furthermore, diabetes is accompanied by low-level systemic inflammation, creating a favorable environment for tumor initiation, as described for pancreatitis.[53] In addition, it was shown that T2DM increases the activation of pancreatic stellate cells (PaSC), which are involved in a desmoplastic reaction, a hallmark of PDAC.[49,53] However, T2DM is also frequently observed as a result of

PDAC, and further research is needed to fully decipher the relationship between the two diseases.[47]

While obesity is often associated with T2DM, it has been established as an independent risk factor for PDAC. Studies showed that a high body mass index (BMI) could be linked to an increased risk of developing PDAC by 50 %.[48] The presence of fat tissue leads to an inflammatory environment, and the secreted cytokines can promote PDAC tumorigenesis.[48,49,53]

A well-established extrinsic risk factor for PDAC is smoking and the consumption of tobacco products. Smoking is not only associated with increased risk of developing PDAC, but smokers also tend to have a worse prognosis once diagnosed, compared to non-smokers.[49] While smoking in general is associated with a higher likelihood of developing multiple cancer types, due to the accumulation of DNA damage, it also increases the risk of pancreatitis and diabetes.[48] Therefore, smoking is also an indirect risk factor for PDAC.

Overall, several factors can be linked to an increased risk of developing PDAC. However, patients are often susceptible to more than one risk factor, and it remains challenging to evaluate the impact of single factors separately.

1.2.2 Tumor evolution

PDAC arises in the exocrine tissue of the pancreas. However, the exact cell type of origin has been a topic of controversy over the past decades. Due to the histological features of PDAC, it has long been a consensus that PDAC originates from ductal cells.[54] The establishment of different mouse models, however, showed that PDAC can also arise from acinar cells.[55,56] While evidence suggests that PDAC can develop from both acinar and ductal cells, the cell of origin appears to determine different routes of tumor evolution and has an impact on both the molecular subtype and patients' survival.[57–60]

Different types of precursor lesions precede the onset of invasive PDAC. The most commonly found lesions are pancreatic intraepithelial neoplasias (PanINs).[61,62] PanINs are microscopically small (<5 mm) lesions within the ductal system, characterized by columnar mucin-producing cells.[61,62] Clinically, PanINs are classified either as low-grade (formerly PanIN-1 and PanIN-2) or high-grade (formerly PanIN-3), depending on the severity of cellular atypia (**Figure 3**), which

includes loss of polarity, nuclear crowding, and increased frequency of mitosis.[61,63] Interestingly, low-grade PanINs do not necessarily escalate towards PDAC, and a significant proportion of individuals with an otherwise healthy pancreas harbor these lesions.[64,65]

Although PanINs resemble ductal morphology, acinar cells are also capable of giving rise to these precursor lesions by undergoing acinar-to-ductal metaplasia (ADM). Upon stress stimuli (e.g., chronic inflammation), features of mature acinar cells, such as the production of digestive enzymes, are lost, while obtaining a duct-like phenotype.[66] ADM is considered a necessary and reversible process to maintain cellular homeostasis after tissue damage.[66,67] However, if the metaplastic cells acquire mutations of Kirsten Ras Oncogene Homolog (KRAS), this re-transition is obstructed.[66,67]

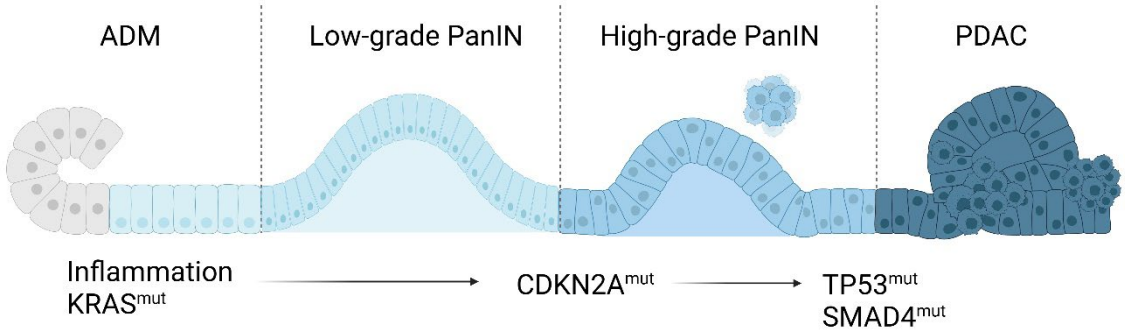

Figure 3 | Tumor evolution of PDAC. Acinar cells initially undergo acinar-to-ductal metaplasia (ADM) in response to stress stimuli, such as inflammation. Oncogenic KRAS mutations then drive the formation of preneoplastic lesions. Accumulation of other genetic alterations, including mutations of tumor suppressor genes CDKN2A, TP53, or SMAD4, further drives tumorigenesis. (Scheme was created with BioRender.com based on Seidel et al.[68]).

Somatic mutations of KRAS are recognized as the key trigger for PanIN development and are detected in over 90 % of low-grade PanINs.[69,70] In high-grade PanINs, additional mutations in tumor-suppressor genes such as CDKN2A, TP53, and SMAD4 (Mothers Against Decapentaplegic Homolog 4) are frequently observed, indicating a gradual escalation in molecular instability during tumorigenesis.[69,70]

Another type of neoplastic lesion is represented by intraductal papillary mucinous neoplasms (IPMNs). IPMNs are larger (> 1 cm) than PanINs, and can therefore be captured with conventional imaging techniques.[71,72] This improves earlier diagnosis, which most likely contributes to the better prognosis of patients with IPMN-associated PDAC.[71] IPMNs are characterized by their cystic morphology and are

either located at the main duct (MD-IPMN), at the branch duct (BD-IPMN), or both (mixed-IPMN).[71,72] Depending on their morphology in combination with their expression profile of mucins (MUC), IPMNs are categorized as either gastric ($MUC5A^+$), intestinal ($MUC5AC^+$ and $MUC2^+$), or pancreatobiliary ($MUC5AC^+$, $MUC1^+$).[71–73] IPMNs are far less studied than PanINs. It has been established, however, that similar genetic alterations drive carcinogenesis.[61,71–73] Oncogenic KRAS variants are present in 50 % to 80 % of IPMNs, often accompanied by mutations of CDKN2A and TP53.[61,72] Unique alterations specifically found in IPMNs but not in PanINs are mutations of Guanine Nucleotide Binding Protein Alpha Stimulating (GNAS), regulating the Cyclic Adenosine Monophosphate (cAMP) cascade and inducing extensive cell proliferation.[61,72,73] Additionally, Ring Finger Protein 43 (RNF43) is a frequently mutated tumor suppressor found in IPMNs.[61,71,72]

PDAC can also arise from mucinous cystic neoplasms (MCNs), a rare type of precursor lesions, accounting for about 10% of neoplasms in the pancreas.[74,75] MCNs are distinguished from other mucin-producing lesions by the presence of the surrounding ovarian-like tissue and are therefore mainly found in women.[74,75] Within this ovarian-like tissue, oestrogen and progesterone receptors seem to promote tumor growth.[74] However, genetic alterations covering the usual suspects of PDAC, including KRAS, CDKN2A, TP53, and GNAS, can also be observed in MCNs.[74,75]

As previously stated, the cell of origin remains a topic of debate. However, recent studies using acinar- or ductal-lineage tracing mouse models show that the emerging tumors share histological similarities while following different routes throughout tumorigenesis. When inducing oncogenic KRAS expression in combination with monoallelic TP53 mutations in acinar cells, a rapid formation of PanINs followed by the transformation to PDAC was observed.[58,59] In contrast, biallelic mutation of TP53 in the presence of oncogenic KRAS was necessary to trigger PDAC formation of ductal cells.[58,59] Notably, ductal-derived tumor models showed fewer or no low-grade PanINs.[57–60] Instead, tumor progression seems to emerge more rapidly compared to acinar-derived cancer models through high-grade PanINs and non-mucinous lesions.[58–60] Moreover, compared to acinar-derived PDAC, ductal-derived PDAC was associated with worse survival and exhibited a

more dedifferentiated phenotype, indicating that ductal-derived tumorigenesis is the more aggressive route.[57,58]

1.2.3 Tumor microenvironment

Desmoplasia is a major hallmark of pancreatic cancer, reflected by a dense and fibrotic stroma surrounding the actual tumor. This tumor-surrounding tissue, referred to as the tumor microenvironment (TME), comprises several non-epithelial components, including fibroblasts and immune cells (**Figure 4**). The complex composition and interplay of the TME not only influence carcinogenesis but also impact treatment response.

A relevant component of the TME comprises a heterogeneous set of fibroblasts. In the healthy pancreas, mesenchymal pancreatic stellate cells (PaSCs) support tissue homeostasis in a quiescent state.[76–79] Upon stimulation due to tissue damage or carcinogenesis, PaSCs become activated and secrete high levels of ECM proteins, such as collagens and laminins.[76–79] Activated stellate cells can be found throughout tumor evolution, including precursor lesions and PDAC.[77,79] However, the most abundant type of cells within the TME are cancer-associated fibroblasts (CAFs), which can originate from PaSCs, as well as bone marrow-derived mesenchymal stem cells, adipose-derived stem cells, endothelial cells, and epithelial cells.[77] So far, different types of CAFs have been described, including myofibroblastic CAFs (myCAFs) and inflammatory CAFs (iCAFs).

The myCAF subtype is characterized by high expression of Alpha Smooth Muscle Actin (αSMA) and spatially assembles in direct proximity to the tumor cells.[80,81] The myCAF phenotype is mainly induced by tumor cell-derived Transforming Growth Factor β (TGFβ), triggering the SMAD2/3/4 signaling cascade. This then results in the expression of contractile proteins and secretion of ECM proteins such as periostin, matrix metalloproteinase-11 (MMP11), and type I collagen.[80–82] The iCAF subtype, on the other hand, shows low expression of αSMA while highly expressing interleukin 6 (IL6) and other cytokines and chemokines.[80,81] In contrast to myCAFs, iCAFs are distributed across the TME at a greater distance from the tumor.[80,81] Tumor cell-secreted interleukin 1 (IL1) is the key modulator, inducing the iCAF phenotype by activating Nuclear Factor Kappa B (NFκB), leading to Janus Kinase/Signal Transducer and Activator of Transcription (JAK/STAT) signaling via LIF Interleukin 6 Family Cytokine (LIF).[80–82] As a result, iCAFs secrete various

cytokines and chemokines, including IL6 as well as C-X-C Motif Chemokine Ligand 2 and 12 (CXCL2/CXCL12).[80–82]

Several other CAF subtypes have been described, including antigen-presenting CAFs (apCAFs), which show high expression of the Major Histocompatibility Complex Class II (MHC class II) family.[80] Interestingly, these CAF subtypes (iCAF, myCAF, and apCAFs) can already be found in PanIN lesions, while iCAFs seem to be absent in IPMN lesions.[83,84]

CAFs can act both as tumor-suppressing and tumor-promoting. For example, iCAFs not only create an immune-suppressive environment but also directly promote tumor growth by releasing anti-inflammatory cytokines.[85] The MHC II-expressing apCAFs are thought to modulate T cells by promoting differentiation towards regulatory T cells (Tregs), thereby enhancing the pro-tumorigenic properties of the TME.[80] As previously described, myCAFs strongly contribute to the fibrotic stroma of PDAC tumors by producing ECM proteins. This protects the tumor from immune infiltration and reduces the penetration of chemotherapeutics, thereby increasing tumor cell survival.[86] Paradoxically, depletion of myCAFs from the TME resulted in more invasive tumors accompanied by worse overall survival.[87] A recent study could also show that in early tumor stages, meflin-positive CAFs can be observed, which have anti-tumor properties by downregulating ECM protein secretion.[88] In later stages, however, these meflin$^+$ CAFs give rise to αSMA$^+$ CAFs, which then promote PDAC progression.[88] Overall, data suggest that CAFs fulfill a dual role within the TME, constraining tumor growth via a mechanical barrier on the one hand, while also contributing to tumor growth through direct tumor-promoting cross-talk and shaping the immune landscape.

Within the PDAC immune landscape, tumor-associated macrophages (TAMs) are the most abundant immune cell type, and distinct TAM subsets can be identified throughout carcinogenesis. Pro-inflammatory M1-polarized macrophages are described to promote ADM and PanIN formation by secreting IL6, Tumor Necrosis Factor α (TNFα), and C-C Motif Chemokine Ligand 5 (CCL5).[89,90] Upon further PDAC progression, the population of pro-inflammatory macrophages shifts towards anti-inflammatory M2-polarized TAMs.[79,89,90] These TAMs modulate the TME via various mechanisms, creating an immune-suppressive environment and thereby contributing to cancer progression. CAF-derived factors, such as IL6, for example,

promote M2-polarization of macrophages, which in turn release myCAF-activating TGFβ.[90] Besides indirectly promoting desmoplasia, TAMs also release MMPs, thereby directly influencing ECM remodeling.[89,90]

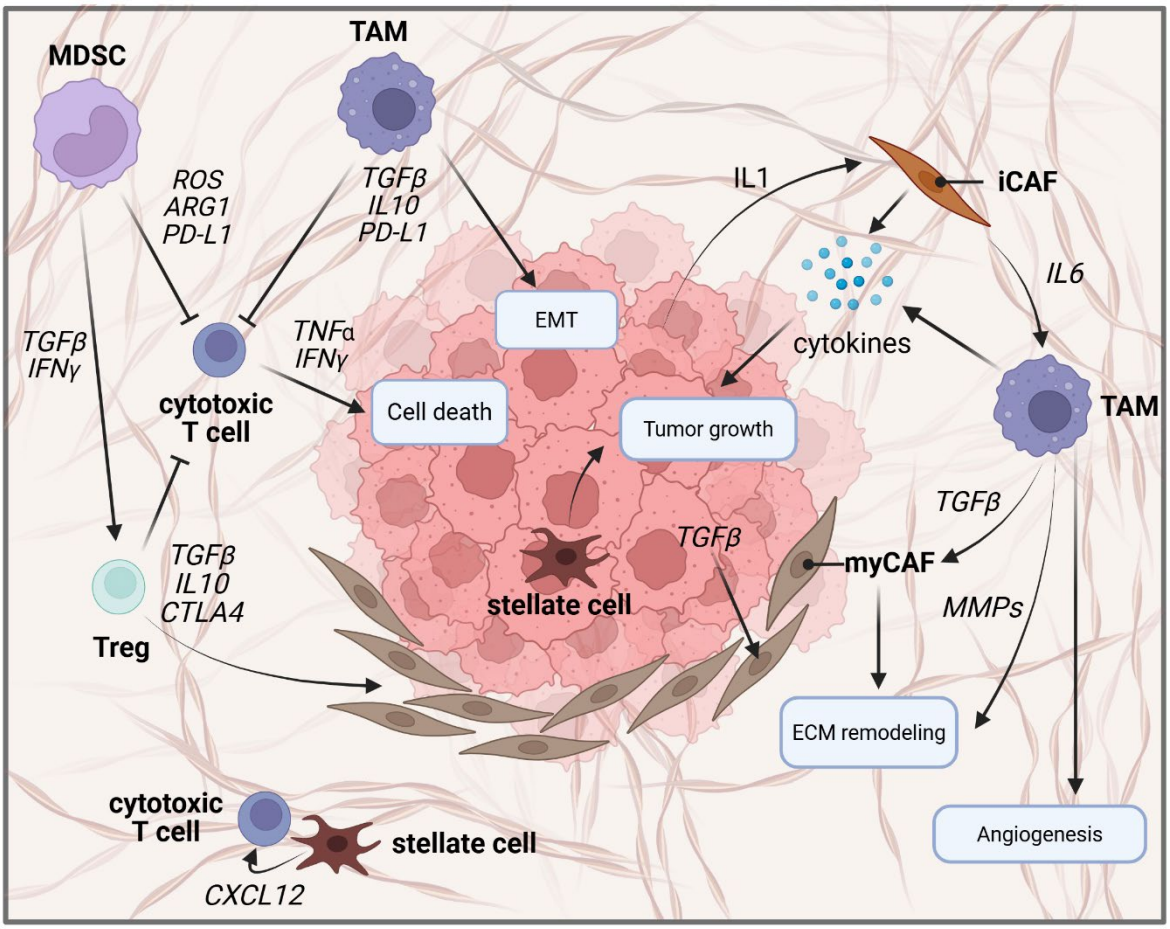

Figure 4 | The tumor microenvironment of PDAC. The tumor cells are surrounded by a complex mixture of non-epithelial cells, including cancer-associated fibroblasts (CAFs) and immune cells. Myofibroblastic CAFs (myCAFs) are located in proximity to the tumor and produce essential components of the extracellular matrix (ECM), thereby generating a fibrotic environment. Inflammatory CAFs (iCAFs) secrete various cytokines that directly promote tumor growth. Tumor-associated macrophages (TAMs) activate myCAF polarization, thereby indirectly promoting desmoplasia, but are also directly involved in ECM remodeling by releasing matrix metalloproteinases (MMPs). Furthermore, TAMs release factors that promote tumor growth, epithelial-to-mesenchymal transition (EMT), and angiogenesis. Cytotoxic T cells induce tumor cell death by releasing cytotoxic agents. However, several other cell types, including TAMs, myeloid-derived suppressor cells (MDSCs), and regulatory T cells (Tregs) inhibit the activity of cytotoxic T cells by inducing T cell exhaustion. This complex cross-talk of different components of the TME creates a highly fibrotic and immunosuppressive environment, generating optimal conditions for tumor growth and metastasis. (Scheme was created with BioRender.com using the template "PDAC Histology" based on Ho et al.[91])

TAMs furthermore affect T cells, resulting in immune escape.[89,90] In addition, TAM-derived factors such as TGFβ, MMPs, and Vascular Endothelial Growth Factor

(VEGF) have an impact on metastasis by increasing angiogenesis and inducing epithelial–mesenchymal transition (EMT) of tumor cells.[89,90]

In addition to TAMs, various subtypes of T lymphocytes are present within the TME. Throughout cancer progression, a change in the composition of these T cell subpopulations can be observed. Within PanIN and IPMN lesions, cytotoxic $CD8^+$ cells are present at elevated levels.[65,92,93] Activated $CD8^+$ T cells recognize tumor cells by direct cell-cell contact, and then release cytotoxic agents, including TNFα and INFγ, which induce apoptosis of the cancer cell.[94] The presence of $CD8^+$ T cells is therefore described as an essential anti-tumor mechanism and correlates with patients' survival.[95,96] However, over the time of cancer progression, this T cell population is dramatically reduced. Within PDAC tumors, only few $CD8^+$ T cells are detected, exhibiting an exhausted (inactivated, non-functional) phenotype and mostly residing in the surrounding stroma.[93]

Several mechanisms are described to interfere with $CD8^+$ T cell infiltration. Stellate cells and CAFs, for example, secrete CXCL12, which attracts and captures $CD8^+$ T cells within the stroma.[77,78,95] Moreover, several cell types, including myeloid-derived suppressor cells (MDSCs), TAMs, and tumor cells, express immune checkpoint modulators.[95] These immune checkpoints include, for example, Programmed Death-1 Ligand (PD-L1) and Cytotoxic T-lymphocyte-associated protein 4 (CTLA4), which, upon binding to their respective receptors, induce T cell exhaustion.[95]

In contrast to $CD8^+$ cells, a $CD4^+$ positive subset of T cells, namely regulatory T cells (Tregs), becomes more abundant in high-grade lesions and fully developed tumors.[77,79,95] Tregs are characterized by the expression of Interleukin 2 Receptor Subunit Alpha (IL2RA; CD25) and Forkhead Box P3 (FOXP3) and their main function remains in the inactivation of cytotoxic T cells, for example, via CTLA4.[95] While a higher prevalence of Tregs was correlated with worse patients outcome[97], depletion of Tregs within the TME surprisingly led to increased tumor progression *in vivo*.[98] This phenomenon was explained by the fact that Tregs express important TGFβ ligands, which induce activation of tumor-restraining αSMA-positive CAFs.[98]

Another crucial immune population within the PDAC TME is represented by MDSCs. Similar to TAMs, MDSCs create an immune-suppressive environment through the release of various stimuli.[76,99,100] MDSCs are recruited to the TME by

Granulocyte-Macrophage Colony-Stimulating Factor (GM-CSF), which is also secreted by tumor cells.[76,99,100] Within the TME, MDSCs release Reactive Oxygen Species (ROS) and Arginase 1 (ARG1), which in turn inhibit the proliferation and activation of T cells.[76,100] Furthermore, MDSC-derived TGFβ and Interferon γ (IFNγ) stimulate Tregs.[79]

Further immune cells which can be found within the TME are neutrophils and mast cells, crucially cross-talking with other cell types and thereby influencing tumor maintenance and progression.

1.2.4 Molecular subtypes of PDAC

As PDAC tumors show great heterogeneity, efforts have been made to establish different subtypes to better tailor diagnostics and therapeutic options.[101] Several studies have investigated the transcriptional landscape of PDAC specimens, subtyping the tumors into distinct classes based on gene expression signatures and mutational profiles (**Table 1**).

Although different terminology for the individual subtypes has been used across studies, PDAC samples can be mainly classified into either classical or basal tumors (also termed squamous or quasi-mesenchymal).[59,101–104] Classical tumors were described as well-differentiated, retaining their epithelial identity, and showing high expression of GATA Binding Protein 6 (GATA6).[59,102,103,105] In contrast, basal tumors acquire a mesenchymal-like phenotype accompanied by hypermethylation of GATA6.[59,102,103,105] Basal tumors were associated with worse survival across all studies and increased metastasis.[59,102,103,105] Interestingly, acinar-derived PDAC signatures could be linked to the classical subtype, while ductal-derived tumors seem to correlate with the squamous phenotype.[58]

Besides the classification within the epithelial compartment, it has been demonstrated that the TME can also be divided into distinct subtypes.[102,105] Moffitt et al., for example, classified the stroma into either normal or activated, independently of the classical or basal tumor subtype, revealing that the activated stroma type correlated with worse overall survival.[102] A similar observation was made by Puleo and colleagues, who additionally described the immune classical subtype, where the presence of an immune-rich stroma correlated with a good prognosis.[105]

Table 1 | Overview of different studies describing molecular subtypes of PDAC. (Table based on Robertson et al.[101])

Study	Molecular Subtypes
Collisson et al. 2011[103] (84 samples from surgical resection, cell lines)	Classical: • high expression of adhesion and epithelial genes • high expression of GATA6 • higher KRAS-dependency • better overall survival compared to QM-PDAC • better response to erlotinib Quasi-mesenchymal (QM): • high expression of mesenchymal genes • low expression of GATA6 • less KRAS-dependent • worse overall survival compared to the classical subtype • better response to gemcitabine Exocrine • expression profile of healthy exocrine tissue
Moffitt et al. 2015[102] (206 samples from surgical resection, cell lines, PDX)	Tumor – classical: • GATA6 overexpression Tumor - basal-like: • worse overall survival compared to the classical subtype • faster tumor growth *in vivo* • higher correlation with metastasis • better response to adjuvant therapy Stroma – normal: • gene expression profile of pancreatic stellate cells Stroma – activated: • expression of ECM-related genes (e.g., collagens) • expression of inflammatory genes • worse median survival compared to normal stroma • faster tumor growth *in vivo*
Bailey et al. 2016[106] (456 samples from surgical resection, cell lines)	Squamous: • inflammation, hypoxia, metabolic reprogramming, TGFβ signaling, MYC pathway activation • associated with TP53 and KDM6A mutations • increased TP63 expression • hypermethylation • loss of endodermal identity • poor prognosis

Table 1 | continued.

Study	Molecular Subtypes
Bailey et al. 2016[106] (456 samples from surgical resection, cell lines)	Pancreatic progenitor • enriched for transcription factors involved in pancreatic development (e.g., *PDX1, FOXA2/3, HNF1B*) • fatty acid oxidation and steroid hormone biosynthesis • co-expression of *MUC5AC* and *MUC1* • correlates with pancreatobiliary IPMNs Aberrantly differentiated endocrine exocrine (ADEX): • subclass of pancreatic progenitor • expression of genes related to mature exocrine and endocrine tissue (e.g., *MIST1, INS, AMY2B, PRSS1*) Immunogenic: • shares characteristics of the pancreatic progenitor class • evidence of immune infiltration • B cell signaling pathways, antigen presentation, CD4+ T cell, CD8+ T cell and Toll-like receptor signaling pathways
Puleo et al. 2019[105] (309 samples from surgical resection)	Pure classic: • low stromal signal • correlated with classical/progenitor subtype of other studies • well-differentiated • good prognosis • fewer *CDKN2A* and *TP53* mutations Immune classic: • presence of immune stroma • correlated with classical/progenitor subtype of other studies • good prognosis Pure basal-like • low stromal signal • correlated with basal subtype of other studies • associated with metastatic spreading • worst prognosis Desmoplastic: • basal association • presence of immune and vascularized stroma components Stroma-activated: • high αSMA, SPARC, and FAP • severe prognosis

1.2.5 KRAS mutations

Genetic alterations in the KRAS gene are the most frequent mutations observed in solid cancers.[107–109] This is also true for PDAC, as over 90% of patients harbour *KRAS* mutations.[70,71,107–109] As a member of the Ras family, the *KRAS* gene, as well as its homologs *NRAS* and *HRAS*, encodes GTPases.[108,109] Upstream of Ras signaling, the epidermal growth factor receptor (EGFR) is activated by the binding of its corresponding growth factors (e.g. EGF).[108,109] This activation leads to the accumulation of guanine nucleotide exchange factors (GEFs) at the Ras protein.[108,109] The Ras protein then undergoes conformational changes and exchanges guanosine diphosphate (GDP) with guanosine triphosphate (GTP).[107–109] The switch from the inactive GDP-bound Ras to the active GTP-bound Ras then triggers numerous downstream signaling cascades, including the Mitogen-Activated Protein Kinase (MAPK) and the PI 3-kinase (PI3K)/AKT/mTOR pathway.[107–109] These pathways are essential for proliferation, cell survival, and differentiation. In a physiological setting, the GTPase-activating protein (GAP) then hydrolyses the GTP, returning the Ras protein to its GDP-bound inactive state.[108,109] However, if *KRAS* is mutated, this hydrolysis is inhibited, resulting in the presence of a constantly active GTP-bound Ras protein and therefore overstimulated growth signaling.[107–109]

Genetic alterations within the *KRAS* gene mainly occur as missense point mutations, most commonly in GCT sequences, altering the conformation of the GTP-binding site.[107–109] In PDAC, the most common forms of *KRAS* mutation are found in codon 12 at exon 2, namely G12D (40-51 %), G12V (33 %), and G12R (12-15 %), but alterations in codon 13 at exon 2 are also observed.[107,108] It remains unclear why *KRAS* mutations are more dominant in pancreatic carcinogenesis compared to *HRAS* and *NRAS*. *KRAS* mutations, however, appear to create optimal conditions for neoplastic transformation in the pancreas.[109] Moreover, it was shown that the different forms of KRAS alterations impact patients' prognosis, with $KRAS^{G12D}$ mutation showing worse prognosis compared to wildtype *KRAS* ($KRAS^{wt}$), $KRAS^{G12V,}$ and $KRAS^{G12R}$.[107,108]

While mutations of the *KRAS* gene are described as a key trigger for initiating neoplasia, it has been shown that *KRAS* alone is not able to further drive the development of PDAC.[55,59,110] For the progression from precursor lesions such as

PanINs to PDAC, additional events are necessary, including pancreatitis and genetic alterations of tumor-suppressor genes such as *TP53* and *CDKN2A* (**Figure 3**).[55,59,110]

Furthermore, Müller and colleagues highlighted the importance of KRAS dosage in PDAC and described different tumor routes depending on $KRAS^{G12D}$ levels. Here, heterozygous $KRAS^{G12D}$ mutations can further lead to $KRAS^{G12D}$ allelic imbalances: focal gain, arm-level gain, or copy number neutral loss of $KRAS^{wt}$.[111] These allelic imbalances are associated with homozygous mutations of *CDKN2A* and correlate with higher $KRAS^{G12D}$ expression levels.[111] Tumors also evolved without allelic imbalances of $KRAS^{G12D}$, in combination with the amplification of alternative oncogenes (e.g. *MYC* and *YAP*).[111] However, $KRAS^{G12D}$ allelic imbalances were associated with a higher metastatic potential, and tumors showed a more dedifferentiated morphology, suggesting that KRAS dosage critically shapes PDAC aggressiveness.[111]

KRAS is a potent and dominant oncogene involved in a broad spectrum of signaling pathways. Therefore, several biological processes are altered, including metabolism. Activating *KRAS* mutations, for example, are linked to increased glucose uptake by upregulating glucose transporters.[112–114] The resulting enhanced glycolysis is followed by increased lactate secretion, enabling rapid ATP production.[112–114] This process, namely the Warburg effect or aerobic glycolysis, is observed across different cancer entities and allows the tumor cells to grow and expand under stress conditions.[112–114] Oncogenic KRAS signaling can also affect lipid metabolism by enhancing intracellular lipid storage through downregulation of hormone-sensitive lipase (HSL), resulting in increased migration and metastasis.[115] *KRAS*-mutated tumors also show dysregulated glutamine metabolism, resulting in the production of non-essential amino acids, such as aspartate, thereby further fueling tumor growth.[114,116]

Furthermore, oncogenic KRAS signaling leads to the secretion of chemokines and cytokines, thereby mediating cross-talk with other cell types of the TME. The KRAS-induced secretome of tumor cells for example includes GM-CSF and IL6, which recruits MDSCs to the TME.[117,118] Additionally, tumor cells release IL10 and TGFβ upon KRAS signaling, which increases the amount of Tregs and enhances M2 polarization of TAMs.[118,119] As described above, TGFβ also promotes the myCAF subytype.[80–82] *KRAS*-mutated tumors also release IL33 and induce IL33 secretion

in CAFs. The presence of IL33 in the TME was linked to reduced cytotoxic CD8+ T cell infiltration.[114,119] In summary, *KRAS*-mutated tumor cells shape the surrounding tissue towards an immune-suppressive environment, thereby creating optimized conditions for tumor growth and progression.

1.2.6 Clinical management of PDAC

Throughout tumor progression, PDAC patients often experience jaundice, abdominal pain, weight loss, and the onset of diabetes.[120,121] In the early stages, however, PDAC is either asymptomatic or accompanied by nonspecific symptoms, including back pain, fatigue, and nausea.[120] This makes an early detection of PDAC extremely challenging, and most patients are therefore diagnosed in advanced stages.

Non-invasive imaging techniques such as computed tomography (CT) or magnetic resonance imaging (MRI) are commonly used for diagnosis.[120–122] Patients are staged following the TNM system according to the Union for International Cancer Control (UICC), based on the primary tumor size (T1-T4), number of regional lymph nodes showing metastasis (N0-N2), and presence of metastasis at distant sites (M0-M1).[121] When imaging results are inconclusive, biopsy for histological examination is necessary to evaluate morphological and genetic alterations.[120–122] Currently, there is only a single serological marker, namely the carbohydrate antigen CA19-9, which is used in clinical practice.[120–122] However, it lacks sensitivity and specificity and is therefore not a reliable resource for screening.[120–122] Elevated levels of CA19-9 are, however, linked to worse overall prognosis, especially for patients undergoing resection.[121]

Therefore, great efforts are being made to improve the earlier diagnosis of PDAC, and promising approaches are currently being investigated. Koa et al., for example, recently introduced pancreatic cancer detection with artificial intelligence (PANDA), a deep learning tool allowing the detection of lesions via CT scan with a sensitivity of 92.9 % and specificity of 99.9 % across 20,530 patients.[123] Furthermore, a wide range of potential novel biomarkers are being explored. For example, elevated serum levels of several microRNAs (miRNAs), short single-stranded RNA molecules involved in post-transcriptional regulation of gene expression, were observed in PDAC patients.[124,125] Additionally, detecting

circulating tumor DNA (ctDNA), DNA released into the bloodstream by dying tumor cells, could be a non-invasive method to support diagnosis and prognosis.[126]

Surgical resection is the method of choice for the treatment of PDAC as it is the only curative option.[121,122] Nevertheless, surgical resection may be accompanied by post-operative complications due to infection and hemorrhage.[120] Moreover, surgery is only applicable if the tumor remains locally restricted to the pancreas.[121] But as PDAC is so often diagnosed at late stages, the majority of patients already show metastatic spreading, and only 10-20 % of patients are eligible for surgical resection.[122]

In about 80 % of cases, patients relapse after surgery, and follow-up treatment is therefore commonly done by adjuvant chemotherapy.[121,127] Chemotherapy is also advised as neoadjuvant treatment for borderline resectable patients, in order to shrink tumor size before surgery.[121] For patients with unresectable and metastatic PDAC, chemotherapy remains the standard of care.[120–122]

Over decades, gemcitabine monotherapy has been the gold standard.[120,122,128] As a deoxycytidine nucleoside analog, gemcitabine is incorporated into the DNA during cell division, leading to the termination of DNA synthesis and consequently to cell death.[128] While adjuvant monotherapy with gemcitabine improved disease-free survival for patients after surgical resection, compared to an untreated observation group (13.4 months vs. 6.7 months), overall survival was not improved much (22.8 months vs. 20.2 months).[129] Gemcitabine was also established as first-line therapy for patients with advanced PDAC, after it was shown to be superior to fluorouracil (5-FU), with a slight improvement in median survival (5.65 months vs. 4.41 months).[130] Despite these advances, outcomes remained disappointing, and therefore several studies aimed to evaluate gemcitabine in combination with other cytotoxic agents, showing a general improvement compared to gemcitabine monotherapy.[131]

Gemcitabine-based therapy in combination with albumin-bound paclitaxel particles (nab-paclitaxel), for example, improved survival and progression-free survival compared to gemcitabine treatment alone.[132] While exploring further treatment regimens in several clinical trials, the combination of fluorouracil, leucovorin, irinotecan, and oxaliplatin (FOLFIRINOX) was presented to have favorable outcomes compared to gemcitabine monotherapy regarding overall survival of the

patients (53.5 months vs. 35.5 months).[133,134] The higher efficiency of FOLFIRINOX, however, was also accompanied by increased toxicity.[134] The European Society for Medical Oncology (ESMO) therefore currently recommends FOLFIRINOX as adjuvant therapy and therapy for advanced disease as a first-line treatment option for patients with a good performance status.[121] If patients lack overall fitness, gemcitabine-nab-paclitaxel is recommended as an alternative.[121]

In summary, currently available chemotherapeutic agents fail to meet the expectations, as the patient's life is prolonged only by a few months. The lack of efficacy of chemotherapeutic regimens in the context of PDAC is still being investigated. It has been established, however, that a majority of patients either show initial chemoresistance or rapidly acquire this resistance over the time of treatment.[135] So far, multiple factors have been described to promote chemoresistance, including the mechanical barrier of dense stroma, reduced expression of nucleoside transporters, epithelial-to-mesenchymal transition, altered cell metabolism, and autophagy.[135–137]

New therapeutic approaches are therefore desperately needed. A significant breakthrough has been made recently, as the first KRAS inhibitors entered the field. Before, KRAS has been considered an undruggable target, as the KRAS protein shows a very high affinity for GTP within the picomolar range and structurally lacks deep pockets for allosteric inhibition.[138,139] Ostrem et al., however, took advantage of the nucleophile cystine side chains and via a compound-screen identified small molecules, which irreversible bind GDP-bound $KRAS^{G12C}$.[140] This led to the development of sotorasib and adagrasib, both FDA-approved $KRAS^{G12C}$ inhibitors for the treatment of non-small cell lung cancer (NSCLC).[138,139] Targeting $KRAS^{G12D}$, the predominant mutant in PDAC, has been even more challenging, as the protein does not harbor cystine residues.[138,141]

Based on the experience gained from the development of adagrasib and additional extensive compound optimization, Mirati Therapeutics introduced MRTX1133, a reversible and selective $KRAS^{G12D}$ inhibitor.[141] MRTX1133 has been proven to be highly potent, blocking KRAS-dependent downstream signaling and drastically reducing tumor growth *in vitro* and *in vivo*.[138,141,142] MRTX113 is therefore currently being evaluated in a phase 1/2 study for treating solid tumors with $KRAS^{G12D}$ mutation (NCT05737706).[143] The efficacy and safety of a second $KRAS^{G12D}$ inhibitor,

namely RMC-9805 (Revolution Medicines) is currently being investigated in a phase 1/1b clinical trial (NCT06040541).[144] RMC-9805 is a covalent tri-complex inhibitor, targeting active (GTP-bound) $KRAS^{G12D}$ after forming a bi-complex with cyclophilin A.[145] Besides targeting specific KRAS mutants, a variety of pan-KRAS inhibitors have been introduced. RMC-6236 and RMC-7977 (Revolution Medicines), for example, are reversible tri-complex inhibitors targeting KRAS ($KRAS^{G12X}$, $KRAS^{G13X}$, $KRAS^{Q61H}$) as well as NKRAS and HKRAS mutants and their corresponding wildtype variants.[146,147]

Despite the great success in developing small-molecule KRAS inhibitors and the promising preclinical and clinical data, primary or acquired resistance to the treatment will be a major challenge to address.[148] The underlying mechanisms involved in resistance are currently being investigated. Here, resistant cells showed amplification in genes such as KRAS, MYC and CDK6 and basal-like tumor cells seem to respond better to KRAS inhibition compared to classical-like cells.[149]

1.2.7 Pancreatic cancer models

In order to tackle the variety of challenges regarding the diagnosis and treatment of PDAC, appropriate models are necessary. So far, several *in vitro*, *in vivo*, and *ex vivo* PDAC model systems are available, paving the way for a better understanding of the disease itself and providing essential tools for identifying novel biomarkers and conducting drug screenings (**Table 2**).

For decades, human PDAC cancer cell lines have been used as the foundation of research. The first PDAC lines were introduced in the 1960s, and several more have been introduced since.[150–152] The spectrum of cell lines used today allows disease modelling sourced from either primary tumors or metastatic sites, harboring different genomic backgrounds.[150,151] Culturing cell lines is relatively cheap and quite easy to handle.[150,151] PDAC cell lines can be expanded almost indefinitely and therefore offer virtually unlimited material.[151] However, due to the *in vitro* cultivation of the cells in a monolayer, the cells adapted to the distinct growth conditions and therefore do not necessarily mirror the true biology of *in vivo* PDAC tumors.[150] The monolayer culture also lacks complexity, and the influence of the TME is not being accounted for.[150,151]

To partially overcome the limitations of cancer cell lines, xenograft models have been established. These xenograft models can include the transplantation of cancer

cell lines (cell line-derived xenograft, CDX) or of patient-derived material (patient-derived xenograft, PDX) into mice.[150,151,153] The human tumor cells are therefore injected either subcutaneously or orthotopically (directly into the pancreas).[151,153] Especially, PDX models better reflect the true biology of the human tumor, with an improved coverage of tumor heterogeneity compared to cancer cell lines.[150,151,153] While the transplants from human tumor tissue often include stromal cells, transplantation is only possible into immunodeficient mice.[150,151,153] Therefore, the influence of the immune compartment is neglected within these models.

Table 2 | Overview of different PDAC models. (Table contents based on [34,36,150-172])

Model system	Advantages	Limitations
Cancer cell lines	• low costs • simple handling • virtually unlimited resource	• may not reflect true *in vivo* biology • lack complexity and TME
Xenografts	• coverage of tumor heterogeneity • better display complexity compared to cell lines	• lack of immune cells • ethical concerns
Genetically engineered mouse models (GEMMs)	• Comparable to human PDAC • Studying precursor lesions possible • Lineage tracing possible	• time-intensive breeding • varying latency time • "off-target" malignancies • species-specific differences • ethical concerns
Patient-derived organoids (PDOs)	• mirrors parental tumors • gene editing possible • potential for personalized medicine	• technically challenging • time-consuming • cost-intensive
Stem cell-derived duct-like organoids (PDLOs)	• genetically defined background • allows modeling of earliest stages • animal-free	• technically challenging • time-consuming • cost-intensive

Genetically-engineered mouse models (GEMMs) represent another invaluable PDAC model platform. The required mutations are therefore introduced into the endogenous locus under a tissue-specific promoter (e.g. Pdx1).[150] A prominent and

well-established PDAC GEMM is the KPC mouse. Here, Lox-STOP-Lox (LSL)-$KRAS^{G12D}$ and LSL-$Trp53^{R172H}$ mice are crossed with mice expressing the Cre-recombinase under the pancreas-specific Pdx1 promoter ($Kras^{LSLG12D/+}$-$p53^{LSL.R172H/+}$ -PdxCre; KPC).[150,154,155] These mice are born with a normal pancreas but then rapidly develop precursor lesions and invasive tumors within weeks.[154,155] GEMMs have contributed to a large share of our knowledge on PDAC today and KPC mice, for example, nicely mirror the biology of tumor evolution of human PDAC.[154,156] GEMMs also allow lineage-tracing, exploring, for example, the cell-of-origin or dissecting transcriptional programs over the time of tumorigenesis.[58,157]

However, GEMM breeding is time-consuming, and tumor latency can vary widely between animals.[154,158] Additionally, promoters such as Pdx1 are also expressed in other tissues and may therefore cause malignancies outside of the pancreas.[154,158] Findings gained from GEMMs can also not always be translated to human PDAC, due to species-specific differences in gene expression.[154,159]

While GEMMs and PDX models have contributed to a significant part in PDAC research, experiments with animals are always accompanied by ethical concerns. Following the 3R principle (replace, reduce, refine), the balance between harm and benefit should always be considered, and animal-free alternative models should be applied whenever possible.[160]

Such animal-free models are represented for example by the use of organoids. Organoids are 3D structures, resembling key features of an organ *in vitro*.[161] In order to generate organoids, cells are usually embedded in ECM-mimicking materials, such as Matrigel or synthetic hydrogels, resulting in self-organized complex structures.[161,162] The cells used to generate organoids can be from various sources, including human resected PDAC tissue.[163,164] These patient-derived organoids (PDOs) conserve the parental tumor characteristics regarding genotype and morphology.[164] Establishing PDOs from primary tumors across different patients allows the investigation of tumor heterogeneity, by reflecting various PDAC subtypes.[163] Moreover, PDOs offer a promising platform for drug screening *in vitro*, thereby predicting a patient's response to chemotherapeutic agents.[151,163] While this is a major step towards personalized medicine, successfully establishing PDOs strongly depends on the amount and quality of the patient material.[163] Furthermore,

organoids in general are technically challenging and expensive, and PDO cultures require several weeks until they can be used for drug testing.[154,163]

Recent approaches include 3D co-culturing of organoids with stromal, immune or endothelial cells, either in conventional cell culture formats or by employing advanced bioprinting techniques.[165–168] Moreover, several PDAC-on-chip systems have been introduced, allowing long-term co-culturing on microfluidic devices, and accounting for the vascular barrier.[169–171] These novel culturing techniques further evolve existing organoid platforms and license improved physiological disease modelling.

PDOs are, however, commonly derived from fully developed tumors, and therefore represent a retrospective snapshot without the possibility to investigate the earliest events of cancer onset. Stem cell-derived duct-like organoids (PDLOs), on the other hand, enable modeling of the earliest events of tumorigenesis in a genetically defined human context.[34,36] Here, pluripotent stem cells are directed towards the pancreatic lineage, resulting in duct-like organoids mimicking the characteristics of human tissue.[34,36] The stem cells can be genetically engineered to harbor inducible oncogene cassettes (e.g. $KRAS^{G12D}$ or $GNAS^{R201C}$) with or without additional mutations (e.g. *CDKN2A*).[34,36,172] While differentiation and generation of these organoids require several weeks and are quite expensive, PDLOs represent a unique platform to model the earliest events of dysplasia in the human context.[34,36,172]

1.3 Aims and objectives

Pancreatic cancer, specifically PDAC, is a highly aggressive disease with a 5-year survival rate ranging between 10 % and 30 %[47,70,120] thereby foreshadowing a devastating prognosis for the afflicted patients. Diagnosis most often occurs in late, advanced stages, while curative treatment options are lacking due to high recurrence rates and rapid development of chemoresistance.

Despite significant efforts and breakthroughs in PDAC research, a full understanding of the complex pathological mechanisms currently remains beyond reach. Especially, the earliest events of dysplasia in the human context are largely unexplored. Knowledge generated from animal models is accompanied by ethical concerns and restricted species-to-species translatability. Human material to investigate early states before cancer onset is extremely scarce, and studies

employing human models such as PDOs are therefore mostly limited to exploring characteristics of end-stage cancers.

It is, however, well established that oncogenic KRAS is not only the most commonly observed genetic alteration in PDAC, playing a pivotal role throughout carcinogenesis, but also represents the root of tumor development. Here, stem cell-derived PDLOs offer the opportunity of modeling the earliest states of dysplasia by allowing inducible oncogene expression within the healthy human duct *in vitro*. Thus, *KRAS*^{G12D}-expressing PDLOs may generate a window into the earliest events upon oncogenic signaling within the human context.

Based on the previous efforts from Breunig & Merkle et al.[34] it was therefore the aim of this work to address the following:

i. In-depth, time-resolved characterization of *KRAS*^{G12D} signaling within the PDLO model by employing scRNA-sequencing

ii. Investigating the role of *KRAS*^{G12D} signaling on the surrounding tissue in a pre-cancer context by establishing various PDLO co-culture systems

iii. Identifying potential *KRAS*^{G12D}-dependent candidates involved in modulating the pre-cancer niche by combining *in silico* and *in vitro* approaches

2. Material and Methods

2.1 Material

2.1.1 Antibodies

List of primary antibodies.

Target	Conjugate	Manufacturer	Cat. Nr.	Applications	Dilution
Anti-CD28	-	BD Pharmingen	555725	T cell activation	2.5 µg/ml
Anti-CD3E	-	BD Pharmingen	555329	T cell activation	5 µg/ml
aSMA	APC	R&D Systems	IC1420A	Flow cytometry	1:20
CD127	PE-CY5	Biolegend	351324	Flow cytometry - T cell panel	5 µl/ml
CD25	FITC	Biolegend	356106	Flow cytometry - T cell panel	5 µl/ml
CD3	PacOrange	Life Technologies	CD0330	Flow cytometry - T cell panel	5 µl/ml
CD4	AF700	Invitrogen	56-0048-82	Flow cytometry - T cell panel	5 µl/ml
CD8	BV650	Biolegend	344729	Flow cytometry - T cell panel	5 µl/ml
ERK1/2	-	Cell Signaling	9102	Western blot	1:1000
GAPDH	-	Merck	G9545	Western blot	1:1000
GP2	-	MBL	D277-3	MACS	1:5000
HA-Tag	-	Cell Signaling	3724S	Flow cytometry	1:1000
HLA-DR	APC-H7	BD Biosciences	561358	Flow cytometry - T cell panel	5 µl/ml
IL6	PE-Cy7	Thermo Scientific	25-7069-42	Flow cytometry	1:10
NKX6-1	APC	BD Pharmingen	563338	Flow cytometry	1:35
NKX6-1	-	DSHB	F55A12	Flow cytometry	1:150
PD1	PE	Invitrogen	12-2799-42	Flow cytometry - T cell panel	5 µl/ml
PDX1	-	R&D	AF2419	Flow cytometry	1:500
PDX1	PE	BD Pharmingen	562161	Flow cytometry	1:35
phospho-ERK1/2	-	Cell Signaling	4377	Western blot	1:1000

List of secondary antibodies.

Target	Manufacturer	Cat. Nr.	Applications	Dilution
Alexa Fluor™ 568 anti-rabbit	Invitrogen	A10042	Flow cytometry	1:500
Alexa Fluor™ 488 anti-mouse	Invitrogen	A-21202	Flow cytometry	1:500
Anti-mouse-HRP	GE Healthcare	NA931	Western blot	1:1000
Anti-rabbit-HRP	GE Healthcare	NA934	Western blot	1:1000

2.1.2 Buffers and solutions

Composition of buffers and solutions.

Buffer/Solution	Composition	
FC buffer (GP2 sort)	DPBS 10 % FBS	
4% PFA solution	DPBS 4 % Paraformaldehyde (PFA) 100 mM sucrose	
MACS buffer (GP2 sort)	DPBS 0.5 % BSA 2 mM EDTA	
Polyacrylamide gel (SDS-PAGE)	<u>Stacking gel:</u> 4 % Acrylamide 0.1 M (pH 6.8) Tris 0.2 % SDS 0.1 % APS 0.1 % TEMED	<u>Resolving gel:</u> 12 % Acrylamide 0.4 M (pH 8.8) Tris 0.2 % SDS 0.1 % APS 0.1 % TEMED
RIPA buffer	50 mM Tris (pH 7.4) 150 mM NaCl 1 mM EDTA 1 % NP40 0.25 % Sodium deoxycholate 0.1 % SDS 1 mM PMSF 1x Phosphatase inhibitor cocktail (PhosSTOP) 1x EDTA-free protease inhibitor cocktail (cOmplete)	
Semi dry buffer	H_2O 44 mM Tris 39 mM Glycine 20 % Methanol	
T cell isolation buffer	DPBS (Ca^{2+} and Mg^{2+} free) 0.1 % BSA 2 mM EDTA	
TBS 10x Buffer (1 Liter, pH 7.6)	H_2O 60.6 g Tris 87.6 g NaCl	
TBST	H_2O 10 % TBS (10x) 0.1 % Tween20	

2.1.3 Cell culture media, supplements, and reagents

List of cell culture media and related supplements and reagents.

Product	Manufacturer	Cat. Nr.
Accutase® solution	Sigma Aldrich	A6964
Bovine Serum Albumin (BSA)	Proliant	68700
Collagenase/Dispase®	Roche	11097113001
Cultrex UltiMatrix RGF BME	R&D Systems	BME001-05
DMEM	Gibco	41965-039
Doxycycline hyclate (Dox)	Sigma Aldrich	D9891
Dulbecco's Balanced Salt Solution (DPBS)	Gibco	14190-094
Fetal bovine serum (FBS)	Pan Biotech	P30-3031
Infliximab	Pharmacy, Ulm University Hospital	-
ITS-X (100x)	Thermo Fisher Scientific	51500056
L-Ascorbic acid	Wako Chemicals	013-12061
L-Glutamine	Sigma Aldrich	G8540
Matrigel© hESC-qualified Matrix	Corning	354277
Matrigel® Growth Factor Reduced (GFR)	Corning	354230
MCDB131	Gibco	10372-019
mTeSR™ Plus	STEMCELL Technologies	100-0276
Penicillin-Streptomycin-solution (P/S)	PAN Biotech	P06-07100
RPMI 1640	Gibco	11875093
TrypLE™ select (10x)	Gibco	A12177-01

Basal media for pancreatic differentiation.

Basal media	Composition
BE1 medium	MCDB131 0.8 g/l Glucose 1.174 g/l Sodium bicarbonate 0.1% or 0.5% fatty acid-free BSA 2 mM L-glutamine
BE3 medium	MCDB131 0.44 g/l Glucose 1.754 g/l Sodium bicarbonate 2% Fatty acid-free BSA 2 mM L-glutamine 44 mg/l L-ascorbic acid 0.5x ITS-X 2% fatty acid-free BSA

2.1.4 Chemicals

List of chemicals.

Product	Manufacturer	Cat. Nr.
Agarose	BD	214010
Ammoniumperoxodisulfat (APS)	Carl Roth	9592.2
Collagen Type I, rat tail	Merck	08-115
cOmplete, EDTA-free Protease Inhibitor cocktail	Roche	11873580001
D-Glucose	Sigma Aldrich	G7528
Digitonin	Promega	G9441
EDTA	AppliChem	A3145-0500
Ficoll® Paque Plus	Cytiva	GE17-1440-02
NaCl	Sigma Aldrich	31434-Kg-R
NP40	Fluka	74385
Paraformaldehyde (PFA)	Sigma Aldrich	P6148-500G
Phosphatase inhibitor Cocktail Tablets PhosSTOP	Roche	4906837001
PMSF	AppliChem	A0999-0500
Ponceau S	AppliChem	A2935-0500
ROTIPHORESE®NF-Acrylamide/Bis-solution	Carl Roth	A124.1
SDS	Serva	20765.03
Sodium Bicarbonate	Sigma Aldrich	S5761-500G
Sodium deoxycholate	Sigma Aldrich	D6750
Sucrose	Sigma Aldrich	S9378
TEMED	Thermo Fisher	17919
Tris	AppliChem	A2264-1000
Triton™ X-100	Sigma Aldrich	T8787

2.1.5 Consumables

List of consumables.

Product	Manufacturer	Cat. Nr.
Cell culture dish (10 cm)	Sarstedt	833902
12-well plate	Sarstdt	833921300
24-well plate	Sarstedt	833922
6-well plate	Sarstedt	833.920
8-well µ-Slide	IBIDI	80806-90
Filter tips (10 µl)	Sarstedt	703010255
Filter tips (200 µl)	Sarstedt	703031255
Filtertips (1000µl)	Sarstedt	703060255
Immobilon-P PVDF membrane	Millipore	IPVH00010
MS columns	Miltenyi Biotec	130-042-201
PCR single tube (0.2 ml)	Sarstedt	72737002
PCR tupe (0.1 ml, 4x stripe)	Biozym	712500
Pierce™ protein concentrator PES, 3K MWCO, 5-20 ml	Thermo Fisher	88515
Reaction tube (1.5 ml)	Sarstedt	72.690.001
Reaction tube (2 ml)	Sarstedt	72691
Screw cap tube (15 ml)	Sarstedt	62554502
Screw cap tube (50 ml)	Sarstedt	62547254
Serological pipette (10 ml, sterile)	Sarstedt	861254001
Serological pipette (25 ml, sterile)	sarstedt	861685001
Serological pipette (5 ml, sterile)	Sarstedt	861.253.001
Syringe filter, 0.2 µm	Sarstedt	83.1826.102
T25 flasks	Greiner	690175
Transwell® 8.0-µm Pore Polycarbonate Membrane Inserts	Corning	3428

2.1.6 Computational tools and packages

List of computational tools.

Tool/Package	Version	Source/Reference
CellRanger	-	10x Genomics
CellChat	v2.1.2	Jin *et al.*[173]
ChIPseeker	v1.46.1	Yu *et al.*[174]
clusterprofiler	v4.14.3	Yu *et al.*[175]
DESeq2	v1.45.3	Love *et al.*[176]
dplyr	v1.1.4	Wickham *et al.*[177]
GenomicRanges	v1.50.2	Lawrence *et al.*[178]
ggplot2	v3.4.0-3.5.1	Wickham *et al.*[179]
GSVA	v1.53.23	Hänzelmann *et al.*[180]
Keras API	-	TensorFlow
Matrix	v1.7.0	Bates *et al.*[181]
Rsubread	v2.12.3	Liao *et al.*[182]
Scanpy	v1.7.0	Wolf *et al.*[183]
SCpubr	v2.0.2	Blanco-Carmona *et al.*[184]
sctransform	v0.4.1	Hafemeister *et al.*[185]
scVelo	v0.3.2	Bergen *et al.*[186]
Seurat	v4.2.0 – 5.1.0	Satija *et al.*[187] Butler *et al.*[188] Hao *et al.*[189,190]
SeuratDisk	v0.0.0.9020-0.0.0.9021	Hoffman *et al.*[191]
stringr	v1.5.1	Wickham *et al.*[192]
survminer	v0.4.9	Kassambara *et al.*[193]
TCGAbiolinks	v2.26.0	Colaprico *et al.*[194] Mounir *et al.*[195]

2.1.7 Cytokines, growth factors and inhibitors

List of cytokines, growth factors and inhibitors.

Product	Manufacturer	Cat. Nr.
Activin A	PeproTech	120-14
CHIR99021	Axon MedChem	1386
EGF	R&D Systems	236-EG-200
FGF10	R&D Systems	345-FG-250
FGF2	Novoprotein	C046
Indolactam V	STEMCELL Technologies	72312
KGF	PeproTech	100-19
LDN-193189	Sigma Aldrich	SML0559
mNoggin	PeproTech	250-38
MSC2530818	Selleckchem	S8387
Nicotinamide	Sigma Aldrich	N0636
Retinoic acid	Sigma Aldrich	R2625
SANT-1	Sigma Aldrich	S4572
Wnt3a	PeproTech	315-20
Y-27632	STEMCELL Technologies	72307
Zinc sulfate ($ZnSO_4$)	Sigma Aldrich	Z0251

2.1.8 Devices

List of devices.

Device	Model/Cat.Nr	Manufacturer
Blotting system	Trans-Blot® SD Semi-Dry Transfer Cell	BioRad
Cell Counter	Casy TTC	OMNI Life Science
Centrifuge (15- and 50-ml tubes)	HERAEUS LABOFUGE 400	Thermo Fisher Scientific
Centrifuge (bench top)	5417C	Eppendorf
Chemiluminescence imaging system	Fusion SL	VILBER
Chromium X	-	10x Genomics
CO2 incubator	HERACELL 240i	Thermo Fisher Scientific
Confocal microscope	TCS SP8	Leica
DynaMag™-2 Magnet	12321D	Invitrogen
Flow cytometer	Attune™ NxT	Thermo Fisher Scientific
Fluorescence microscope	BZ-X Series	Keyence
Fluorescence microscope	Axio Observer 7	Zeiss
Live cell imaging system	Incucyte® S3 live-cell	Sartorius
Microplate reader	Infinite M200 Pro	Tecan
MicroTissues® 3D Petri Dish® micro-mold spheroids	Z764019-6EA	Sigma Aldrich
NovaSeq 6000	S2 flow cell	Illumina
OctoMACS™ Separator	130-042-109	Miltenyi Biotec
Real-time PCR cycler	QuantStudioTM 3	Thermo Fisher Scientific
Real-time PCR cycler	Rotor-Gene Q (9001862)	Qiagen

2.1.9 Kits and ready-to-use reagents

List of kits and ready-to-use solutions.

Product	Manufacturer	Cat. Nr.
Anti-Mouse IgG MicroBeads	Miltenyi Biotec	130-048-401
Dead Cell Removal Kit	Miltenyi Biotec	130-090-101
CellTracker™ Blue CMAC	Invitrogen	C2110
CellTracker™ Green CMFDA	Invitrogen	C2925
Chromium Single Cell 3' Library and Gel Bead Kit v3.1	10x Genomics	1000268
Click-iT™ Plus EdU Alexa Fluor™ 647-Kit	Thermo Fisher Scientific	C10634
DNeasy Blood & Tissue Kit	Qiagen	69504
Dynabeads™ Untouched™ Human T Cells Kit	Invitrogen	11344D
EBioscience™ DRAQ5™	Invitrogen	65-0880-92
GEM-X Flex Human Transcriptome Probe Kit v2	10x Genomics	1000900
GEM-X Flex Sample Preparation v2 Kit	10x Genomics	1000781
GeneJET RNA Purification Kit	Thermo Fisher Scientific	K0732
GreenMasterMix No Rox	Genaxxon	M3150.0200
Human TNF alpha ELISA Kit	Thermo Fisher Scientific	KHC3012
iScript™ cDNA Synthesis Kit	BioRad	1708891
MinElute PCR Purification Kit	Qiagen	28004
Monarch® Total RNA Miniprep Kit	New England Biolabs	T2010S
Normal Donkey Serum	Biozol	LIN-END9010
Pan T Cell Isolation Kit, human	Miltenyi Biotec	130-096-535
Pierce™ BCA Protein Assay Kit	Thermo Fisher Scientific	A55864
SuperSignal West Dura Kit	Thermo Fisher Scientific	34075
Tagment DNA Enzyme and Buffer Small Kit	Illumina	20034197
TaqMan™ Universal PCR Master Mix	Thermo Fisher Scientific	4304437
ViaDye™ Red Fixable Viability Dye Kit	Cytek® Biosciences	SKU R7-60008

2.1.10 Primers and oligos

List of qPCR primers (self-designed, produced by Biomers).

Target	Forward sequence	Reverse sequence
ACTA2	5´-AGATCAAGATCATTGCCCC-3´	5´-TTCATCGTATTC CTGTTTGC-3´
CXCL2	5´-TGCAGGGAATCTCAAG-3´	5´-TGAGACAAGCTGCCCA-3´
CTGF	5´-CCTGGTCCAGACCACAGAGT-3´	5´-TGGAGATTTTGGGAGTACGG-3´
GAPDH	5´-TCGGAGTCAACGGATTTG-3´	5´-CAACAATATCCACTTTACCAGAG-3´
IL-6	5´-GCAGAAAAAGGCAAAGAATC-3´	5´-CTACATTTGCCGAAGAGC-3´
POSTN	5´-TGTCACTGTTAATTGTGCTC-3´	5´-CTGCTCTAAAAGATGAAAGGTC-3´

List of customized probes used for co-culture scRNA-seq data set (produced by Biomers).

Probe	Sequence
LHS	CCTTGGCACCCGAGAATTCCA-ATTACGGGGCCGTCGGAGGGGAAGT
RHS-BC001	phospho-TGGTGCCGCGCAGCTTCACCTTGTA-ACGCGGTTAGCACGTA-NN-ACTTTAGG-CGGTCCTAGCAA
RHS-BC002	phospho-TGGTGCCGCGCAGCTTCACCTTGTA-ACGCGGTTAGCACGTA-NN-AACGGGAA-CGGTCCTAGCAA
RHS-BC003	phospho-TGGTGCCGCGCAGCTTCACCTTGTA-ACGCGGTTAGCACGTA-NN-AGTAGGCT-CGGTCCTAGCAA
RHS-BC004	phospho-TGGTGCCGCGCAGCTTCACCTTGTA-ACGCGGTTAGCACGTA-NN-ATGTTGAC-CGGTCCTAGCAA
RHS-BC005	phospho-TGGTGCCGCGCAGCTTCACCTTGTA-ACGCGGTTAGCACGTA-NN-ACAGACCT-CGGTCCTAGCAA
RHS-BC006	phospho-TGGTGCCGCGCAGCTTCACCTTGTA-ACGCGGTTAGCACGTA-NN-ATCCCAAC-CGGTCCTAGCAA
RHS-BC007	phospho-TGGTGCCGCGCAGCTTCACCTTGTA-ACGCGGTTAGCACGTA-NN-AAGTAGAG-CGGTCCTAGCAA
RHS-BC008	phospho-TGGTGCCGCGCAGCTTCACCTTGTA-ACGCGGTTAGCACGTA-NN-AGCTGTGA-CGGTCCTAGCAA
RHS-BC009	phospho-TGGTGCCGCGCAGCTTCACCTTGTA-ACGCGGTTAGCACGTA-NN-ACAGTCTG-CGGTCCTAGCAA
RHS-BC010	phospho-TGGTGCCGCGCAGCTTCACCTTGTA-ACGCGGTTAGCACGTA-NN-AGTGAGTG-CGGTCCTAGCAA
RHS-BC011	phospho-TGGTGCCGCGCAGCTTCACCTTGTA-ACGCGGTTAGCACGTA-NN-AGAGGCAA-CGGTCCTAGCAA
RHS-BC012	phospho-TGGTGCCGCGCAGCTTCACCTTGTA-ACGCGGTTAGCACGTA-NN-ACTACTCA-CGGTCCTAGCAA
RHS-BC013	phospho-TGGTGCCGCGCAGCTTCACCTTGTA-ACGCGGTTAGCACGTA-NN-ATACGTCA-CGGTCCTAGCAA
RHS-BC014	phospho-TGGTGCCGCGCAGCTTCACCTTGTA-ACGCGGTTAGCACGTA-NN-ATCATGTG-CGGTCCTAGCAA
RHS-BC015	phospho-TGGTGCCGCGCAGCTTCACCTTGTA-ACGCGGTTAGCACGTA-NN-AACGCCGA-CGGTCCTAGCAA
RHS-BC016	phospho-TGGTGCCGCGCAGCTTCACCTTGTA-ACGCGGTTAGCACGTA-NN-ATTCGGTT-CGGTCCTAGCAA

List of probes and primers used for TaqMan™ assay

Target	Probe/primer
endogenous KRAS (3'UTR of exon 5)	Thermo Fisher Scientific (Hs02739788_cn)
KRAS exon 3 (self-designed)	Probe: FAM probe (5'-/56-FAM/TCG ACA CAG/ ZEN/ CAG GTC AAG AAG AGT A/3tABkFQ/-3', IDT) Primer: for_5'GAAGCAAGTAGTAATTGATGGAGAA-3', rev_5'-CCAGTCCTCATGTACTGGTC-3'
TaqMan™ Copy Number Reference Assay, RNase P	Thermo Fisher Scientific (4403328)

2.1.11 Software

List of used software.

Software	Application	Devoloper
GSEA desktop software (v4.3.3)	Gene set enrichment analysis	UC San Diego and Broad Institute
ChatGPT	AI-assisted troubleshooting during computational analysis	OpenAI
Enrichr	Gene list enrichment	Ma'ayan Laboratory, Icahn School of Medicine at Mount Sinai
FlowJo (v 10.8.1)	Flow cytometry data analysis	FlowJo LLC
Grammarly	Improvement of grammar and spelling	Grammarly Inc.
Incucyte® software (v2022B Rev2)	Analysis of live cell imaging data	Sartorius
Prism v9	Data analysis and visualization	GraphPad
R (v 3.4.4 – v4.4.1)	Data analysis and visualization	R Core Team
R Studio	Integrated development environment (IDE) for R	Posit, PBC

2.2 Cell culture methods

2.2.1 Cultivation of human embryonic stem cells (hESCs)

Cultivation of hESCs and differentiation towards the pancreatic lineage was approved by the Robert Koch Institute (79th Authorization under the Stem Cell Act, AZ 3.04.02/0084). The hESC line HUES8 was obtained from Harvard University (RRID: CVCL_B207) and cultured at 5 % CO_2, 5 % O_2, and 37°C on hESC-qualified Matrigel-coated plates in mTeSR Plus. Cells were passaged twice a week upon confluency (80-100 %). Therefore, cells were detached from the plate by incubating with TrypLE for approximately 5 min, then resuspended in DMEM. After centrifugation at 300 x g for 4 min, cells were re-seeded in a ratio of 1:8 using fresh mTeSR plus supplemented with 10 µM Y-27632 for the first 24 h after passaging.

2.2.2 Cultivation of human pancreatic stellate cells (PaSCs)

PaSCs, kindly provided by Prof. Matthias Löhr (Karolinska Institute, Stockholm), were isolated from a chronic pancreatitis patient and immortalized using the catalytic subunit of hTERT and SV40 large T antigen. The cells were maintained at 37°C under a 5 % CO_2 atmosphere in DMEM supplemented with 10% fetal bovine serum (FBS) and P/S (100 IU/mL penicillin and 100 µg/mL streptomycin sulfate). Passaging was performed when cells reached approximately 90 % confluency, by detaching the cells with TrypLE for 10 min and reseeding in a ratio of 1:10 in fresh media.

2.2.3 Gene editing of hESCs and PaSCs

Dr. Jessica Lindenmeyer (former Internal Medicine I, Ulm University Hospital), generated the doxycycline-inducible $KRAS^{G12D}$ hESC line using a piggyBac transposon system.[34,196] Therefore, a PB-TAC-ERP2-(N-HA)KRAS_G12D plasmid was generated by employing a multi-step PCR approach followed by gateway cloning. The plasmid, together with a transposase-expression vector, was transfected into the cells via nucleofection. Clones, in which the construct was successfully integrated, were further enriched by puromycin selection.

The GFP-labelling of PaSCs was performed by Paul Lopatta (Institute of Molecular Oncology and Stem Cell Biology, Ulm University Hospital). Therefore, LentiX-cells were transfected by adding 8 µg of pLac eGFP vector, 5.5 µg psPAX2 vector, and 2 µg pMD2 vector, and 70 µl of PEI (1 mg/ml in 20 mM HEPES and 150 mM NaCl

at pH 7.4) diluted in DMEM for 4 hours. After 2 and 4 days, the media was collected and lentivirus particles were concentrated with the Lenti-X concentrator. The virus concentrate was then used to transduce the PaSCs, which were selected with Neomycin for 7 days.

2.2.4 Generation and cultivation of pancreatic duct-like organoids (PDLOs)

Differentiation of hESCs towards the pancreatic lineage was done as described in previously published protocols.[34,35,197] The hESCs were seeded on plates, pre-coated with either GFR-Matrigel© or Ultimatrix (1:18 in DMEM). By adding day 0 media after 24 h (70-95 % confluency), the differentiation process was initiated, and the media was changed daily according to **Table 3**.

On day 13, pancreatic progenitors (PPs) were detached with TrypLE, followed by magnetic-activated cell sorting (MACS), thereby increasing the GP2-positive population. Therefore, cells were blocked in FC buffer for 30 min on ice, before adding GP2-antibody diluted 1:5000 in FC buffer for 1 h on ice. After washing cells in FC buffer three times, anti-mouse IgG MicroBeads were added and incubated for another 15 min on ice. Cells were again washed three times and re-diluted in MACS buffer before loading the cells onto columns for magnetic sorting. For dome culture, 40,000 purified PP cells were then seeded in 50 µl Matrigel® or UltiMatrix droplets, and media was added once the domes solidified. For sandwich cultures, a layer of Matrigel® or UltiMatrix was added to 12-well plates before adding 100,000 PPs in day 13 media + 5 % Matrigel® or UltiMatrix. Matrigel® and UltiMatrix were adjusted to a protein concentration of 9 mg/ml with DMEM before use. Every 3 to 4 days the media was changed and, after 27 to 29 days of pancreatic differentiation, PDLOs were passaged once. 2 to 4 days after passaging, PDLOs were treated with 3 µg/ml Doxycycline (Dox) to induce $KRAS^{G12D}$ expression. PDLOs were reseeded or harvested by adding Collagenase/Dispase® solution (1:100 in DMEM) for 2 h at 37°C to digest the Matrigel® or UltiMatrix. To dissociate the organoid structures into single cells, PDLOs were incubated in Accutase® solution for 30 min at 37°C. Follow-up experiments, including co-culture assays, were performed using PDLO media, if not stated otherwise.

Table 3 | Stage-specific media composition for pancreatic differentiation.

Day	Compound	Concentration
	BE1 + 0.1 % BSA	
0	Activin A CHIR99021	100 ng/ml 2 µM
1-2	Activin A FGF2	100 ng/ml 5 ng/ml
	BE1 + 0.5 % BSA	
3-5	FGF10 Wnt3a Vitamin C	50 ng/ml 3 ng/ml 0.25 mM
6-8	mNoggin SANT-1 Retinoic acid Glucose Indolactam V	50 ng/ml 0.25 µM 1 µM 16 mM 500 nM
	BE3 + 2 % BSA	
9-12	LDN-193189 EGF Nicotinamide Indolactam V Glucose SANT-1	200 nM 100 ng/ml 10 mM 500 nM 16 mM 0.25 µM
13-19	Nicotinamide ZnSO4 Y-27632 EGF FGF10 KGF MSC2530818	10 mM 10 µM 10 µM 50 ng/ml 50 ng/ml 50 ng/ml 50 nM
from 20 onwards (PDLO medium)	Nicotinamide ZnSO4 EGF FGF10 Matrigel® or UltiMatrix	10 mM 10 µM 50 ng/ml 50 ng/ml 5 % (sandwich culture only)

2.2.5 T cell isolation

The German Red Cross blood bank provided buffy coats from healthy donors. Written consent was obtained from donors, allowing the use of the samples for research purposes and the experiments were approved by the Ethics commission of Ulm University (#460/23). Buffy coats were carefully layered onto Ficoll-PaqueTM PLUS, after diluting 1:1 with DPBS. Peripheral blood mononuclear cells (PBMCs) were then collected after centrifugation for 20 min at 800 x g, followed by washing in DPBS three times. PBMCs were then either cryo-preserved in heat-inactivated FBS + 10 % DMSO or directly subjected to T cell isolation. T cell isolation was achieved with the Dynabeads™ Untouched™ Human T Cells Kit (Invitrogen). Therefore, PBMCs were resuspended in T cell isolation buffer and incubated with the antibody cocktail at 4°C for 15 min. After washing the cells in T cell isolation buffer once, the Dynabeads™ were added for 20 min at room temperature (RT) on a rotating device. Using the DynaMag™-2 Magnet, T cells were enriched in the supernatant. The freshly isolated T cells were then activated overnight in RPMI supplemented with 10 % FBS and 1 % P/S on anti-CD3E and anti-CD28 antibody pre-coated plates.

2.3 Global analysis techniques

2.3.1 Sample preparation and sequencing for scRNA-seq analysis

Within the scope of this work, two distinct single-cell RNA sequencing (scRNA-seq) datasets were generated. For the first data set, mono-cultures of PDLOs after different time points of Dox treatment were sequenced (time-series data set). For the second data set, PDLOs after 7 days of Dox treatment were analyzed, either in mono-culture or in bi-culture with T cells or PaSCs (co-culture data set).

The samples for the time-series data set were generated by Dr. Jessica Lindenmeyer (former Internal Medicine I, Ulm University Hospital), Dr. Michael Melzer (Institute of Molecular Oncology and Stem Cell Biology, Ulm University Hospital) and Dr. Sandra Wiedenmann (Helmholtz Pioneer Campus, Helmholtz Munich). PDLOs were harvested as described above after 1, 3, 5, and 7 days of Dox treatment and untreated PDLOs from day 1 and day 7 were included as controls. However, the day 1 control was later excluded from downstream analysis, as the sample did not meet the quality criteria. The cells were then initially cryo-preserved (in DMEM supplemented with 10% FBS and 10% DMSO) after harvesting and later thawed

again for sequencing. The Dead Cell Removal Kit was used to remove any cell debris or dead cells. Library preparation was done with the Chromium Single Cell 3' Library and Gel Bead Kit v3.1, and sequencing was run on a NovaSeq 6000 S2 flow cell system. In order to capture the expression of the $KRAS^{G12D}$ construct, the corresponding sequence was incorporated into the reference genome (GRCh38) file before the CellRanger pipeline was called on the raw sequencing files.

To generate the samples for the co-culture data set, PDLOs were Dox-treated for 4 days. Then either T cells (10-fold of cells to the number of initially seeded PDLO cells) or PaSCs (1.5-fold of cells to the number of initially seeded PDLO cells) were added. One condition also included the addition of 10 µg/ml infliximab to Dox-treated PDLOs, and samples were harvested after 3 days of co-culture. The GEM-X Flex Sample Preparation v2 Kit was used to fix the cells, strictly following the manufacturer's protocol (CG000782). Library preparation and sequencing were performed by the Biomedical Sequencing Facility at the CeMM Research Center for Molecular Medicine of the Austrian Academy of Sciences. Therefore, the Chromium X and the Chromium Human Transcriptome Probe Set v1.1.0 were utilized to generate multiplexed libraries, according to the "GEM-X Flex Gene Expression for Multiplexed Samples" user guide (CG000787). The Chromium Human Transcriptome Probe Set v1.1.0 was extended by the addition of self-designed customized probes, targeting the mCherry reported sequence in order to capture the expression of the $KRAS^{G12D}$ construct (see 2.1.10 Primers and oligos for oligo sequences). The multiplexed samples were sequenced in two independent runs. While the first run included all samples of the mono- and bi-cultures, the second run was only performed on the bi-cultures. Both runs were sequenced on a NovaSeq 6000 device. Pre-processing of the raw sequencing files was also performed by the Biomedical Sequencing Facility at the CeMM Research Center for Molecular Medicine of the Austrian Academy of Sciences with the CellRanger Multi -pipeline (v9.0.0).

2.3.2 ATAC-sequencing

After 3, 5, and 7 days of Dox treatment, PDLOs were harvested as described above. For the tagmentation of 50,000 cells per sample, the 2x TD (Tagment DNA Buffer) and TDE1 (Tagment DNA Enzyme) from the Tagment DNA Enzyme and Buffer Kit were used together with 1% Digitonin, and 50x cOmplete, EDTA-free Protease

Inhibitor cocktail. Samples were incubated at 37°C for 30 min before purifying the DNA fragments with the MinElute Kit. Sequencing was performed by the Biomedical Sequencing Facility at the CeMM Research Center for Molecular Medicine of the Austrian Academy of Sciences on a NovaSeq 6000 instrument using a paired-end protocol. Bowtie2 was used to align the reads against the human reference genome GRCh38, and peak calling was performed with MACS2. The R package GenomicRanges v1.50.2 allowed filtering, excluding peaks that were present in less than 10 samples. Bam files were used as input for the *featureCounts* function of the Rsubread package 2.12.3, generating read counts. To identify differentially accessible regions, the DESeq2 package was utilized. The differentially accessible regions were annotated with the ChIPseeker package.

2.3.3 Mass spectrometry for proteome analysis

To reduce Matrigel®-related contamination of samples, PDLOs were reseeded into 1196 microwell-chips. The microwell-chips were kindly provided by Dr. Sandra Wiedenmann[198]. On day 25 of pancreatic differentiation, PDLOs were harvested as described above. A total of 717,000 cells were added per chip (equal to 600 cells per microwell) in 700 µl of media. After the cells settled for 1h at 37°C, another 2.3 ml of media was added and Dox treatment was initiated on day 27. The PDLOs were harvested after 7 days of Dox treatment by flushing the microwell-chips with cold DPBS, and RIPA buffer was used to lyse the cells. Peptides were generated by tryptic digestion of 10 µg lysate. Mass spectrometry was performed on a Q-Exactive HF-X device by the Metabolomics and Proteomics Core (MPC) at the Helmholtz Munich.

2.3.4 Data availability

The generated sequencing data have been deposited in the Gene Expression Omnibus (GEO) data repository and are available under the GEO accession numbers GSE284392 (scRNA-seq time-series), GSE312209 (scRNA-seq co-culture) and GSE284390 (ATAC-seq).

2.4 Computational analysis

2.4.1 Pre-processing of the PDLO scRNA-seq data sets

The Python package Scanpy v1.7.0 was utilized for the initial processing of the time-series data set, which was performed by Dr. Sandra Wiedenmann (Helmholtz Pioneer Campus, Helmholtz Munich). The raw count matrix of each individual

sample was therefore filtered to exclude cells with more than 1,200 detected genes and more than 15 % of mitochondrial counts and to exclude genes that were found in less than 3 cells. The filtered raw count matrixes were then merged and log-normalized. The resulting AnnData object was then converted from h5ad file format to h5seurat file format with SeuratDisk v0.0.0.9020, allowing further analysis in R.

The raw counts of the co-culture data set showed some discrepancies between the individual probes for the same gene (e.g. mean raw count for KRT19 across all cells: probe 1 = 3.4007, probe 2 = 0.0225, probe 3 = 0.0059). Probes were therefore excluded if their mean raw count across all cells was below 20% of the best-performing probe for the same gene, aiming to reduce potential bias based on variance in probe performance. This filtering step was performed in R with the aid of the Matrix v1.7-0, dplyr v1.1.4 and the stringr v1.5.1 packages. For the first sequencing run, 37,651 of initially 54,582 probes remained, while 39,069 of 54,582 probes were kept for the second sequencing run. As the Human Transcriptome Probe Set v1.1.0 includes 18,526 genes, the filtered probe matrix averages to approximately two probes per gene. The mean count of all remaining probes was then calculated per gene and cell. The filtered raw count matrices of both sequencing runs were then merged with Seurat v5.0.0, before excluding cells with less than 300 or more than 8,000 unique features or more than 30 % mitochondrial counts.

2.4.2 *KRAS*^{G12D}-dependent grouping of cells and multilayer deep learning

To group the cells of the time-series data set based on their KRAS^{G12D} expression, the normalized KRAS^{G12D} expression values were used as input for k-means clustering. Therefore, the R package stats v4.2.2 was used to run distance matrix computation (*dist* function) before hierarchical clustering (*hclust* function) was performed, followed by k-means grouping (*cutree* function with k=3).

Dr. Medhanie Mulaw (Single cell Sequencing Unit, Ulm University) then utilized the Keras/TensorFlow deep learning model to identify gene expression classifiers that distinguish the k-means-based KRAS^{G12D} groups. The workflow was applied as described previously.[199] The model consisted of an input layer with 16 units, followed by three hidden layers of 16 units each, and a final output layer with 3 units for multiclass classification. For kernel initialization and activation, a Glorot uniform initializer and hyperbolic tangent activation were applied. For the final layer prediction, softmax was used, and for model optimization, along with a

categorical cross-entropy loss measurement, a stochastic gradient descent optimizer was employed. Training of the model was done with 200 iterations using 65 % of the dataset, while the other 35 % was used for validation.

Within the co-culture data set, the PDLO cells were grouped using the normalized mCherry expression values, which were then used as input for k-means clustering as described above for the time-series data set. However, only 20% of the cells showed detectable levels of mCherry, although the mCherry fluorescence signals were as expected before harvesting the samples and should have therefore yielded a higher number of mCherry-positive cells. Therefore, mCherry-negative cells were additionally annotated using the time-series data set as reference and performing Seurat's anchor-based label transfer. Combining both methods resulted in a total of 45 % $KRAS^{high}$ or $KRAS^{intermediate}$ cells within the PDLO population.

2.4.3 Normalization, dimension reduction, and identification of differentially expressed genes (DEGs) of the PDLO scRNA-seq data sets

For the normalization, dimension reduction, and identification of differentially expressed genes (DEGs) the R package Seurat (v4.2.0 – 5.1.0) was used for both the time-series data set and the co-culture data set. For visualization, ggplot2 v3.4.0-3.5.1 and SCpubr v2.0.2 were additionally employed.

The 1,452 genes from the deep learning model (deep learning classifiers) were used as *VariableFeatures* for the time-series data set. After scaling, principal component analysis (PCA) was run on the first 50 PCs. For nearest-neighbor graph construction and Uniform Manifold Approximation and Projection (UMAP) dimensional reduction, 30 PCs were used. To identify DEGs, Seurat's function *FindMarkers* was employed, using DESeq2 for testing and excluding genes beyond a threshold of 0.2 for log2FC and <0.05 for the p-value.

The *NormalizeData* function was run on default settings for the co-culture data set, thereby log-normalizing the raw counts. The top 2,000 variable features were then used to scale the normalized counts and dimension reduction (PCA, nearest-neighbor graph construction and UMAP) was computed based on the first 30 PCs. Cells that were only present in the PDLO monocultures were assigned as PDLOs, while additional clusters in the bi-culture conditions were annotated as either T cells or stellate cells accordingly. Cell-type-specific marker expression (e.g., *KRT19* for

PDLOs, *CD3E* for T cells, and *ACTA2* for stellate cells) was examined to confirm cell type annotation. The different cell types were then further analyzed separately:

PDLOs: All PDLO cells were extracted, normalized again with the *NormalizeData* function on default settings, and scaled based on the deep learning classifiers. While the first 50 PCs were used for PCA, the first 10 dimensions were employed for nearest-neighbor graph construction, as well as UMAP dimensional reduction. Raw counts were then normalized and scaled again with sctransform v0.4.1, before using the *FindMarker* function (threshold of 0.2 for log2FC and <0.05 for the p-value) to identify DEGs between conditions. To investigate the similarity between the PDLOs from the co-culture data set and the PDLOs from the time-series data set, the cells from both data sets were merged, and anchor-based CCA integration was computed with the *IntegrateLayers* function. The *BuildClusterTree* (reduction = "integrated.cca") function was then used to visualize similarity between the groups.

T cells: All T cells were extracted, and the functions *NormalizeData* and *ScaleData* were rerun on default settings. The first 50 PCs were used for PCA while the first 10 dimensions were utilized for and nearest-neighbor graph construction, as well as UMAP dimensional reduction. Cluster 5 (44 cells) was excluded from further analysis as the cells did not express relevant levels of CD3. Based on the expression of CD4 and CD8, the remaining clusters were grouped accordingly. All T cells, as well as the CD4 and CD8 subsets, were separately normalized and scaled again with sctransform v0.4.1, followed by the identification of DEGs with the *FindMarker* function.

Stellate cells: All stellate cells were extracted, and the functions *NormalizeData* and *ScaleData* were rerun on default settings. Using the first 50 PCs, PCA was computed and nearest-neighbor graph and UMAP were constructed based on the first 30 dimensions. After running sctransform v0.4.1, *FindMarkers* was called to determine DEGs.

2.4.4 Gene set enrichment

To rank DEGs based on their significance while also accounting for the directionality (up- or downregulated), the negative base-10 logarithm of a gene's p-value was multiplied by the sign of the respective log2-fold change value. The ranked DEG list was then used as input to compute gene set enrichment analysis (GSEA) with the GSEAPreranked tool of the GSEA desktop software v4.3.3. The online tool Enrichr

was further used to investigate gene set enrichment of DEGs within KEGG pathways, Gene Ontology (GO) terms, and HALLMARK gene sets, independent of their ranking. The R package clusterprofiler v4.14.3 allowed the generation of gene-concept networks (cnet plots). Seurat's function *AddModuleScore* was used to calculate the average expression of entire gene sets on a single-cell level. Module scores were, for example, also computed for the stellate cells of the co-culture scRNA-seq data set, using CAF signatures from Elyada et al.[80] and Toa et al.[200]. The individual cells were then annotated according to the CAF subtype with the highest module score. If the highest module score for a cell was smaller than the mean score of all cells, the cell was labeled "non-assigned".

2.4.5 Velocity analysis

The Python package scVelo v0.3.2 was employed to compute splicing kinetics within the time-series scRNA-seq data set, allowing the analysis of trajectory routes. Using SeuratDisk v0.0.0.9021, the Seurat object was therefore converted to an AnnData object. The AnnData object, including UMAP embeddings, was merged with the corresponding loom files, filtered and normalized (min_shared_counts=20, n_top_genes=2000). The dynamical mode was then applied to estimate velocities. Partition-based graph abstraction (PAGA) construction was performed on default settings.

2.4.6 Survival analysis of the TCGA-PAAD data set

The TCGAbiolinks package v2.26.0 was used to download the TCGA-PAAD data set, which was then filtered for primary tumors. The log-transformed TPM values from the RNA-seq of all remaining patient samples were used as input for gene set variation analysis with the GSVA package v1.53.23. The top 50 DEGs of the comparisons $KRAS^{high}$ PDLOs vs. $KRAS^{low}$ PDLOs and $KRAS^{intermediate}$ PDLOs vs. $KRAS^{low}$ PDLOs (time-series data set) were used as gene sets. Samples with a score greater than 0.2 were assigned as "high gene set enrichment", while the remaining samples (score < 0.2) were annotated as "low gene set enrichment". The survminer package v0.4.9 was then used to create survival curves.

2.4.7 Reprocessing of publicly available scRNA-seq data sets

Peng et al. published scRNA-seq data from 24 PDAC and 11 healthy samples[201], which was downloaded from the Genome Sequence Archive (PRJCA001063). Using

Seurat, cells with more than 8,000 genes and 10 % mitochondrial counts were excluded. After normalization of the raw counts (*NormalizeData*), data was scaled based on the top 2,000 variable features. The first 50 PCs were used to compute PCA, followed by nearest neighbor and UMAP construction on the first 20 dimensions. Metadata, including cell-type annotations, was provided by the authors and used without further adaptation.

Carpenter et al. published a scRNA-seq data set of pancreatic tissues derived from healthy donors, partially harboring PanIN lesions, and from PDAC tissue.[65] The data set was downloaded from the NIH Gene Expression Omnibus database (GSE229413). Preprocessing of the data set was done with Seurat, following the pipeline published by the authors. Cells with less than 200 unique genes and more than 15% mitochondrial counts were therefore excluded. All cells labeled as fibroblasts were then extracted, followed by log-normalization of raw counts. Using the reciprocal PCA, anchor-based integration was computed before nearest-neighbor graph construction was done on the first 30 dimensions and UMAP reduction was performed on the first 15 dimensions.

2.4.8 Integration of a published PDAC scRNA-seq data set with PDLO scRNA-seq data set

Using Seurat v4.0.6, the data set from Peng et al.[201] was merged with the time-series PDLO data set. A list containing both objects separately was generated with the *SplitObject* function, followed by normalization and the identification of variable features (n = 4000) for each data set individually. Integration anchors were then identified, on which the data sets were then integrated. PCA was performed on the top 500 variable features from the integrated assay and nearest-neighbor graph construction was done on the first 15 dimensions. The UMAP was constructed on the first 30 dimensions.

2.4.9 Grouping of PDAC samples based on deep learning classifiers

Ductal cells of the reprocessed data set from Peng et al.[201] were extracted, and raw counts were normalized and scaled with sctransform v0.4.1. The average expression for each gene was computed per patient and the pseudo-bulked count matrix was then restricted to the machine learning classifiers. K-means clustering was then performed as described for the time-series data set with the stats package v4.2.2

(*dist, hclust, cutree* with k =3). The resulting groups were then assigned as either $KRAS^{high}$, $KRAS^{intermediate}$, or $KRAS^{low}$, according to their KRAS expression.

2.4.10 Cell-cell communication analysis

The R package CellChat v2.1.2 was used for cell-cell communication analysis. Unless stated otherwise, communication probability and aggregated cell-cell communication networks were computed as described in the CellChat package vignette, running the respective functions on default settings.

The preprocessed data set from Carpenter et al.[65] was used, including only cells from the healthy donors and restricting the cell types to epithelial cells, T cells, macrophages, endothelial cells, fibroblasts, B cells and natural killer cells. The remaining cells were then merged with the PDLO time-series data set into a Seurat object. Normalization was performed with sctransform v0.4.1 and the normalized count matrix was then used as input for the standard CellChat pipeline.

For the scRNA-seq data set from Peng et al.[201], analysis was performed on the integrated (PDLO-PDAC) data set as well as on the KRAS-grouped PDAC data set (without PDLOs). The KRAS-grouped PDAC data set was split into three separate Seurat objects: $KRAS^{high}$, $KRAS^{intermediate}$ and $KRAS^{low}$. The raw counts of each Seurat object were again normalized with sctransform v0.4.0, before creating the respective CellChat objects, on which the CellChat pipeline was then applied. The integrated PDLO-PDAC data set was not filtered, and the SCT assay was directly used as input for the CellChat pipeline.

For the PDLO co-culture scRNA-seq data set, monocultures were excluded, and sctransform v0.4.1 was applied to the remaining cells from the bi-culture conditions. The human protein-protein interaction (PPI) network was used to smooth the gene expression values. The communication probabilities were computed based on the truncated mean before aggregated cell-cell communication networks were constructed. To allow pairwise analysis of the treatment conditions, this workflow was also applied for the untreated, Dox-treated, or infliximab-Dox-treated bi-cultures separately. The *mergeCellChat* function was then used to compare communication patterns between the individual CellChat objects.

2.5 *In vitro* assays

2.5.1 Co-culturing of matrix-embedded organoids and T cells ("InterOMaX")

The INTERaction with Organoid-in-MatriX ("InterOMaX") platform was applied as described previously[202] in collaboration with Dr. Yuan-Na Lin and Anton Lahusen (Internal Medicine I, Ulm University Hospital). To generate the chips, 2 % agarose in DPBS was heated and poured into the 81-well MicroTissues® 3D Petri Dish® micro-molds. Once the agarose chips solidified, molds were carefully removed, and 50,000 PDLO cells were seeded per chip. The cells were allowed to form organoid-like structures for 24 h before being treated with Dox for 4 days. Collagen type 1 and Matrigel® were then mixed in a ratio of 7:3 and added to the chips, thereby embedding the organoids. The embedded organoids were carefully transferred to chamber slides. T cells were isolated and activated overnight as described above before incubating with 1 µM CellTracker™ Green CMFDA for 30 min at 37°C. The stained T cells were then added to the chamber slides, with 500,000 cells per chamber. After 3 days, the co-cultures were imaged using the BZ-X Series Keyence fluorescence microscope. Infiltrated T cells were quantified using ImageJ (Macro Watershed Segmentation technique).

2.5.2 Co-culturing of PDLOs and T cells with cancer-on-chip platform

The cancer-on-chip platform has been established previously, and experiments were performed in collaboration with Dr. Tengku Ibrahim Maulana and Dr. Claudia Teufel (Department of Microphysiological Systems, Eberhard Karls University Tübingen). Informed consent was obtained from healthy individuals before collecting whole blood and the procedure was approved by the Ethical Committee of the Eberhard Karls University Tübingen (No. 495/2018-BO02). Isolation of T cells was performed with the Pan T Cell Isolation Kit according to the manufacturer's protocol. PDLOs were harvested without dissociating the organoid structures, resuspended in pure Matrigel® and loaded into chambers of PDMS chips, with approximately 30 PDLOs per chip. Chips were connected to a perfusion system, allowing the PDLO media to flow through a microfluidic channel. After 4 days of Dox treatment, T cells were added through the perfusion system with 200,000 T cells/chip at a flow rate of 20 µL/h after they were stained with 10 µM of Cell Tracker CMFDA. Co-cultures were then imaged with the Axio Observer 7 fluorescence microscope, and infiltrated T cells were quantified with ImageJ software.

2.5.3 Generating conditioned media from PDLOs

PDLOs were grown in sandwich cultures as described above. After 6 days of Dox treatment, all medium was aspirated, and the matrix-PDLO layer was washed once by adding DPBS for 5 min. Per well, 1 ml of blank DMEM (without any additional supplements) was added. After 24 h, the medium containing the PDLO secretome was collected and pooled for different wells of the same treatment condition. To remove cell debris, the conditioned medium was strained through a syringe filter (0.2 µm) before storing at -20°C.

2.5.4 Transwell® migration assay

T cells were isolated and activated as described above (T cell isolation) before seeding 500,000 T cells in blank DMEM (without any additional supplements) into Transwell® 8.0-µm Pore Polycarbonate Membrane Inserts. Simultaneously, PDLO conditioned medium was added to a 24-well plate (500 µl/well). The Trasnwell® inserts were then placed into the 24-well plate, allowing the T cells to migrate from the upper compartment towards the lower compartment containing PDLO conditioned media. After 2 h at 37°C, T cells from both compartments were harvested separately and quantified using the CASY cell counter. The proportion of migrated cells was calculated by normalizing the amount of T cells in the lower compartment to the total number of cells per well (sum of upper and lower compartment).

2.5.5 Multiplex flow cytometry analysis of T cells

Flow cytometry of T cells using a multiplex immune panel was performed by the Core Facility Immune Monitoring of the Medical Faculty at Ulm University (DFG-funded under the project number 514808265). T cells were isolated and activated as described above (T cell isolation). For 72 h, T cells were cultured in PDLO-derived conditioned media. Antibodies were diluted in DPBS containing 0.5 % BSA and added to the T cells for 30 min at 4°C in the dark. After washing the cells with DPBS containing 0.5 % BSA, flow cytometry was performed using the Cytek Aurora spectral flow cytometer and the data was analyzed using FlowJo software v10.81.

2.5.6 Live imaging of PDLO-PaSC co-cultures

PDLOs were passaged onto 96-well plates, which were layered with UltiMatrix (50 µl/well). After 4 days of Dox treatment, GFP-positive PaSCs were added at 50,000

cells per well. Using the Incucyte® S3 live-cell imaging system, the co-cultures were automatically imaged every 12 hours. Quantification of the total green area was done using the Incucyte® software, implementing top-hat segmentation.

2.5.7 Indirect co-culture of PDLOs and PaSCs

After 4 days of Dox treatment, PDLOs were passaged into fresh Matrigel® domes (50 µl) on 12-well plates, without disrupting the organoid structure (Accutase solution was not used). Within the same well, a second Matrigel® dome was placed, containing 70,000 PaSCs. After 72 h, the medium was removed, and a pipette tip was used to scrape off each dome separately. The PDLOs and PaSCs were therefore not mixed and could be analyzed individually.

2.5.8 Enzyme-Linked Immunosorbent Assay (ELISA)

Conditioned medium was concentrated by centrifuging 1 ml of conditioned medium at 4,000 x g for 20 min in Pierce™ protein concentrators. The remaining 300 µl conditioned media were then used as input for the Human TNFα-ELISA Kit. The assay was performed by strictly following the manufacturer's protocol, and absorbance was measured at 450 nm using the Infinite M200 Pro plate reader. TNFα concentrations were determined by interpolating the absorbance values with the standard curve.

2.5.9 EdU staining for cell cycle analysis

PDLOs were incubated with 10 µM EdU for 4 h at 37°c before harvesting the cells as described above (Generation and cultivation of pancreatic duct-like organoids (PDLOs)). After fixation in 4 % PFA and 100 mM sucrose on ice for 20 min, 5 % normal donkey serum and 0.1 % Triton-X in PBS were added for 30 min. Incubation with primary anti-HA-tag antibody was performed overnight at 4°C, followed by exposure to secondary antibody on ice for 90 min. EdU staining was then achieved with the Click-iT EdU Alexa Fluor 647 Assay Kit and the Attune™ NxT flow cytometer was used to measure the samples.

2.5.10 Quantitative real-time PCR

Either the Gene-JET RNA Purification Kit or the Monarch® Total RNA Miniprep Kit was used for RNA isolation before performing cDNA synthesis with the iScript cDNA Synthesis Kit. In order to run quantitative real-time PCR (qPCR), cDNA was combined with the GreenMasterMix (2x) No ROX and the respective primers.

Samples were analyzed on the Rotor-Gene Q, and normalized gene expression was calculated using the ddCT method.

2.5.11 Taqman™ Copy Number Assay

Using the DNeasy Blood & Tissue Kit, genomic DNA (gDNA) was isolated from hESCs, patient-derived organoids (PDOs) and cancer cell lines. The concentrations of gDNA were adjusted to 3-5 ng/µl per sample before adding to TaqMan™ Universal PCR Master Mix, including respective probes and primers. Quantification was done by using the QuantStudio™ 3 Real-time PCR machine and relative copy numbers were calculated with the ddCT method.

2.5.12 Western Blot

Protein lysates were generated by incubating the cells in RIPA buffer on ice for 30 min. Using the Pierce™ BCA Protein Assay Kit, protein concentrations were determined after diluting the lysates 1:8 in H2O. Total protein concentrations were then adjusted between the samples accordingly, subjecting equal amounts for separation by SDS-PAGE. Proteins were then transferred to a PVDF membrane with the Trans-Blot® SD Semi-Dry Transfer Cell system using semidry transfer buffer, and the transfer was validated with Ponceau staining. After membranes were blocked in TBST buffer containing 5 % BSA, primary antibody was added overnight at 4°C, followed by incubation with secondary antibodies for 1 h at RT. Proteins were detected using the SuperSignal West Dura Kit and imaging of the membranes with the Chemiluminescence Imaging – Fusion SL system. ImageJ software was used to quantify the intensities of the protein bands.

2.5.13 Flow cytometry

Cells were fixed in 4% PFA and 100 mM sucrose for 20 min on ice before permeabilization, and blocking was performed in 5 % normal donkey serum and 0.1 % Triton-X in PBS for another 30 min. Primary antibodies were added overnight at 4°C before incubating with secondary antibodies for 90 min on ice. Conjugated antibodies were directly added after permeabilization and incubated for 90 min on ice. Samples were then measured using the Attune™ NxT flow cytometer, and FlowJo software was used for data analysis.

2.5.14 Statistical analysis

GraphPad Prism was used for data analysis and visualization of *in vitro* experiments, if not otherwise stated. Statistical testing was performed as described in the respective figure legends.

3. Results

3.1 KRAS^{G12D}-expressing PDLOs as a pre-cancer model

To deepen the understanding of human KRAS^{G12D} signaling in a pre-cancer context, stem cell-derived pancreatic duct-like organoids (PDLOs) were employed as an *in vitro* model. A polyclonal hESC line harboring a transgenic doxycycline-inducible mCherry-KRAS^{G12D}-HA-tag construct was directed towards the pancreatic lineage, allowing the generation of healthy duct-like structures, in which oncogene signaling can be induced.

3.1.1 Time-resolved single-cell RNA sequencing of *KRAS^{G12D}*-expressing PDLOs

A time-resolved single-cell RNA sequencing (scRNA-seq) data set of *KRAS^{G12D}*-expressing PDLOs was generated to capture the earliest oncogene-dependent transcriptional dynamics (time-series scRNA-seq data set).

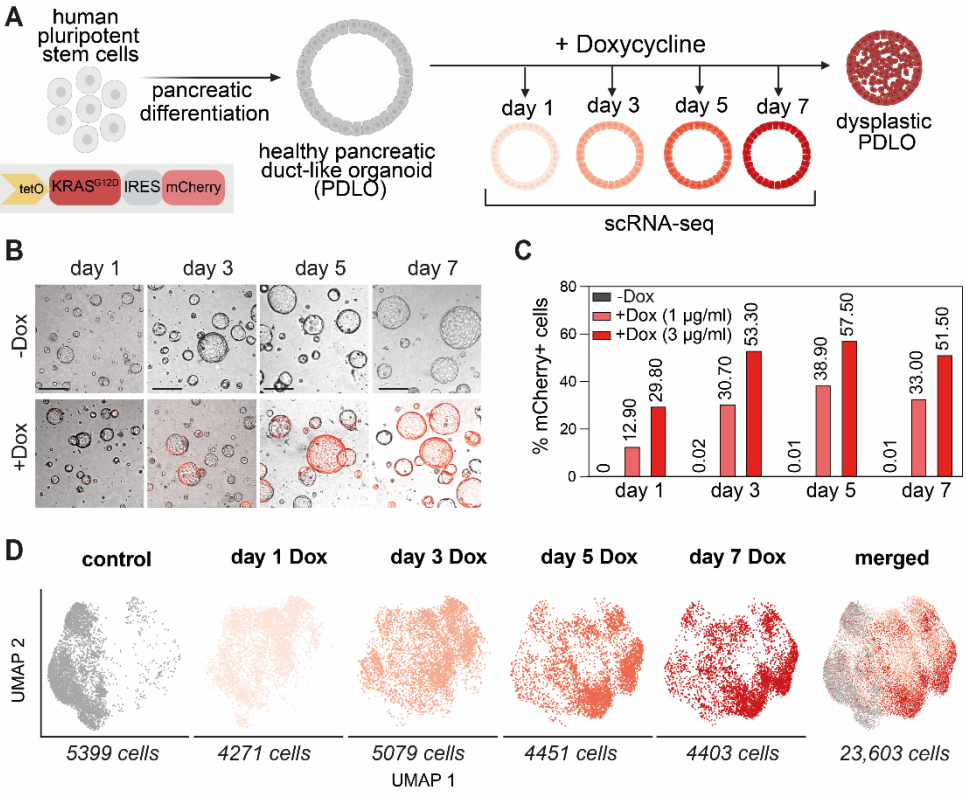

Figure 5 | Single-cell RNA sequencing of PDLOs after different timepoints of doxycycline treatment. (**A**) Schematic overview of PDLO generation and sampling for scRNA-seq. (**B**) Brightfield images of PDLOs used for scRNA-seq overlayed with the red mCherry signal. Scale bar = 250 µm. (**C**) Quantification of mCherry-positive cells after Dox treatment by flow cytometry. (**D**) Uniform manifold approximation and projection (UMAP) graphs showing the cells of each time point after Dox treatment. (Scheme was created with BioRender.com and figure was modified from Allgöwer et al.[203] under CC BY 4.0, https://creativecommons.org/licenses/by/4.0/)

The PDLOs were sampled on day 1, 3, 5, and 7 after inducing *KRAS*^{G12D} expression by doxycycline (Dox, 3 µg/ml) treatment (**Figure 5A**). The PDLOs morphologically resembled ductal structures, while organoid size increased over time (**Figure 5B**). A robust transgene expression upon Dox treatment was confirmed by observing the mCherry reporter signal, with more than 50 % mCherry-positive cells from day 3 onwards (**Figure 5B-C**). After filtering out low-quality cells, the time-series scRNA-seq data set contained a total of 23,603 cells, and untreated PDLOs from day 7 served as control (**Figure 5D**).

To confirm the ductal identity of the sequenced PDLOs, the expression of cell type-specific gene markers was investigated. The cells did not display relevant levels of stemness- (*NANOG, SOX2*), acinar- (*PRSS1, PTF1A*), endocrine- (*GCG, CHGA*), or endothelial-related (*PECAM1, VWF*) genes (**Figure 6A**). A moderate expression of progenitor-related genes, such as *PDX1* (and *NKX6-1*), was observed for some cells, predominantly in the control sample (**Figure 6A-B**). The majority of cells, however, showed strong expression of *KRT19* and other ductal markers, such as *SOX9* and *CLDN1*, thereby validating successful ductal differentiation.

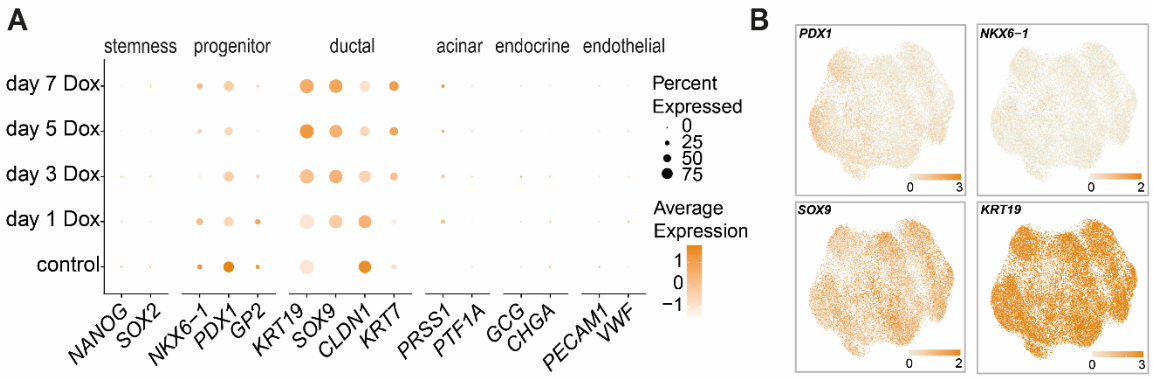

Figure 6 | PDLOs are of ductal identity. (**A**) Dot plot displaying cell type-specific gene expression within the different samples. (**B**) UMAP graphs showing expression of pancreatic progenitor gene marker *PDX1* and *NKX6-1* as well as expression of ductal genes *SOX9* and *KRT19*. (Figure was modified from Allgöwer et al.[203] under CC BY 4.0, https://creativecommons.org/licenses/by/4.0/)

3.1.2 Doxycycline treatment efficiently induces KRAS^{G12D} expression and canonical KRAS signaling in PDLOs

Transfection of the hESCs with the *KRAS^{G12D}*-construct was performed with the PiggyBac transposon system, which inserts the respective sequence at TTAA sites across the genome. To ensure that KRAS copy numbers remain within a physiological range, copy number analysis was done on hESCs, PDAC cell lines, and PDOs (**Figure 7A-B**). The genetically engineered hESCs lines KRAS1 (used for time-series scRNA-seq data set) and KRAS2 showed ~5-fold increased number of *KRAS* copies relative to the parental line (harboring only the endogenous *KRAS^{WT}*). KRAS-mutated PDAC lines and PDOs ranged between 2- and 3-fold *KRAS* copies, relative to the respective wild-type lines. Within the time-series scRNA-seq data set, *KRAS^{G12D}* expression was stable across all time points upon Dox treatment, while expression of endogenous *KRAS^{WT}* was not affected (**Figure 7C**).

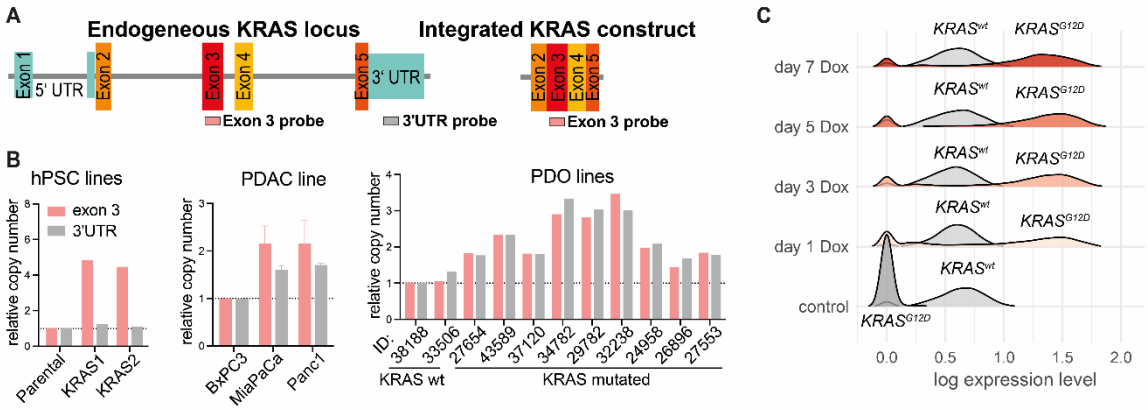

Figure 7 | KRAS copy number and expression. (**A**) Probes used for KRAS copy number analysis either targeted the 3' untranslated region of the endogenous locus (3'UTR) or exon 3. The exon 3 probe detects the endogenous sequence as well as the integrated KRAS^{G12D} construct. (**B**) KRAS copy numbers of hESCs, PDAC cell lines, and PDOs relative to the respective KRAS wild-type lines (parental hESCs, BxPC3, and PDO#38188). (**C**) Ridge plot of KRAS^{G12D} and endogenous KRAS^{WT} expression for the different time-points of Dox treatment within the scRNA-seq data set. figure was modified from Allgöwer et al.[203] under CC BY 4.0, https://creativecommons.org/licenses/by/4.0/)

Canonical KRAS signaling, such as the MAPK cascade, PI3K-mTOR signaling, and the NFκB pathway, was also found to be upregulated within the time-series scRNA-seq data set (**Figure 8A**). This was further validated by analyzing protein levels of phosphorylated ERK (pERK), a well-established downstream target of KRAS signaling (**Figure 8B**). The KRAS-PDLOs showed a gradual increase in pERK relative to ERK over the time of Dox treatment, while this was not observed in the untreated samples. Moreover, pERK levels remained low in Dox-treated parental

PDLOs, thereby excluding effects of the doxycycline treatment itself. Despite fewer KRAS copy numbers, PDAC lines and PDOs show comparable levels of pERK (relative to ERK) as observed in Dox-treated KRAS-PDLOs (Figure 8C).

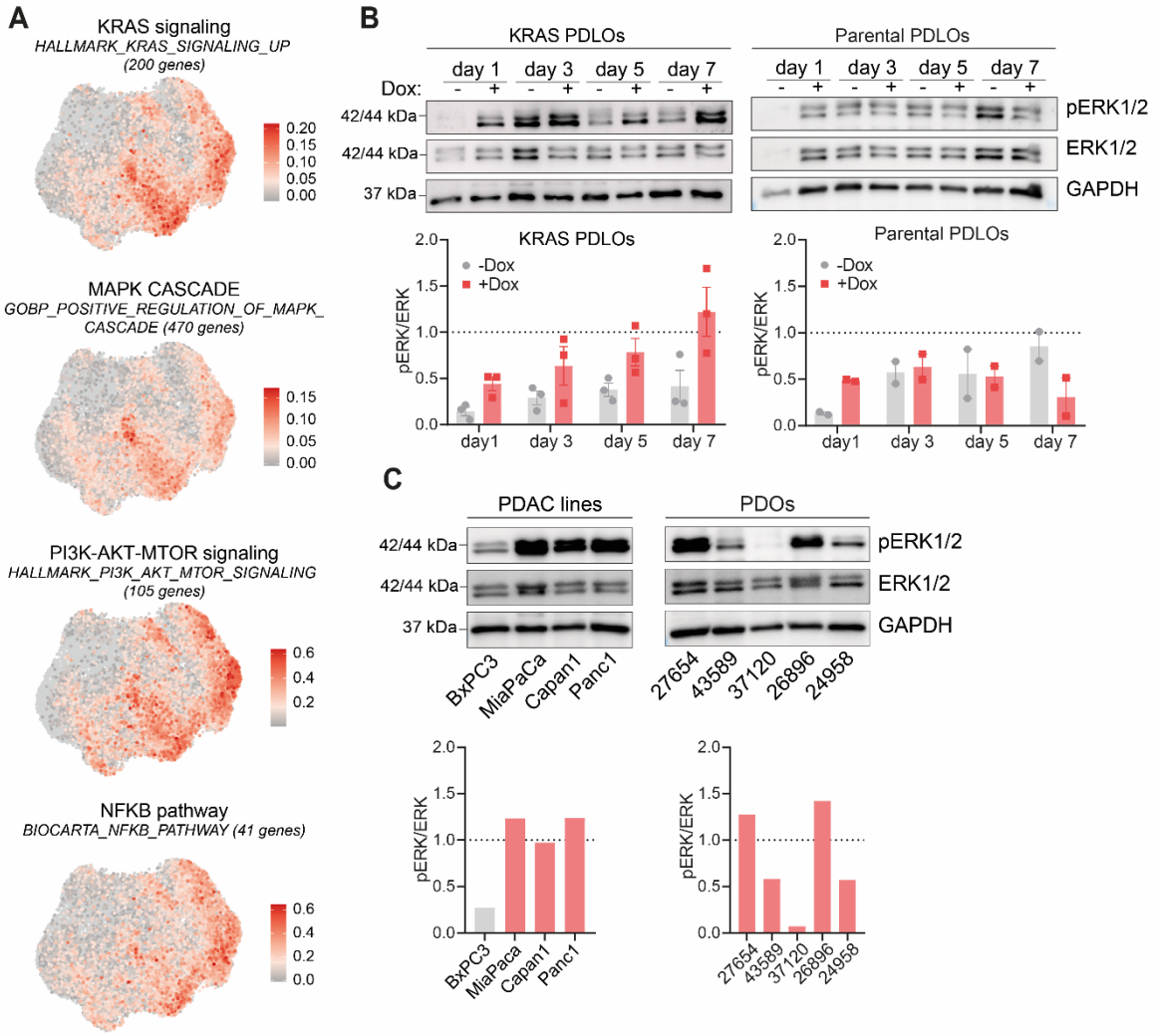

Figure 8 | PDLOs exhibit canonical KRAS signaling after Dox treatment. (**A**) UMAPs showing the module score (averaged expression) per cell of gene sets related to canonical KRAS signaling. (**B**) Protein levels of phosphorylated ERK (pERK) and ERK after different time-points of Dox treatment in KRAS-PDLOs (left, n = 3) and parental PDLOs (right, n =2). Per sample, pERK levels were normalized to ERK levels. GAPDH served as housekeeping gene. (**C**) Protein levels of pERK and ERK in PDAC cell lines (left, n=1) and PDOs (right, n=1). Per sample, pERK levels were normalized to ERK levels. GAPDH served as housekeeping gene. (Figure was modified from Allgöwer et al.[203] under CC BY 4.0, https://creativecommons.org/licenses/by/4.0/)

3.1.3 KRAS^{G12D} correlates with epithelial-to-mesenchymal transition (EMT) and alters the cell-cycle

Previous work linked *KRAS^{G12D}* expression in PDLOs to oncogene-induced senescence and EMT after 9 days of Dox treatment.[34] This was also observed in the time-series scRNA-seq data set. *KRAS^{G12D}* expression was positively correlated with EMT and senescence across the different time points, whereas correlation with the proliferation marker *MKI67* was strongest on day 1, before declining at later time points (**Figure 9A**).

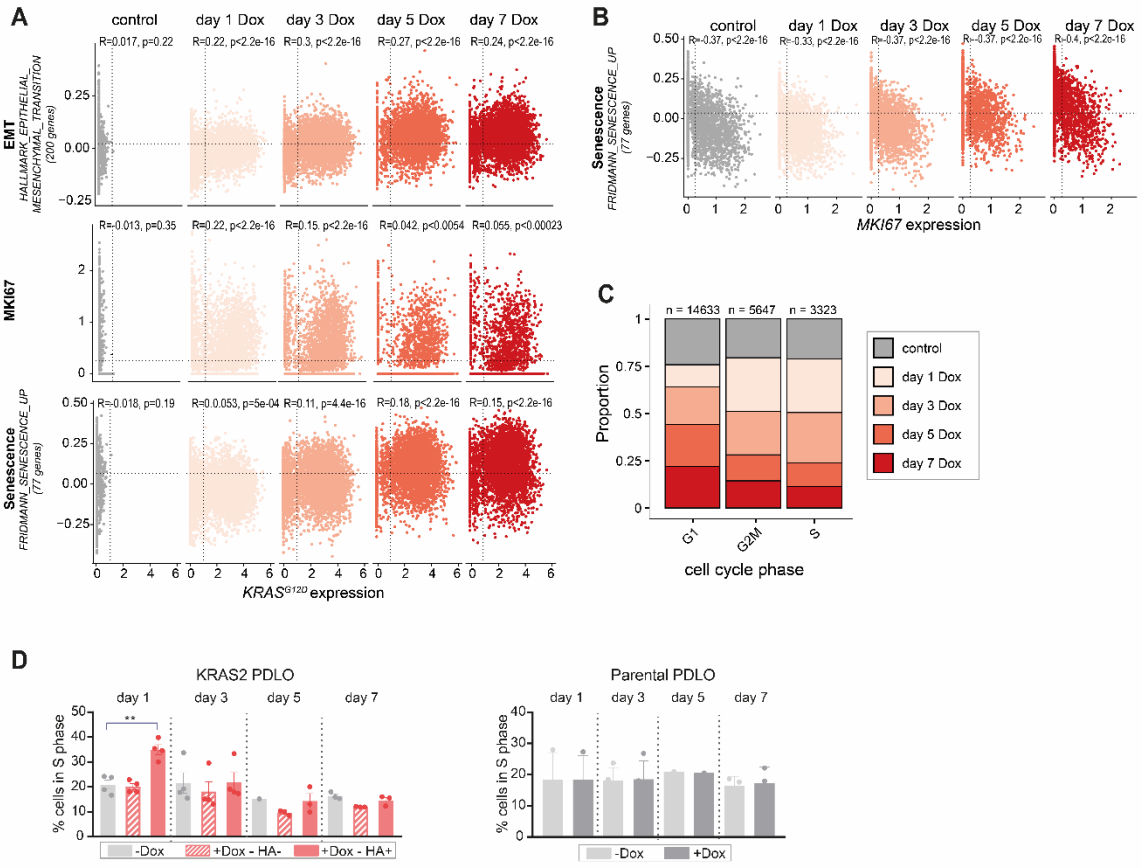

Figure 9 | KRAS^{G12D} induces EMT and senescence in PDLOs. (**A**) Scatter plot depicting the correlation between KRAS^{G12D} expression and module scores (averaged expression) of gene sets for EMT and senescence as well as *MKI67* expression within the time-series scRNA-seq data set. R = Pearson's correlation coefficient. (**B**) Scatter plot displaying the correlation between MKI67 expression and module score of senescence-related genes within the time-series scRNA-seq data set. (**C**) Proportion of individual time points for the different cell cycle phases (**D**). EdU-based cell cycle analysis of PDLOs after different time points of Dox treatment (n = 4). Unpaired t-test: **, p<0.01. (Figure was modified from Allgöwer et al.[203] under CC BY 4.0, https://creativecommons.org/licenses/by/4.0/)

This trend also emerges when analyzing the relationship between senescence and proliferation across all cells over the time course of Dox treatment (**Figure 9B**).

Cell cycle scoring of individual cells showed increased proportions of *KRAS*^{G12D}-expressing PDLOs from day 1 in S- and G2M-phase, while cells of later time points remain in G1-phase (**Figure 9C**). EdU-based cell cycle analysis *in vitro* with a second KRAS line (KRAS2 PDLO) confirmed that there is a significant increase in proliferation in *KRAS*^{G12D}-expressing PDLOs (+Dox and HA+) on day 1, after which the proportion of cells in the S-phase decreases again (**Figure 9D**). In the parental PDLOs, no differences were observed upon Dox treatment.

3.1.4 KRAS-PDLOs show enrichment of neoplasia signatures

To inquire whether the PDLO model can capture transcriptomic changes related to human pre-cancer lesions, the expression of a neoplasia signature, derived from spatial transcriptomics of PanIN lesions[83], was analyzed within the time-series scRNA-seq data set. Indeed, this neoplasia signature gradually increases over the time of Dox treatment (**Figure 10A**). A similar trend is observed for *TFF1* expression (**Figure 10B**), which was described as a key marker of PanINs[83].

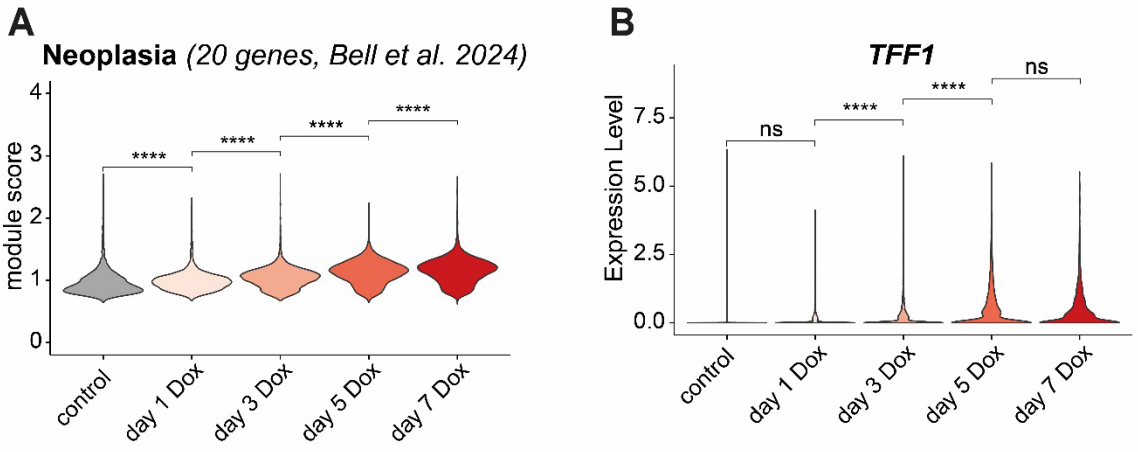

Figure 10 | The expression of PanIN-related genes gradually increases over the time of Dox treatment. (**A**) Module score (averaged expression) of a neoplasia signature, derived from a spatial transcriptome data set of human PanINs[83] over the time of Dox treatment. (**B**) *TFF1* expression over time of Dox treatment. Unpaired t-test: ****, p<0.0001; ns, p>0.05. (Figure was modified from Allgöwer et al.[203] under CC BY 4.0, https://creativecommons.org/licenses/by/4.0/)

To further examine gene regulatory programs associated with carcinogenesis, bulk ATAC-sequencing of PDLOs was performed on days 3, 5, and 7 after Dox treatment. Principal component analysis (PCA) showed KRAS-dependent variance between the samples (**Figure 11A**). Moreover, the number of differently accessible regions drastically increases over time of Dox treatment when compared to the matching untreated samples, further pinpointing *KRAS*^{G12D}-dependent changes in chromatin

dynamics after only a few days (Figure 11B). When analyzing these differently accessible regions, Gene Ontology (GO) term analysis revealed the enrichment of several terms related to ECM remodeling and cell motility as well as inflammation, indicating the presence of *KRAS*^{G12D}-dependent niche preparatory programs within the PDLO model (Figure 11C).

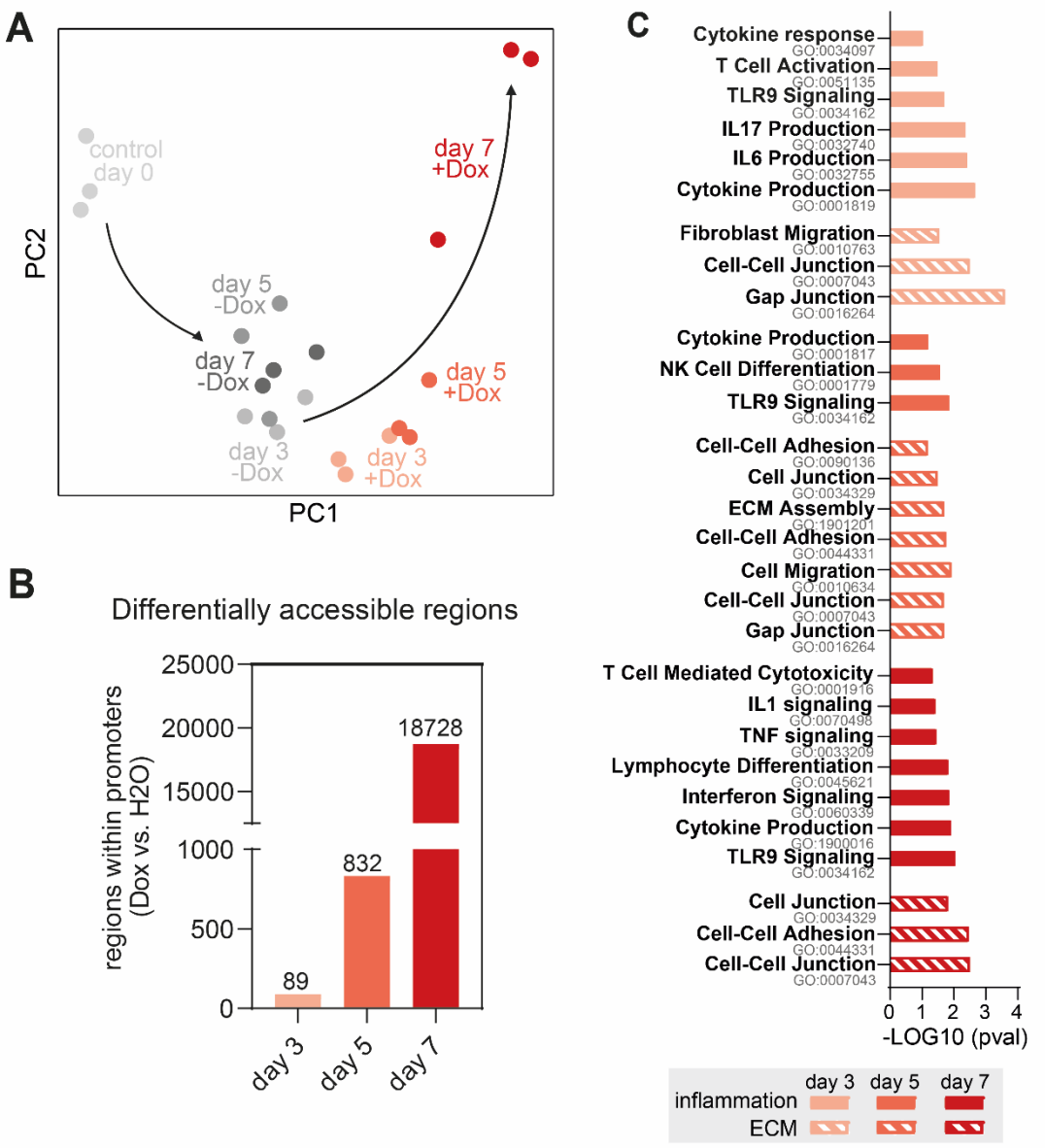

Figure 11 | ATAC-sequencing of PDLOs reveals KRAS-dependent changes in chromatin dynamics. (**A**) Principal component analysis (PCA) displaying the variance in chromatin accessibility between the different ATAC samples. (**B**) Number of differently accessible regions when comparing the Dox-treated samples to the time-matched untreated samples. (**C**) Gene ontology (GO) analysis of genes from differently accessible regions between the Dox-treated samples and the time-matched untreated samples. (Figure was modified from Allgöwer et al.[203] under CC BY 4.0, https://creativecommons.org/licenses/by/4.0/)

The gene signatures from Moffitt et al.[102], describing either the classical or basal tumor subtype, were then used to investigate whether the cells from the time-series scRNA-seq data set can be assigned to either of the two.

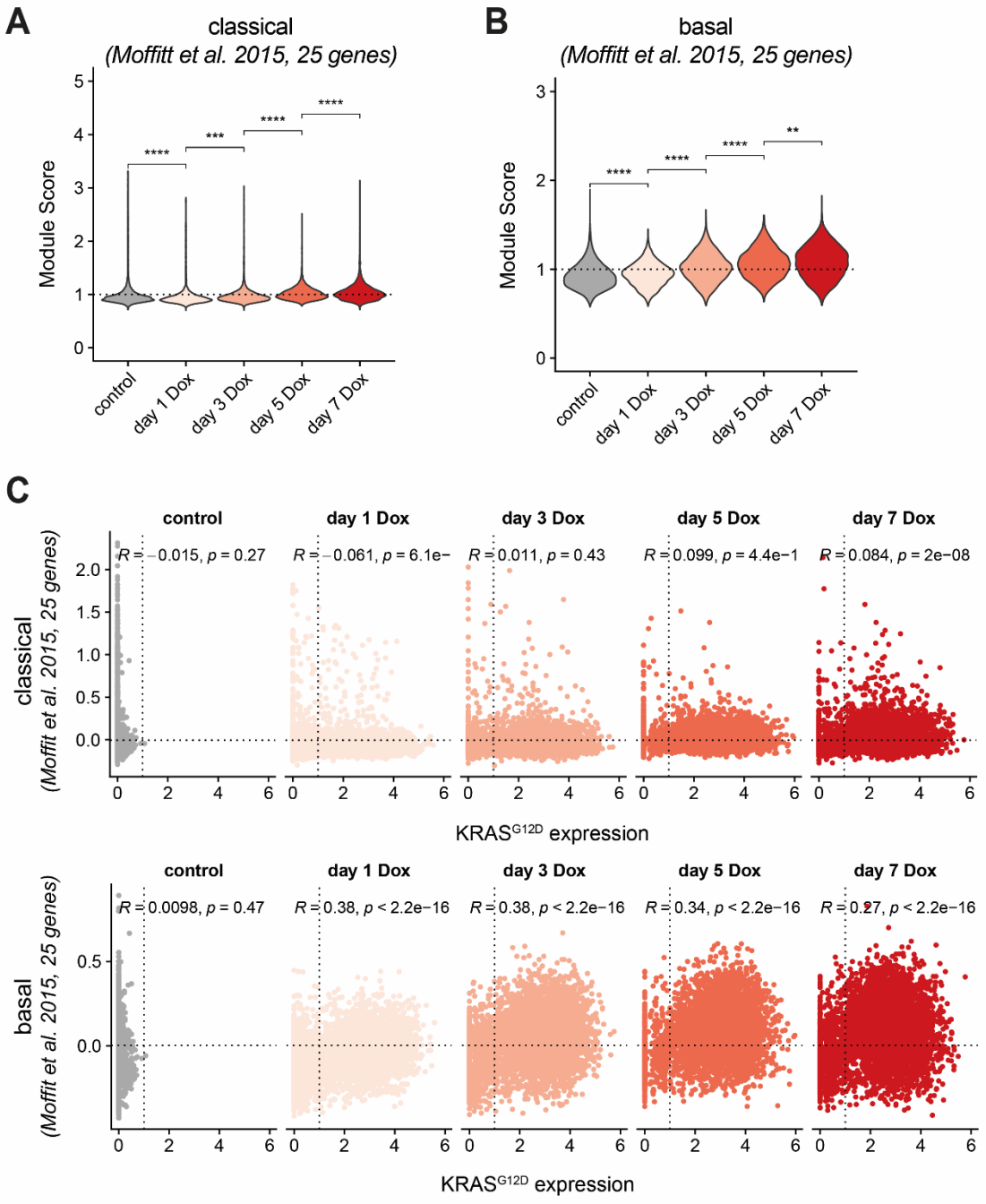

Figure 12 | KRAS^{G12D} expression correlates with the gene signature of basal tumors. (**A**) Module score of genes related to the classical PDAC subtype[102] in the different time points of Dox treatment. Unpaired t-test: ****, p<0.0001; ***, p<0.001. (**B**) Module score of genes related to the basal PDAC subtype[102] in the different time points of Dox treatment. Unpaired t-test: ****, p<0.0001; **, p<0.01. (**C**) Correlation of classical (top) and basal (bottom) genes and *KRAS^{G12D}* expression across different time points of Dox treatment. R = Pearson's correlation coefficient.

While few cells show strong expression of genes related to the classical signature, overall, more cells seem to be enriched for the basal signature (**Figure 12A-B**). This is also reflected by a stronger correlation of *KRAS^{G12D}* expression and the average expression of basal genes (**Figure 12C**).

3.2 KRAS^{G12D} induces niche-preparatory signatures

3.2.1 KRAS-dependent grouping of cells

To further investigate *KRAS^{G12D}*-dependent signatures within the PDLO model, the cells of the time-series scRNA-seq data set were grouped based on their KRAS^{G12D} expression employing k-means clustering (k = 3). The resulting three groups therefore showed different *KRAS^{G12D}* expression levels and were annotated accordingly: KRAS^{high}, KRAS^{intermediate,} and KRAS^{low} (**Figure 13A**). The KRAS^{low} group included cells with either no KRAS^{G12D} expression or very low KRAS^{G12D} expression and included cells from all time points (**Figure 13A-B**). This reflects the semi-stochastic integration of the KRAS^{G12D} transgene, resulting in cell-to-cell variability within the polyclonal cell line. The KRAS^{high} and KRAS^{intermediate} group included cells from all time points of Dox treatment. UMAPs showed that the KRAS^{low} cells mainly cluster apart from the KRAS^{high} cells, while the KRAS^{intermediate} group mostly overlaps with the KRAS^{high} (**Figure 13C**). Velocity analysis followed by partition-based graph abstraction (PAGA) construction, predicting developmental trajectories, revealed that the KRAS^{intermediate} group is not an intermediate cell state but independently arises from KRAS^{low}, in parallel to the KRAS^{high} group (**Figure 13D**). This can again be explained by the heterogenic integration of the KRAS^{G12D} transgene.

When identifying differently expressed genes (DEGs) between the groups, it became apparent that the differences between KRAS^{high} and KRAS^{intermediate} are very subtle. When comparing each group to both other groups, KRAS^{high} and KRAS^{intermediate} partially share the top DEGs (**Figure 13E**). No significant DEGs were found when directly comparing the two groups, and when comparing both to KRAS^{low}, the majority of DEGs overlapped (**Figure 13F**). The unique genes found in the comparison between KRAS^{high} vs. KRAS^{low}, which were not present when comparing KRAS^{intermediate} vs. KRAS^{low}, could be linked to enhanced KRAS signaling (e.g., MAPK and PI3K-Akt signaling). DEGs which were only found in the comparison

KRAS^{intermediate} vs KRAS^{low} but not in KRAS^{high} vs. KRAS^{low}, were related to cell-cell adhesion (**Figure 13F**).

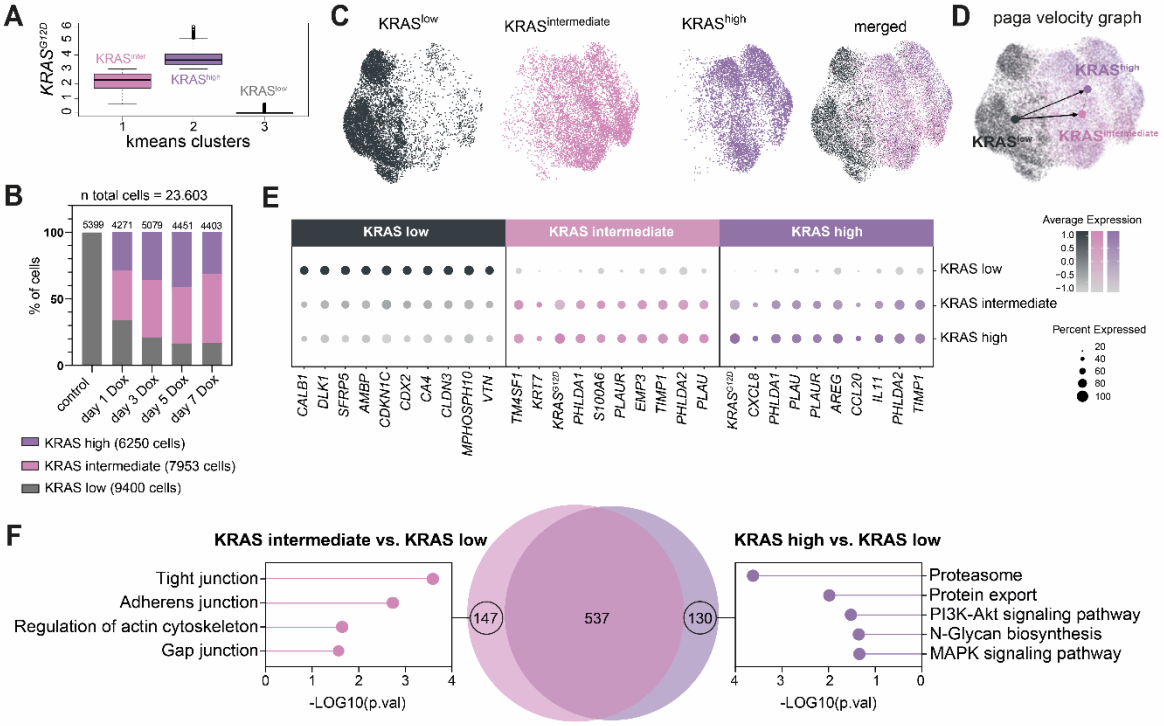

Figure 13 | KRAS-dependent grouping of cells. (**A**) KRAS^{G12D} expression levels of k-means clusters (k = 3) of cells from the time-series scRNA-seq data set are displayed as the median with corresponding extremes. (**B**) Proportions of the KRAS groups within the different time points. (**C**) UMAP of the k-means-based KRAS groups. (**D**) Partition-based graph abstraction (PAGA) graph showing the relation between the KRAS groups based on velocity. (**E**) Average expression of the top 10 differently expressed genes (DEGs) when comparing each group to both other groups. (**F**) Number of DEGs when comparing KRAS^{high} or KRAS^{intermediate} to KRAS^{low}, (unique and overlapping) with corresponding KEGG pathway analysis of the unique DEGs. (Figure was modified from Allgöwer et al.[203] under CC BY 4.0, https://creativecommons.org/licenses/by/4.0/)

3.2.2 *KRAS^{G12D}*-expressing PDLO transcriptome is clinically relevant

To assess whether the DEGs identified between the KRAS groups are relevant in advanced stages of the disease, PDAC patient data were analyzed. The top 50 DEGs from the comparisons KRAS^{high} vs. KRAS^{low} and KRAS^{intermediate} vs. KRAS^{low} were used as input to calculate gene set variance scores for RNA sequencing data of PDAC samples within The Cancer Genome Atlas (TCGA). Patients were then grouped based on these scores, revealing that survival was significantly reduced in the groups showing high enrichment of the PDLO-derived KRAS^{high} or KRAS^{intermediate} gene signatures (**Figure 14A**).

Further, it was of interest to assess how the PDLOs transcriptionally position within cells of healthy and PDAC tissue. Therefore, the PDLO cells from the time-series scRNA-seq data set were integrated with the cells from the data set of Peng et al.[201], consisting of 24 PDAC samples and 11 healthy samples. The resulting UMAP revealed that the PDLOs transcriptionally bridge healthy and malignant ducts in the human samples, with KRAS^{low} cells clustering in close proximity to the healthy duct, while KRAS^{intermediate} and KRAS^{high} cells were arranged closer to the malignant ductal cells of PDAC patients (**Figure 14B**).

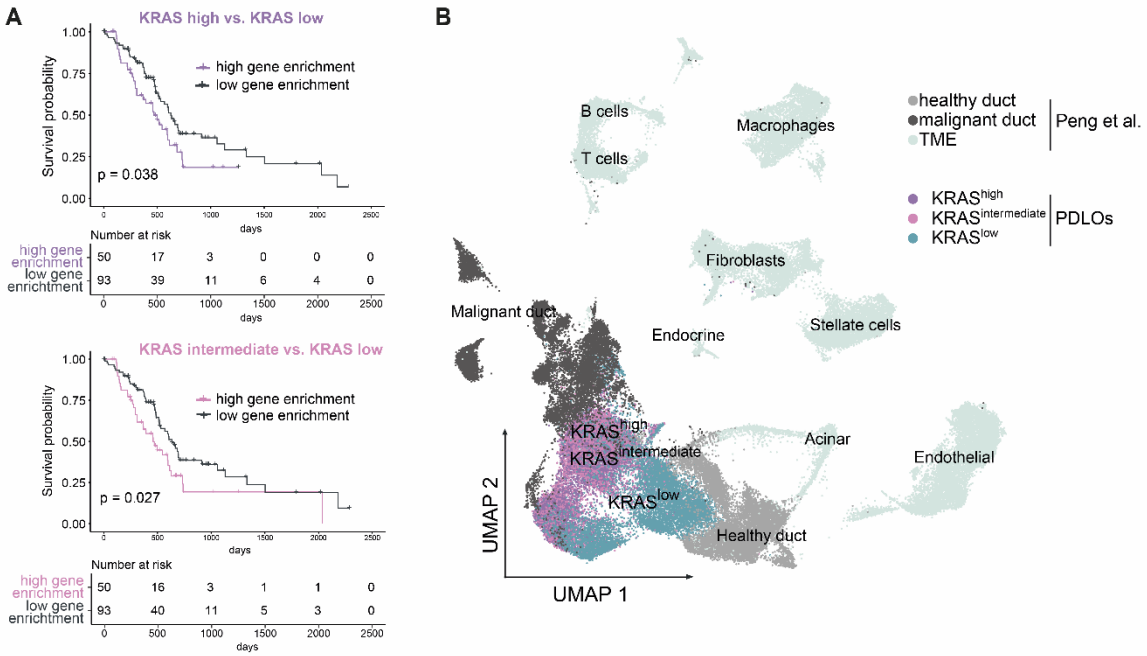

Figure 14 | *KRAS^{G12D}*-expressing PDLO transcriptome is clinically relevant. (**A**) Survival of TCGA-PAAD patients grouped by gene set variance of top 50 DEGs when comparing either KRAS^{high} vs. KRAS^{low} (top) or KRAS^{intermediate} vs. KRAS^{low} (bottom). P values were calculated using log-rank test. (**B**) UMAP of integrated time-series scRNAseq data set and the data set from Peng et al.[201] consisting of 24 PDAC samples and 11 healthy samples. (Figure was modified from Allgöwer et al.[203] under CC BY 4.0, https://creativecommons.org/licenses/by/4.0/)

3.2.3 KRAS^{G12D} induces ECM- and inflammation-related signaling

To gain a deeper understanding of the *KRAS^{G12D}*-dependent transcriptional changes occurring in the PDLO model, the DEGs identified when comparing either KRAS^{high} or KRAS^{intermediate} cells to the KRAS^{low} group were subjected to GO term analysis. Manually grouping the enriched GO terms into umbrella terms showed that altered gene expression of KRAS^{high} and KRAS^{intermediate} cells can be linked to essential cancer-related biological processes, such as metabolism, angiogenesis, and

proliferation (Figure 15A). Interestingly, a relevant proportion of GO terms were related to inflammation and extracellular matrix (ECM) remodeling. These terms included, for example, cytokine signaling and inflammatory response, as well as cell-matrix adhesion and cell motility (Figure 15B). Indeed, a variety of genes related to inflammation and ECM remodeling could be found to be dysregulated in the KRAS^{high} and KRAS^{intermediate} group (compared to KRAS^{low}), including cytokines, chemokines, collagens, interleukins, and integrins (Figure 15C). Several of these candidates were also upregulated in the proteome of Dox-treated PDLOs when compared with untreated PDLOs (Figure 15D).

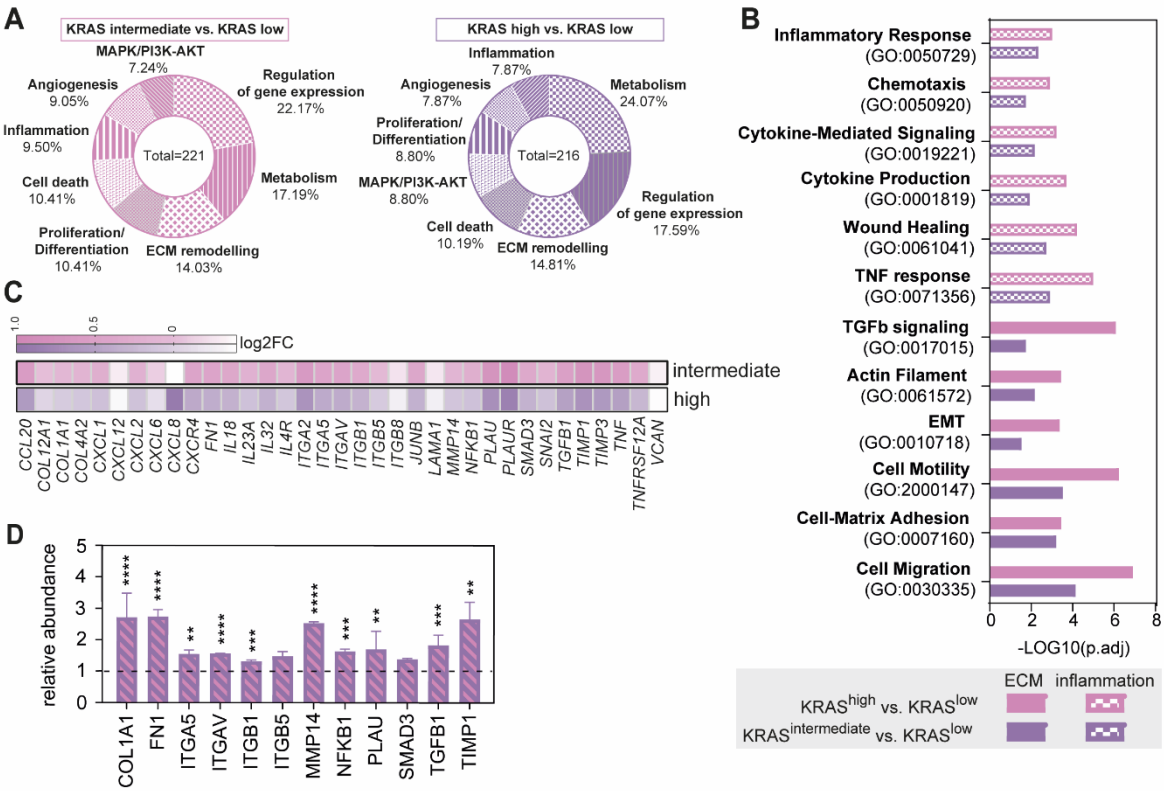

Figure 15 | KRAS^{G12D} induces ECM- and inflammation-related gene signatures. (**A**) Distribution of manually grouped GO terms enriched for DEGs of KRAS^{high} and KRAS^{intermediate} when compared to KRAS^{low}. (**B**) Significance of GO terms related to inflammation and ECM remodeling enriched in KRAS^{high} and KRAS^{intermediate} when compared to KRAS^{low}. (**C**) Log2 fold-change (log2FC) values of selectively chosen inflammation and ECM-related genes dysregulated in KRAS^{high} and KRAS^{intermediate} when compared to KRAS^{low}. (**D**) Relative abundance of proteins in PDLOs after 7 days of treatment compared to untreated PDLOs. Mean ± SD, n=1 in triplicates. Unpaired t-test **, p<0.01, ***, p<0.001; ****, p<0.0001. (Figure was modified from Allgöwer et al.[203] under CC BY 4.0, https://creativecommons.org/licenses/by/4.0/)

3.2.4 Deep learning identifies KRAS classifier signature

Using a deep learning algorithm, a gene signature was defined, allowing the prediction of whether a cell is of $KRAS^{high}$, $KRAS^{intermediate,}$ or $KRAS^{low}$ identity. Although the $KRAS^{high}$ and $KRAS^{intermediate}$ cells showed remarkable similarity regarding DEGs, the deep learning approach could correctly predict the cell identity within the time-series scRNA-seq data set with over 95% accuracy for all three groups (**Figure 16A**). The top 5 % of predictive genes (n =1,452 genes) are further referred to as deep learning classifiers or classifier signature. Within this classifier signature, genes relevant to pancreatic development and maturation, such as *PDX1, ONECUT1*, and *CFTR*, mainly correlated with the $KRAS^{low}$ group, while several cytokines and ECM-related genes (e.g., *CXCL8, ITGAV, TNF, TGFB1* and *IL32*) correlated with the $KRAS^{intermediate}$ and $KRAS^{high}$ group (**Figure 16B**). However, to accurately predict cell identity, the entire signature is needed, and classification cannot be restricted to single genes.

To test the classifier signature outside of the PDLO model, the data set from Peng et al.[201] was used. Therefore, the patient samples, using only the ductal cells, were grouped based on the expression of the 1,452 classifier genes using k-means clustering (k = 3). The deep learning classifiers robustly grouped all healthy samples into a single group, while the tumor samples were distributed across the remaining two groups (**Figure 17A**). Based on *KRAS* expression, the three groups were then annotated as high, intermediate, or low (**Figure 17B**). The samples annotated as intermediate and high showed a gradual increase in malignant ductal cells, while healthy ductal and endothelial cells were lost (**Figure 17C**). Interestingly, an increase in stromal and immune cells could be observed in the high and intermediate groups. Moreover, the samples from the high group showed greater tumor dedifferentiation, perineural invasion, and significantly greater vascular invasion than those from the intermediate group (**Figure 17D**). Cell-cell communication additionally revealed a gradual increase in interaction strength for the individual cell types across the different KRAS groups (**Figure 17E**).

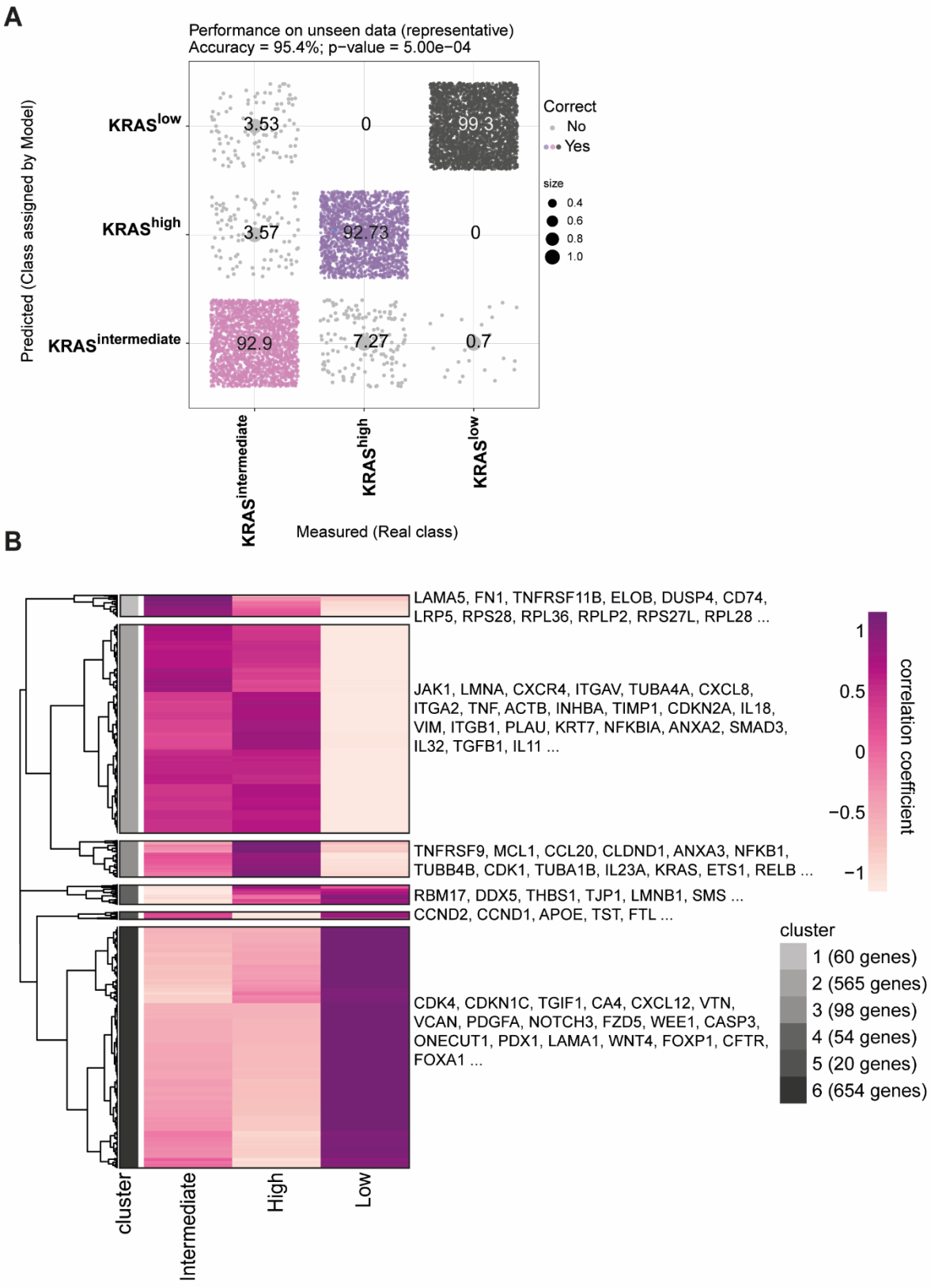

Figure 16 | Deep learning identifies classifier genes accurately predicting KRAS group identity. (**A**) Confusion matrix showing the predicted and actual classifications of KRAS groups on the validation data set (35% of the entire data set). (**B**) Correlation coefficients of the top 5 % predictive genes (n = 1,452) for the KRAS groups. (*Figure was modified from Allgöwer et al.*[203] *under CC BY 4.0, https://creativecommons.org/licenses/by/4.0/)*

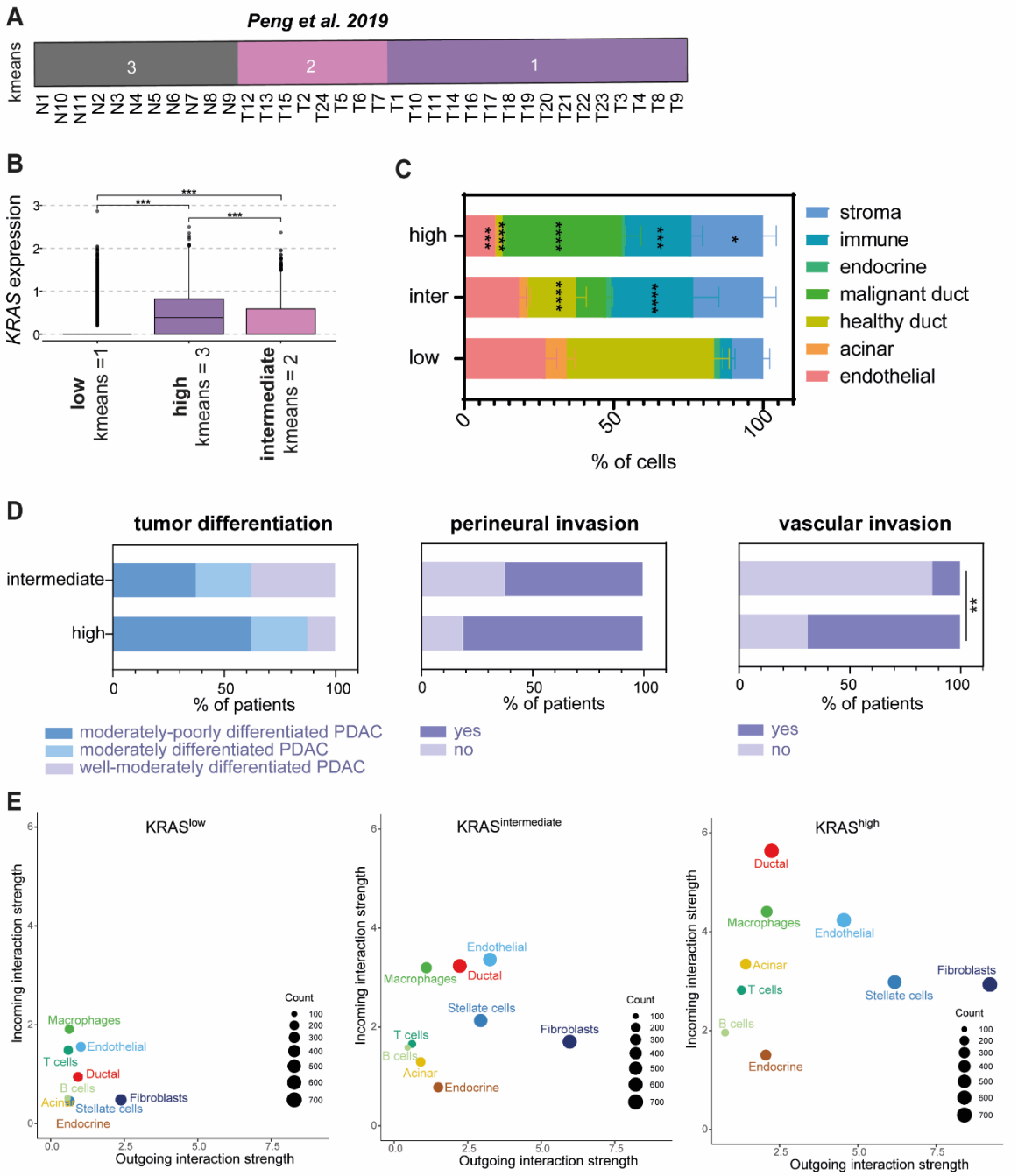

Figure 17 | Grouping of PDAC patients based on deep learning classifiers. (**A**) Samples from Peng et al.[201] (N= healthy, T= tumor) were grouped based on deep learning classifiers using k-means clustering (k = 3). (**B**) KRAS expression of samples from Peng et al. grouped by k-means based on deep learning classifiers. Wilcoxon test ***, p<0.0001. (**C**) Proportions of different cell-types in the grouped samples from Peng et al.[201] Two-way ANOVA: *, p<0.05; ***, p<0.001; ****, p<0.0005. (**D**) Tumor differentiation (left), perineural invasion (middle), and vascular invasion (right) of PDAC samples from Peng et al.[201] grouped by k-means based on KRAS deep learning classifiers. Chi-square test **, p<0.01. (**E**) Incoming and outgoing interaction strength of different cell types in the grouped samples from Peng et al.[201]. (Figure was modified from Allgöwer et al.[203] under CC BY 4.0, https://creativecommons.org/licenses/by/4.0/)

3.3 KRAS^{G12D} induces T cell shielding and activates PaSCs *in vitro*

The time-series scRNA-seq data set showed enrichment of inflammation- and ECM-related signatures in *KRAS^{G12D}*-expressing PDLOs, indicating that KRAS^{G12D} may modulate the surrounding tissue at a very early stage, thereby preparing a "pre-tumor niche" and creating favorable conditions for cancerogenesis. To validate this *in vitro*, different co-culture platforms were used to investigate the impact of *KRAS^{G12D}*-expressing PDLOs on T cells and pancreatic stellate cells (PaSCs). The co-culture experiments were conducted with a polyclonal KRAS^{G12D} line, and the cultures therefore included PDLO cells of all previously defined KRAS groups (KRAS^{low}, KRAS^{intermediate}, and KRAS^{high}).

3.3.1 KRAS^{G12D} reduced T cell infiltration and migration

Employing the previously established Interaction with Organoid-in-MatriX (InterOMaX) platform[202], the infiltration of healthy PBMC-derived T cells towards matrix-embedded PDLOs with or without Dox treatment was observed. Significantly fewer T cells were found infiltrating the Dox-treated organoids compared to the untreated PDLOs (**Figure 18A**). A similar "shielding" effect could be recognized when employing a cancer-on-chip system[204], where T cells were perfused via a microfluid channel (**Figure 18B**).

To investigate whether direct cell-cell contact is necessary to achieve this shielding effect or if the *KRAS^{G12D}*-derived secretome is sufficient to drive reduced T cell migration, Transwell® assays were performed. Here, it could be observed that fewer T cells migrate towards the conditioned media of Dox-treated PDLOs compared to the conditioned media of untreated PDLOs (**Figure 18C**). Moreover, no differences in migration were found for the conditioned media of parental PDLOs, which were either treated with Dox or not, thereby excluding an impact of the Dox treatment itself.

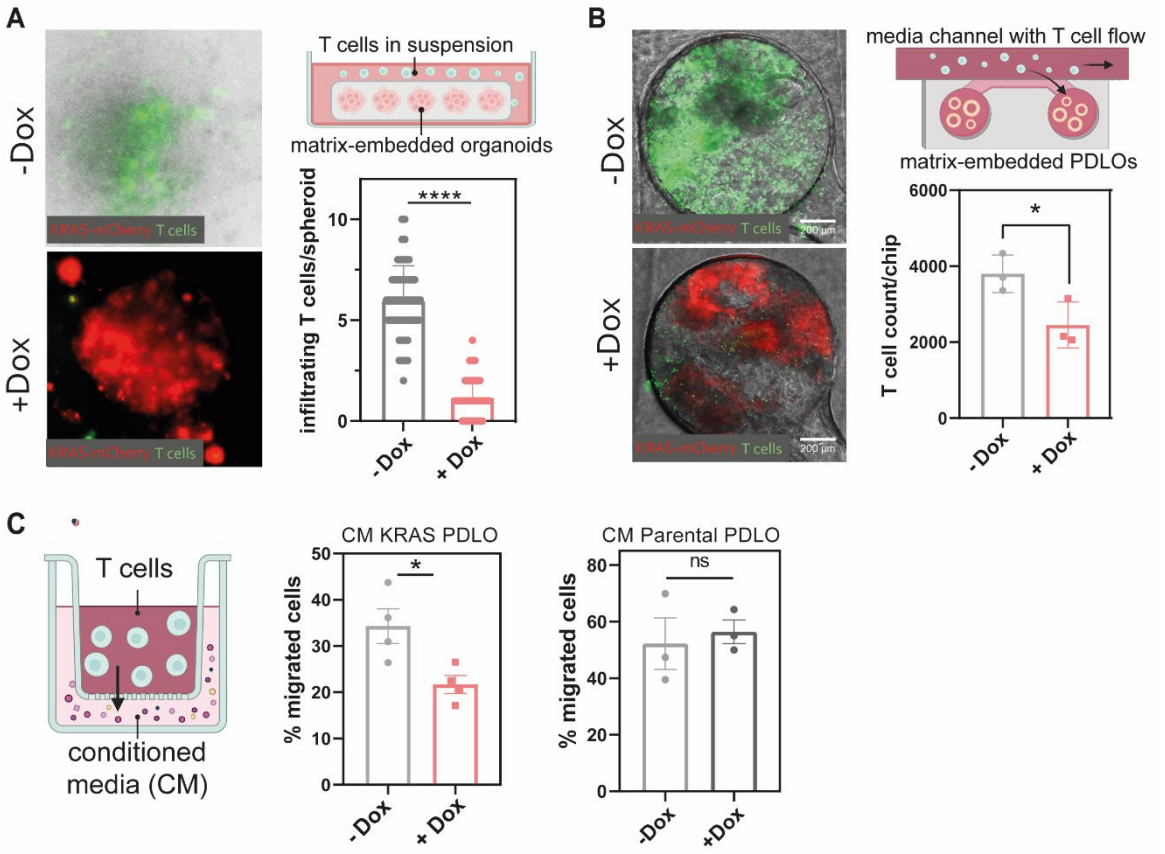

Figure 18 | *KRAS*^{G12D}-expression in PDLOs reduces T cell infiltration and migration. (**A**) Representative images and corresponding quantification of healthy PBMC-derived T cells infiltrating matrix-embedded organoids after 72 h of co-culture. Mean ± standard deviation (SD) of 3 independent experiments, including a total of 5 different T cell donors. Unpaired t-test ****, p<0.0001. (**B**) Representative images and corresponding quantification of healthy PBMC-derived T cells infiltrating matrix-embedded PDLOs via a microfluid channel. Mean ± SD, n=1 with 3 chips/condition. Scale bar = 200 µm. (**C**) Proportion of T cells that migrated towards PDLO-derived conditioned media. Mean ± standard error of mean (SEM) of 4 independent experiments. Unpaired t-test *, p<0.05. (Schemes of co-culture systems were created with BioRender.com and figure was modified from Allgöwer et al.[203] under CC BY 4.0, https://creativecommons.org/licenses/by/4.0/)

As the *KRAS*^{G12D}-induced secretome sufficiently reduced T cell migration, healthy PBMC-derived T cells were cultured in PDLO-derived conditioned media and analyzed by flow cytometry to assess whether differences in T cell subtypes could be observed. However, no differences in the proportions of CD4+ or CD8+ cells were found between the T cells cultured in conditioned media derived from Dox-treated PDLOs compared to conditioned media from the untreated PDLOs (**Figure 19A**). Furthermore, the T cells did not show changes in viability (**Figure 19B**), exhaustion, or activation (**Figure 19C**).

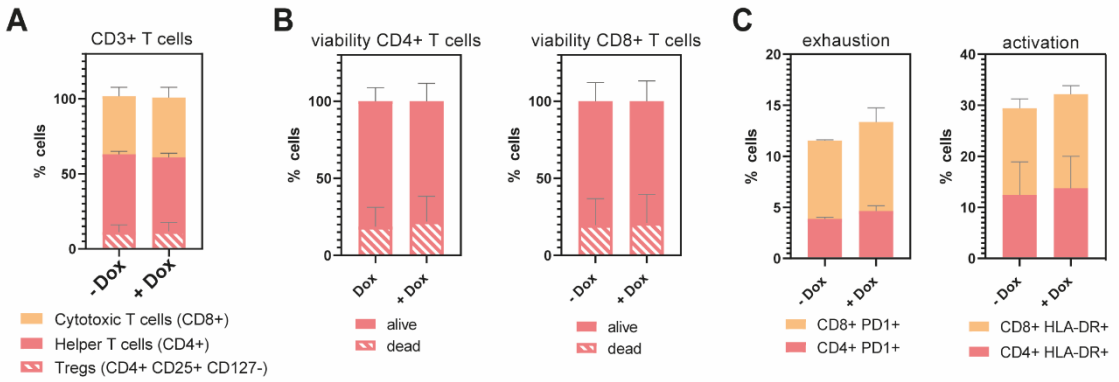

Figure 19 | Conditioned medium from *KRAS*^{G12D}-expressing PDLOs does not alter T cell subtypes. (**A**) Proportions of CD8+ and CD4+ T cells after culturing in PDLO-derived conditioned media for 72 h, analyzed by flow cytometry. Mean ± SD, n=2. (**B**) Viability of CD4+ and CD8+ T cell subsets after culturing in PDLO-derived conditioned media for 72 h, analyzed by flow cytometry. Mean ± SD, n=2. (**C**) Proportions of activated or exhausted CD4+ and CD8+ T cells after culturing in PDLO-derived conditioned media for 72 h, analyzed by flow cytometry. Mean ± SD, n=2. (Figure was modified from Allgöwer et al.[203] under CC BY 4.0, https://creativecommons.org/licenses/by/4.0/)

3.3.2 KRAS^{G12D} activates human pancreatic stellate cells (PaSCs)

Activated PaSCs are omnipresent throughout tumor evolution in PDAC, play a pivotal role in carcinogenesis, and are described as a major source of CAFs.[76–79] As the time-series scRNA-seq data set revealed ECM remodeling signatures upon KRAS^{G12D} expression, it was therefore assessed whether *KRAS*^{G12D}-expressing PDLOs are capable of activating PaSCs.

When directly co-culturing PDLOs with PaSCs, no differences were observed within the first 48 h. However, after 60 h, PaSCs in the presence of Dox-treated PDLOs displayed an altered growth behavior compared to PaSCs co-cultured with untreated PDLOs (**Figure 20A-B**). The PaSCs expanded over a greater area, indicating increased activation and proliferation in the presence of *KRAS*^{G12D}-expressing PDLOs. When co-culturing PaSCs with parental PDLOs, no differences were observed between untreated and Dox-treated conditions (**Figure 20C**).

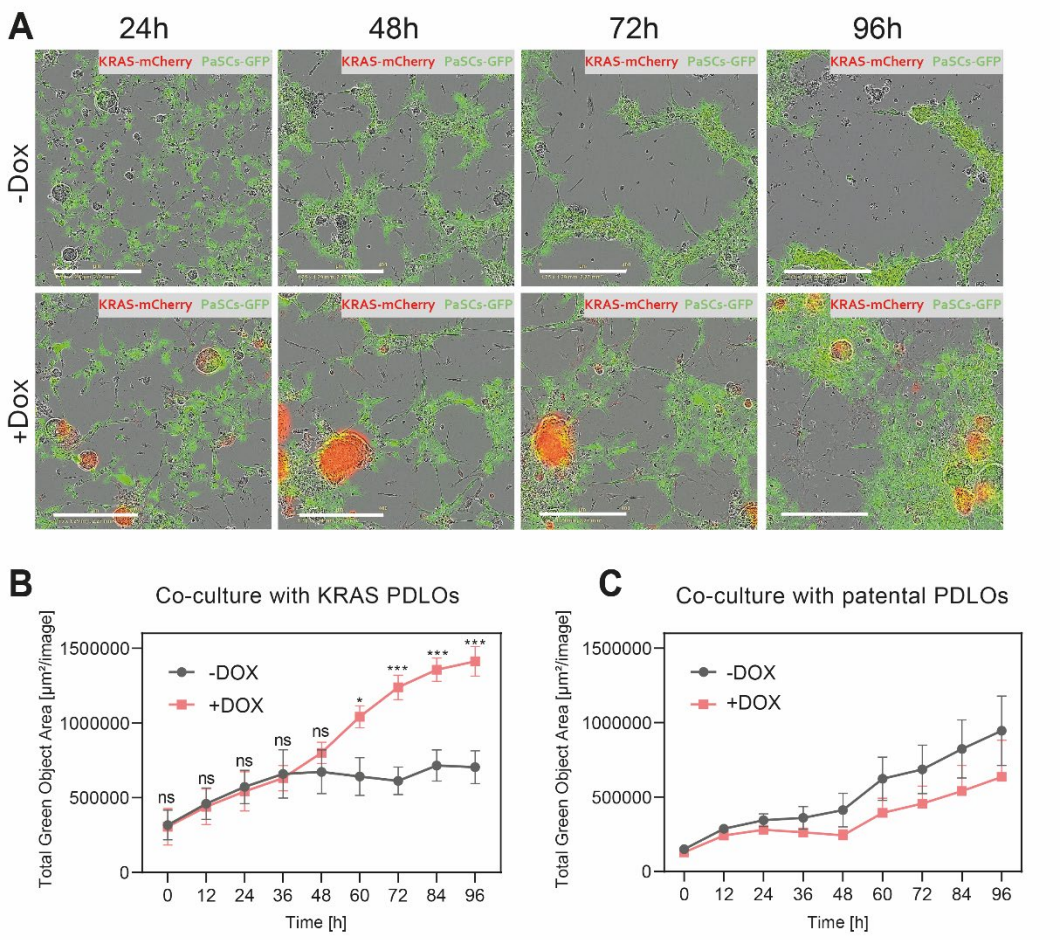

Figure 20 | *KRAS*^{G12D}-expressing PDLOs induce proliferation of PaSCs. (A) Representative images of GFP-labeled PaSCs co-cultured with KRAS-PDLOs captured by live-cell imaging. Scale bar = 400 µm. (**B**) Total green area of GFP-labeled PaSCs co-cultured with KRAS-PDLOs captured by live-cell imaging. Mean ± SEM, n=3. Unpaired t-test ***, p<0.001; ****, p<0.0001. (**C**) Total green area of GFP-labeled PaSCs co-cultured with parental PDLOs captured by live-cell imaging. Mean ± SEM, n=3. (Figure was modified from Allgöwer et al.[203] under CC BY 4.0, https://creativecommons.org/licenses/by/4.0/)

To investigate whether *KRAS*^{G12D}-expressing PDLOs additionally influence CAF polarization of PaSCs, the expression of canonical CAF markers was assessed. An indirect co-culturing format was used, in which bidirectional crosstalk between PDLOs and PaSCs occurs without direct cell-cell contact, allowing separate analysis of the PaSCs. Here, PaSCs co-cultured with Dox-treated PDLOs displayed the most substantial increase in expression for *ACTA2* (myCAF marker) and *CXCL2* (iCAF marker), however, also showing increased expression for the other markers used (**Figure 21A**). When culturing PaSCs in PDLO-derived conditioned media, a similar trend was observed, showing upregulation of both myCAF and iCAF markers when exposed to the secretome of *KRAS*^{G12D}-expressing PDLOs (**Figure 21B**). However, relative expression levels were overall lower than in the indirect co-

culturing format, indicating that bidirectional crosstalk enhances CAF differentiation to a greater extent. Relevant upregulation of CAF marker expression was not observed when using conditioned media from parental PDLOs, thereby underpinning a KRAS-dependent effect rather than a Dox-dependent effect on CAF differentiation. A significant increase of αSMA (*ACTA2*) could also be found on protein level for PaSCs cultured in the *KRAS*^{G12D}-derived secretome, accompanied by a slight increase in IL6 (**Figure 21C**). In summary, KRAS^{G12D}-expressing PDLOs do not seem to direct PaSCs towards a specific CAF subpopulation (myCAF or iCAF), but instead induce global CAF polarization.

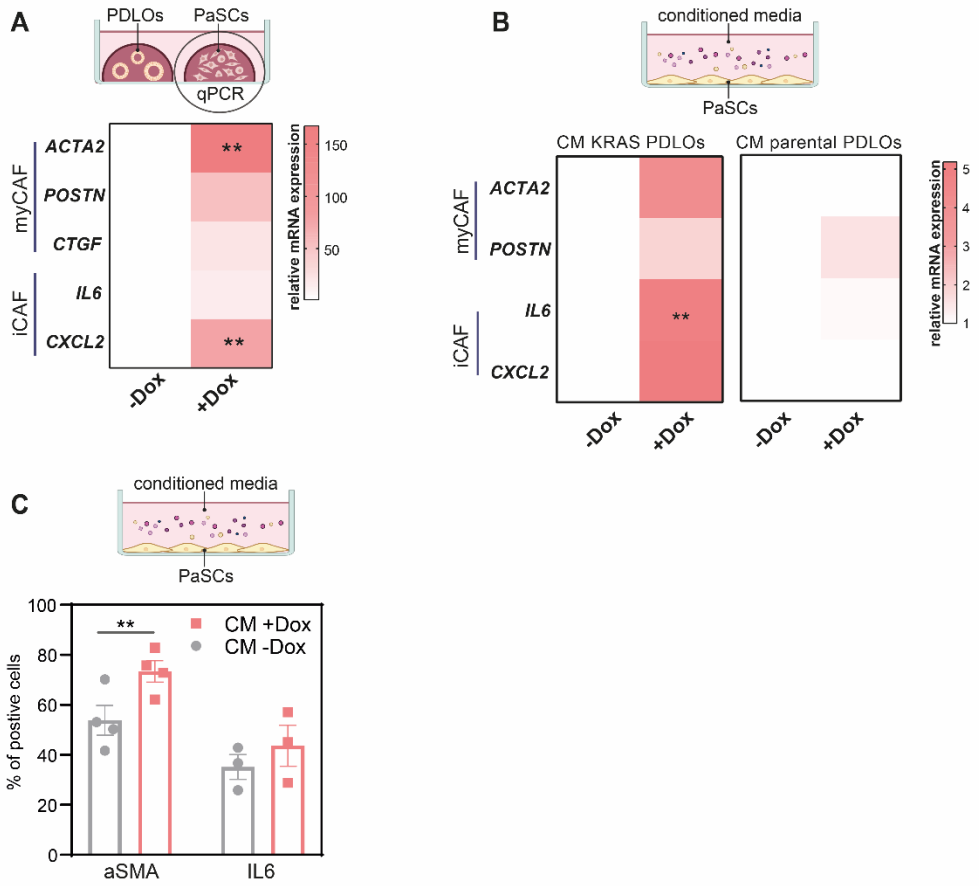

Figure 21 | *KRAS*^{G12D}-expressing PDLOs induce CAF polarization of PaSCs. (**A**) Gene expression of canonical CAF markers in PaSCs after 72h of indirect co-culture with PDLOs. The mRNA levels are shown relative to the untreated (-Dox) condition after normalization to GAPDH was performed. Mean, n=3, unpaired t-test**, p<0.01. (**B**) Gene expression of canonical CAF markers in PaSCs after culturing in PDLO-derived conditioned media (CM) for 72 h. The mRNA levels are shown relative to the untreated (-Dox) condition after normalization to GAPDH was performed. Mean, n=3, unpaired t-test**, p<0.01. (**C**) Proportions of aSMA+ and IL6+ PaSCs after culturing in PDLO-derived conditioned media (CM) for 72 h, analyzed by flow cytometry. Mean ± SEM, n=4 for aSMA, n=3 for IL6, unpaired t-test **, p<0.01. (Schemes of co-culture systems were created with BioRender.com and figure was modified from Allgöwer et al.[203] under CC BY 4.0, https://creativecommons.org/licenses/by/4.0/)

3.4 TNFα as a potential *KRAS^{G12D}*-dependent mediator of niche preparation

3.4.1 Cell-cell communication analysis predicts TNFα as a potential candidate for *KRAS^{G12D}*-dependent niche modelling

To pinpoint potential *KRAS^{G12D}*-dependent signaling pathways involved in inducing T cell shielding and PaSC activation *in vitro*, the PDLO cells from the time-series scRNA-seq data set were merged with publicly available data sets. This allowed the prediction of cell-cell communication patterns *in silico*.

To investigate interactions between PDLOs and healthy, pre-cancerous niche cells, the data set from Carpenter et al. was used.[65] This scRNA-seq data set was generated from healthy pancreatic tissue from 6 donors, of which 4 harbored sporadic, low-grade PanIN lesions. Cell-cell communication analysis of the merged data sets revealed that the overall interaction strength (outgoing and incoming) was highest in PDLOs, whereas the incoming interaction strength was most pronounced in KRAS^{high} and KRAS^{intermediate} PDLOs (**Figure 22A**). Interestingly, cells derived from healthy donors with PanIN lesions also showed increased interaction strength compared with the respective cell types from donors without lesions. Within the outgoing signaling patterns, the TNF and TGFβ pathway are predicted to be sourced from KRAS^{high} and KRAS^{intermediate}, but not from KRAS^{low}, while incoming signaling patterns show that KRAS^{high} and KRAS^{intermediate} seem to be more prone for ECM-related pathways such as the COLLAGEN, THBS, and FN1 pathways (**Figure 22B**).

Analyzing the TNF pathway network in more detail showed that KRAS^{high} and KRAS^{intermediate}, but not KRAS^{low}, are predicted to be the source of TNF signaling (sender, ligand source) but also mediate TNF signaling between other cell types (mediator; **Figure 22C**). Most cell types within the data set are predicted to be receivers (receptor source) of TNF signaling. A similar pattern is observed when obtaining the interaction strengths of the ligand-receptor pair *TNF-TNFRSF1A* (**Figure 22D**). KRAS^{high} and KRAS^{intermediate} (as well as macrophages) are depicted as a ligand source, while most other cell types seem to be receivers via the *TNFRSF1A* receptor. Interestingly, T cells from healthy donors without PanIN lesions were not predicted to be involved in the TNF signaling axis. In contrast, T cells from healthy donors with PanIN lesions are expected to be recipients of TNF signaling.

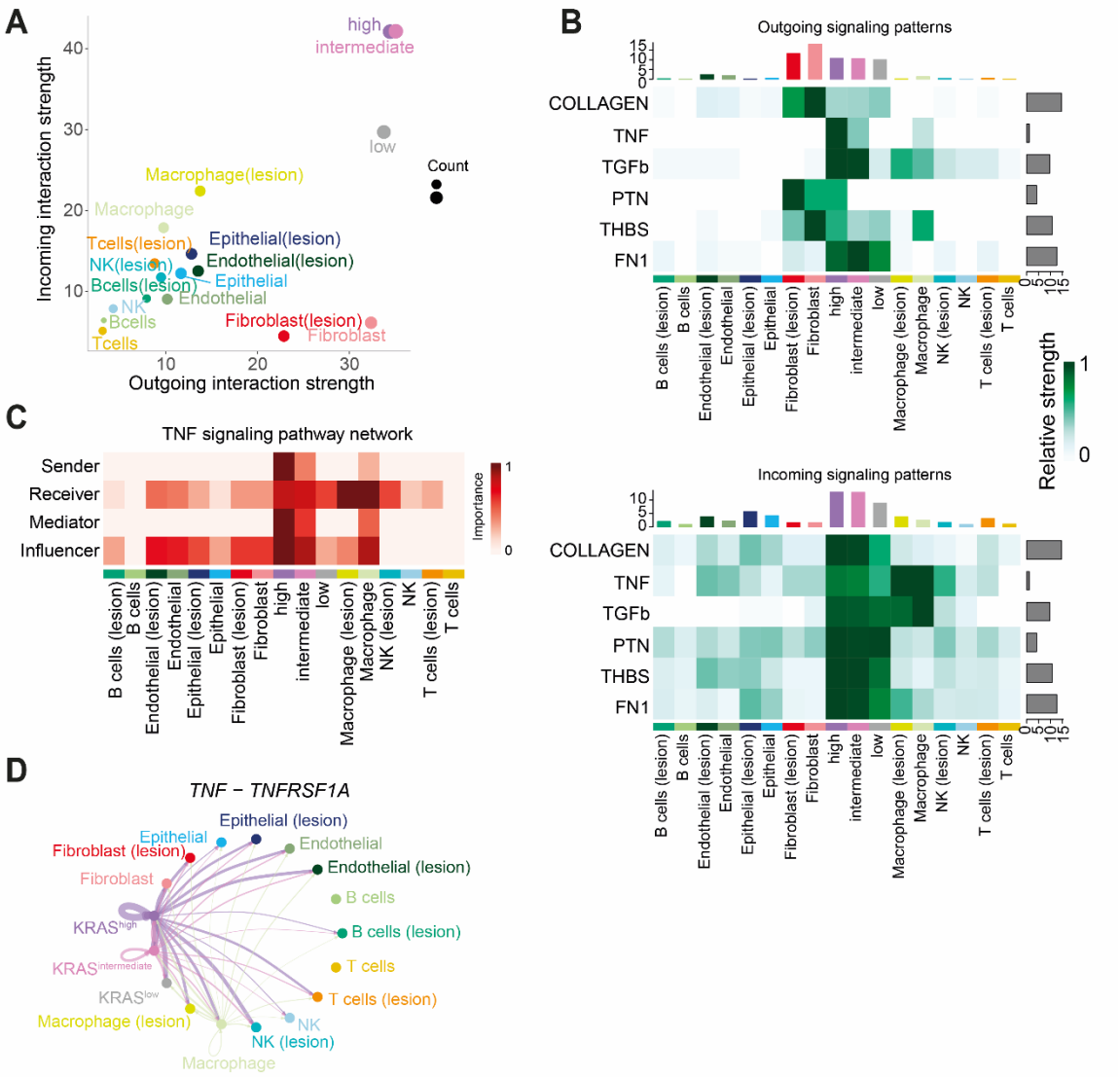

Figure 22 | Cell-cell communication analysis within the healthy niche. (**A**) Predicted outgoing and incoming interaction strengths of PDLOs and different cell types derived from healthy pancreatic tissue[65] with and without PanIN lesions. (**B**) Outgoing (top) and incoming (bottom) signaling patterns of selected pathways in PDLOs and different cell types derived from healthy pancreatic tissue[65] with and without PanIN lesions. (**C**) The role of PDLOs and different cell types derived from healthy pancreatic tissue[65] with and without PanIN lesions in the TNF signaling network. (**D**) Predicted interaction strength and directionality of the ligand-receptor pair TNF-TNFRSF1A in PDLOs and different cell types derived from healthy pancreatic tissue[65] with and without PanIN lesions. (Figure was modified from Allgöwer et al.[203] under CC BY 4.0, https://creativecommons.org/licenses/by/4.0/)

To investigate potential communication patterns of PDLOs within the TME of PDAC tissue, PDLOs were combined with the data set from Peng et al.[201] *in silico*. Remarkably, KRAS^{high} and KRAS^{intermediate} cells show interaction strengths similar to those of the malignant ductal cells (**Figure 23A**). The PDLO cells of KRAS^{high} and KRAS^{intermediate} showed stronger outgoing signaling for pathways such as IL6 and TGFβ compared to KRAS^{low}, while being more prone to respond to COLLAGEN and FN1 (**Figure 23B**). As observed in the analysis of the healthy niche, the TNF pathway was predicted to be an outgoing signal for KRAS^{high} and KRAS^{intermediate}, but not for KRAS^{low}.

The PDLO cells of KRAS^{high} and KRAS^{intermediate} were identified as a unique TNF ligand source (sender), while also having direct (mediator) or indirect (influencer) impact on TNF signaling between other cell types (**Figure 23C**). In contrast to the cell types of the healthy niche, the TME cells of PDAC tissue are predicted to receive TNF signaling not only via the *TNFRSF1A* receptor. T cells, for example, appear to respond exclusively via the *TNFRSF1B* receptor (**Figure 23D**).

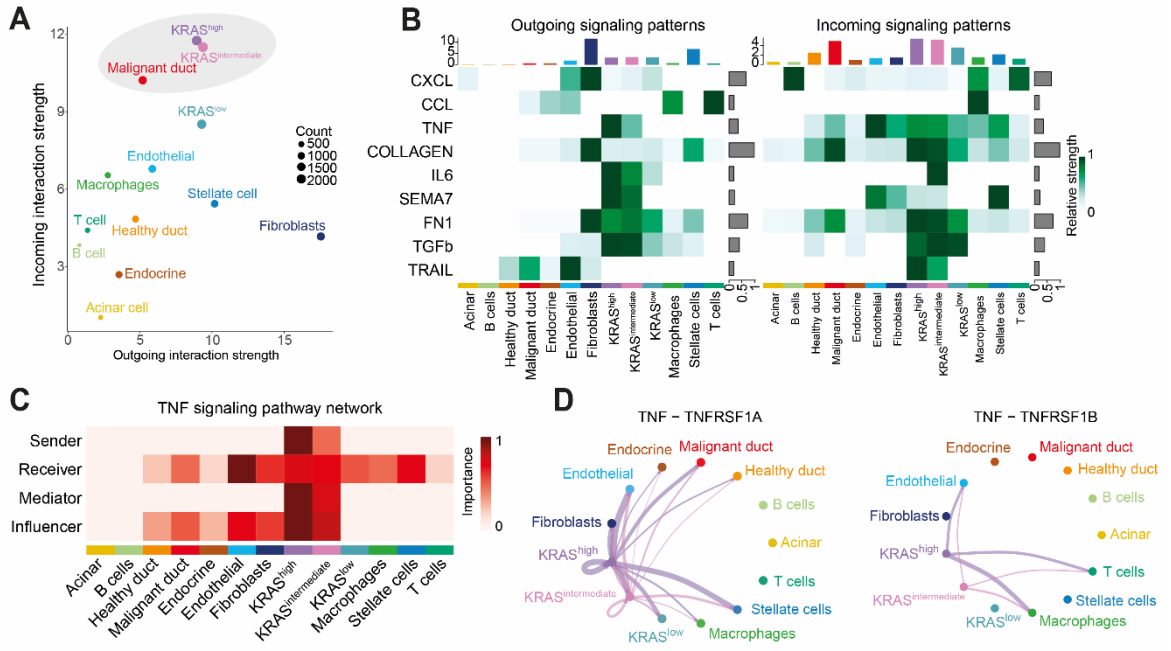

Figure 23 | Cell-cell communication analysis within the PDAC TME. (**A**) Predicted outgoing and incoming interaction strengths of PDLOs and cell types of the PDAC TME.[201] (**B**) Outgoing (left) and incoming (right) signaling patterns of selected pathways in PDLOs and different cell types of the PDAC TME.[201] (**C**) The role of PDLOs and cell types of the PDAC TME[201] in the TNF signaling network. (**D**) Predicted interaction strength and directionality of the ligand-receptor pairs TNF-TNFRSF1A (left) and TNF-TNFRSF1B (right) in PDLOs and cell types of the PDAC TME.[201] (Figure was modified from Allgöwer et al.[203] under CC BY 4.0, https://creativecommons.org/licenses/by/4.0/)

Focusing on communication patterns between *KRAS*^{G12D}-expressing organoids and T cells as well as stromal cells (stellate cells and fibroblasts), ligand-receptor pairs were filtered to be predicted uniquely sourced from KRAS^{high} and KRAS^{intermediate} but not from KRAS^{low} PDLO cells. For the analysis with the healthy data set (**Figure 24A**) as well as the analysis with the PDAC TME cells (**Figure 24B**), several ECM-related ligand-receptor pairs were identified in this context, including, for example, *COL1A1* or *COL6A1*-(*ITGA1* + *ITGB1*) or *THBS4-CD47*. Interestingly, several ligand-receptor pairs overlapped between the analysis of healthy and PDAC cells, including *PTN-SDC2*, *SEMA7A*-(*ITGA1* + *ITGB1*), *SPP1- CD44* and *TNF-TNFRSF1A*.

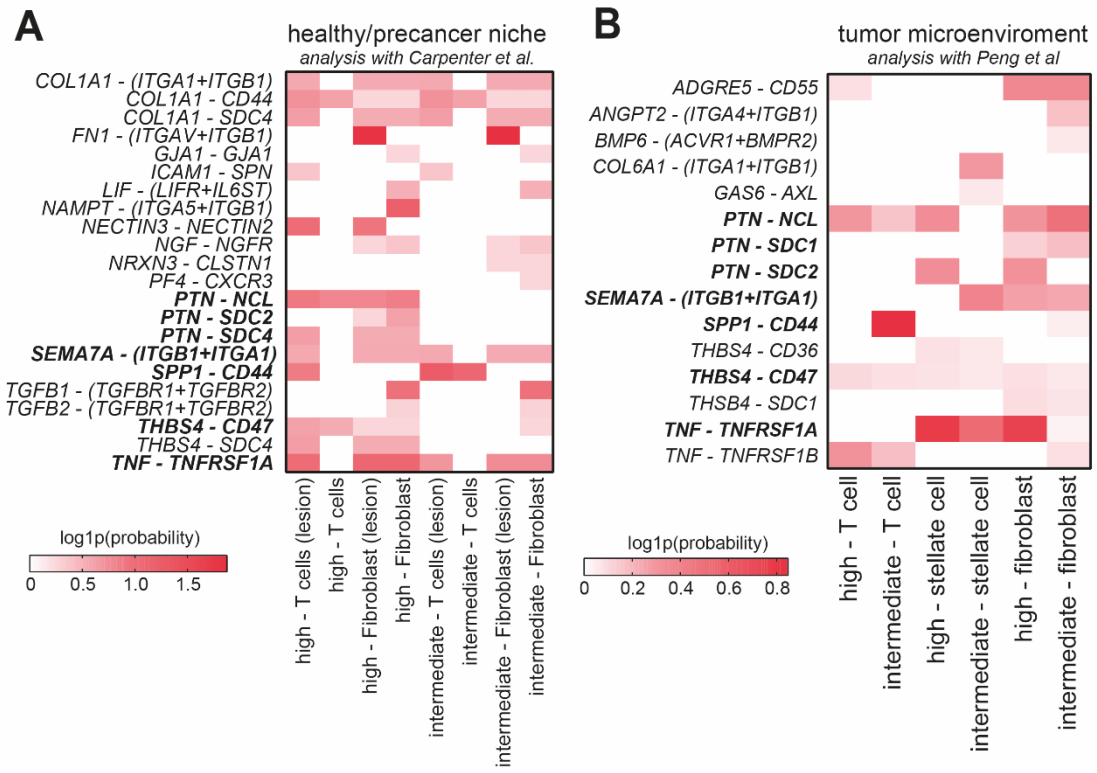

Figure 24 | Unique ligand-receptor pairs sourced from *KRAS*^{G12D}-expressing PDLOs. Interaction probability of ligand-receptor (LR) pairs between PDLOs and T cells or stromal cells (fibroblasts and stellate cells) derived from (**A**) healthy pancreatic tissue[65] or (**B**) PDAC samples[201]. Ligand-receptor pairs were filtered to be predicted in KRAS^{high} and KRAS^{intermediate}, but not in KRAS^{low} cells, and overlapping pairs between both analyses are highlighted in bold. (Figure was modified from Allgöwer et al.[203] under CC BY 4.0, https://creativecommons.org/licenses/by/4.0/)

3.4.2 TNFα is upregulated in *KRAS*^{G12D}-expressing PDLOs and is involved in T cell shielding and PaSC activation

As TNF was predicted to be a potential central candidate in *KRAS*^{G12D}-dependent modulation of niche cells, TNF expression in PDLOs was investigated in greater detail. Indeed, a gradual increase of TNF expression upon Dox treatment was observed in the time-series scRNA-seq data set (**Figure 25A**). Expression of genes related to TNF signaling (via NFκB) could also be directly correlated with KRAS^{G12D} expression within the PDLOs (**Figure 25B**). This was further confirmed by Gene Set Enrichment Analysis (GSEA), showing that the DEGs, which were upregulated in the Dox-treated samples (compared to the untreated control) were enriched within the HALLMARK_TNFA_SIGNALING_VIA_NFKB gene set (**Figure 25C**). Several of these enriched genes found in the scRNA-seq data also showed increased chromatin accessibility (**Figure 25D**).

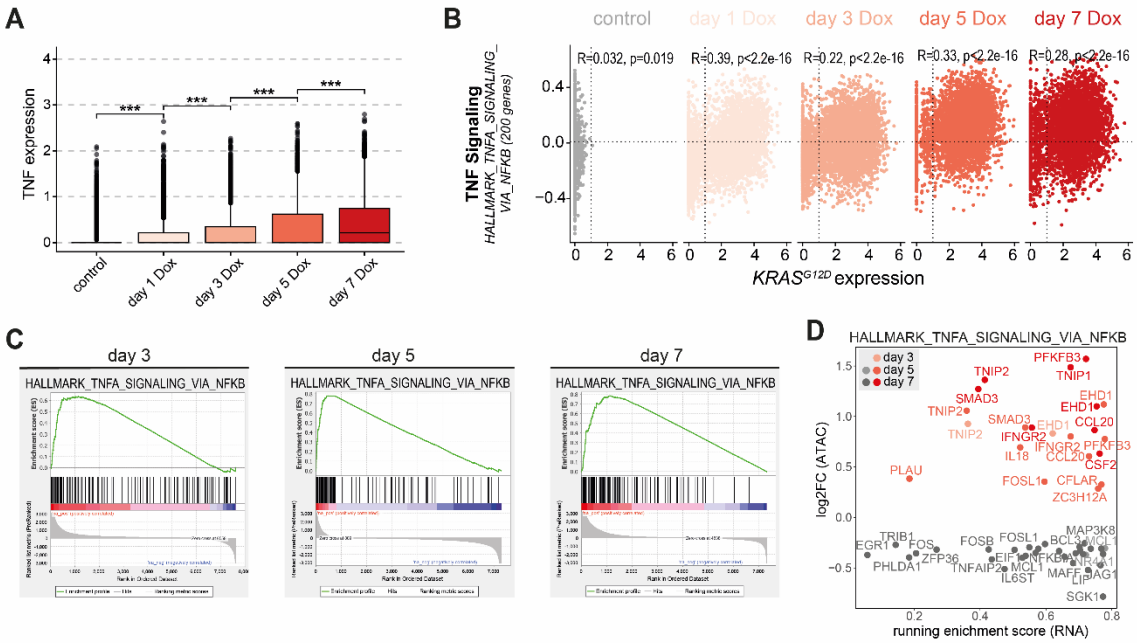

Figure 25 | *KRAS*^{G12D}-dependent TNF signaling in PDLOs. (**A**) TNF gene expression in the time-series scRNA-seq data set over the time of Dox treatment. Wilcoxon test ***, p<0.001. (**B**) Correlation between KRAS^{G12D} expression and module scores of TNF signaling-related genes in the time-series scRNA-seq data set over the time of Dox treatment. (**C**) Gene set enrichment of pre-ranked DEGs between Dox-treated samples and control against the HALLMARK_TNFA_SIGNALING_VIA_NFKB gene set. (**D**) Enrichment score of core enriched genes of GSEA against the HALLMARK_TNFA_SIGNALING_VIA_NFKB gene set from time-series scRNA-seq data set and corresponding log2FC values from the ATAC-seq data set (red = positive log2FC values, grey = negative log2FC values). (Figure was modified from Allgöwer et al.[203] under CC BY 4.0, https://creativecommons.org/licenses/by/4.0/)

TNFα protein levels were therefore further assessed in the PDLO-derived conditioned media. While varying concentrations at baseline (untreated PDLOs) were observed between different pancreatic differentiation experiments, a stable increase of TNFα levels was found in the conditioned media derived from Dox-treated PDLOs across all differentiations (**Figure 26A**).

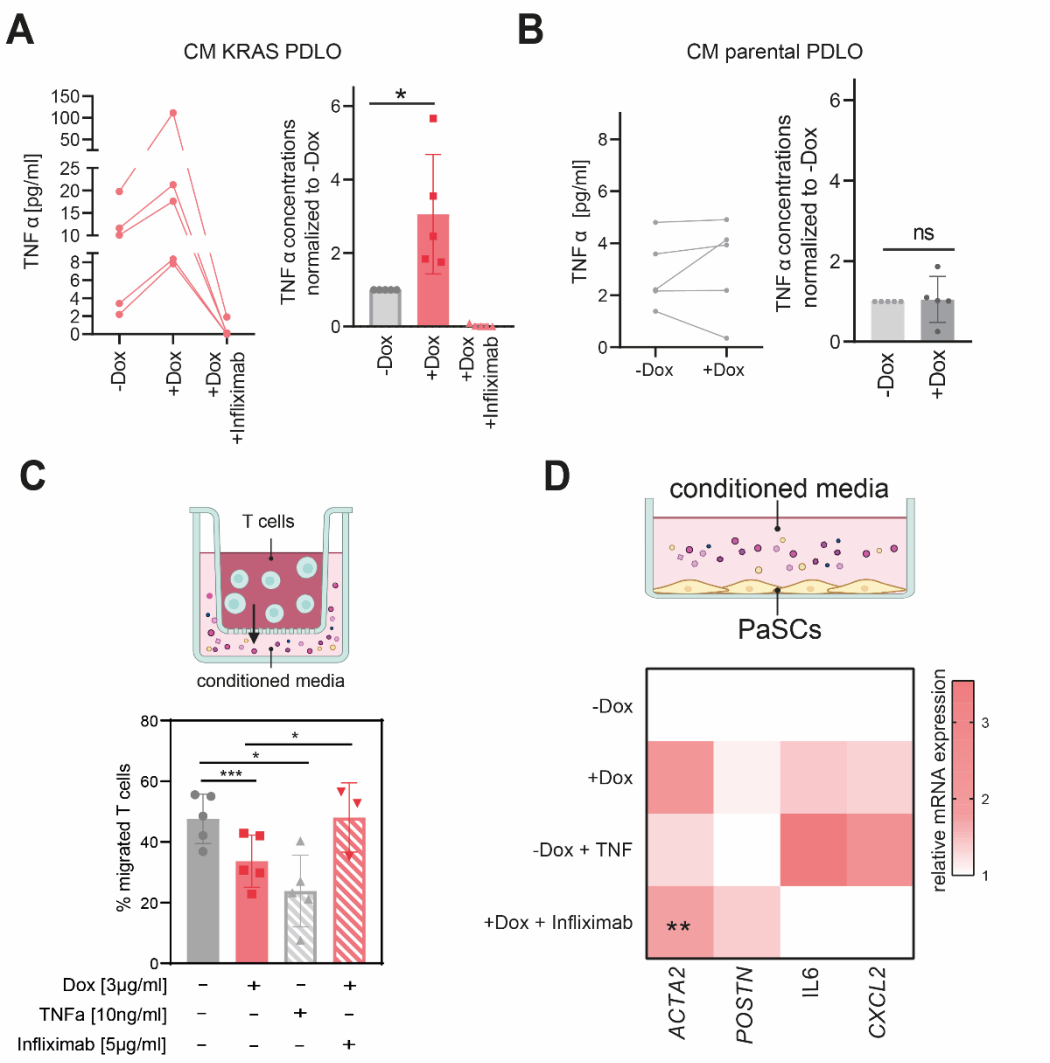

Figure 26 | TNFα secretion is *KRAS*^{G12D}-dependent and reduces T cell migration while inducing PaSC activation. (**A**) TNFα concentrations in conditioned media derived from KRAS-PDLOs (left) and corresponding TNFα levels normalized to the untreated control (right). Mean ± SD, n = 5. Paired t-test *, p<0.05. (**B**) TNFα concentrations in conditioned media derived from parental PDLOs (left) and corresponding TNFα levels normalized to the untreated control (right). Mean ± SD, n = 5. Paired t-test ns, p>0.05. (**C**) Proportions of T cells that migrated towards conditioned media derived from KRAS-PDLOs. Mean ± SEM, n=4. One-way ANOVA *, p<0.05; ***, p<0.001. (**D**) Gene expression of canonical CAF markers in PaSCs after culturing in PDLO-derived conditioned media. The mRNA levels are shown relative to the untreated (-Dox) condition after normalization to GAPDH was performed. Mean, n=4, unpaired t-test**, p<0.01. (Schemes were created with BioRender.com and figure was modified from Allgöwer et al.[203] under CC BY 4.0, https://creativecommons.org/licenses/by/4.0/)

Adding infliximab, a TNF-neutralizing antibody, to conditioned media derived from Dox-treated PDLOs diminished TNFα levels. Within the conditioned media of parental PDLOs, no changes in TNF levels occurred upon Dox treatment (**Figure 26B**), thereby supporting that TNFα secretion is indeed *KRAS*^{G12D}-dependent within the PDLO model.

The influence of TNFα on T cell migration was then assessed by repeating the Transwell® assay, additionally spiking the conditioned media of untreated PDLOs with recombinant TNFα and neutralizing TNFα in the conditioned media derived from Dox-treated PDLOs with infliximab (**Figure 26C**). As observed in the previous experiments, significantly fewer T cells migrated towards the conditioned media of Dox-treated PDLOs compared to the conditioned media of the untreated PDLOs. The presence of TNFα in the conditioned media of untreated PDLOs, however, strongly reduced migration. In contrast, TNF-neutralization within the *KRAS*^{G12D}-derived secretome lead to more attraction of T cells, thereby highlighting the involvement of TNFα in T cell migration.

The same conditions were used on PaSCs, culturing the cells in conditioned media of PDLOs and adding either recombinant TNFα or infliximab. While the conditioned media of Dox-treated PDLOs resulted in an upregulated gene expression of both myCAF- (*ACTA2* and *POSTN*) and iCAF-related (*IL6* and *CXCL12*) markers, additional TNFα neutralization with infliximab directed the PaSCs towards a myCAF phenotype (**Figure 26D**). The addition of recombinant TNFα to the conditioned media of untreated PDLOs predominantly increased the expression of *IL6* and *CXCL2*, indicating polarization of PaSCs towards iCAFs.

3.5 Single-cell RNA sequencing of PDLO co-cultures

To enable global analysis of the *KRAS*^{G12D}-dependent effects on niche cells in a pre-cancer context, a second scRNA-seq data set of PDLOs in co-culture was generated (co-culture scRNA-seq data set). This data set included monocultures of PDLOs as well as bi-cultures of PDLOs with either T cells (bi_Tcells) or PaSCs (bi-stellate, **Figure 27A-B**). The cultures were either left untreated (-Dox), treated with Dox to induce *KRAS*^{G12D}-expression (+Dox), or Dox-treated with the addition of infliximab to neutralize TNFα (+Dox +infliximab). In total, 60,003 cells (25,590 PDLOs, 4,208 T cells, and 30,205 PaSCs) passed quality metrics and were included in downstream analysis (**Figure 27C-D**). Cell types were annotated based on the clusters present in the different culture conditions (**Figure 27E**), which was further validated by cell-type-specific marker gene expression (**Figure 27F**).

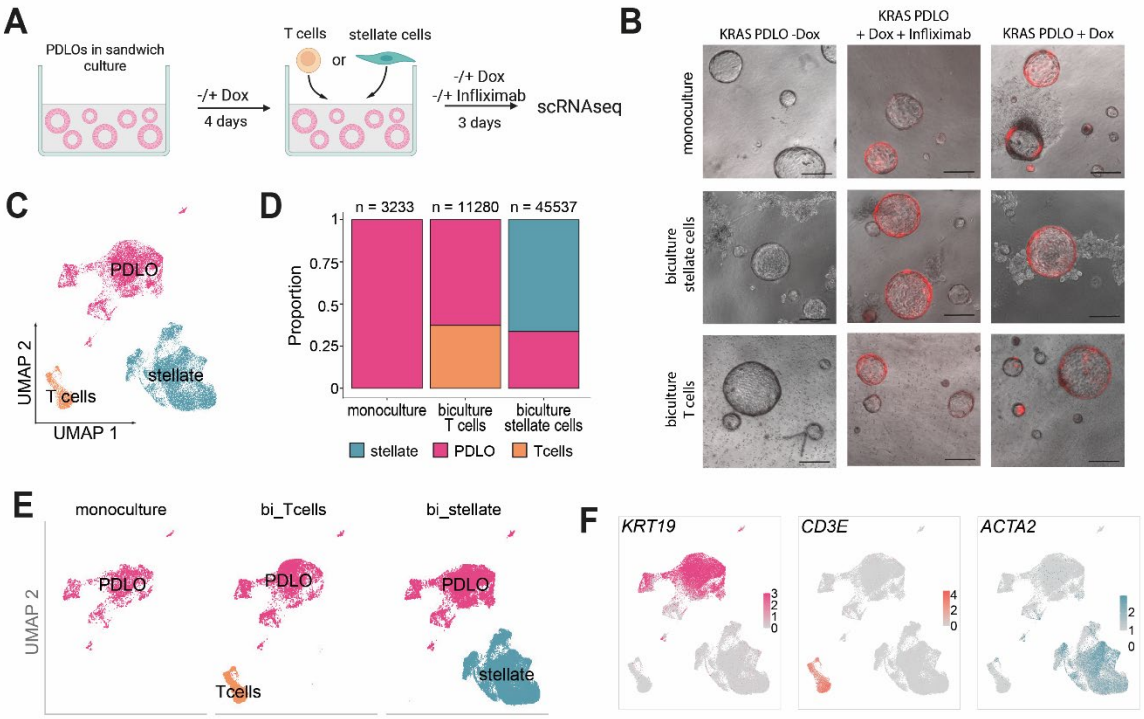

Figure 27 | Single-cell RNA sequencing of PDLO co-cultures. (**A**) Schematic overview of sample generation for scRNA-seq of PDLO bi-cultures with either T cells or stellate cells (generated with BioRender). (**B**) Representative images of PDLO co-cultures before sample harvesting. Scale bar = 250 µm. (**C**) UMAP of all cells in the co-culture scRNA-seq dataset. (**D**) Proportions of PDLOs, T cells, and stellate cells in the different culture conditions. (**E**) UMAPs of the individual culture conditions. (**F**) UMAP of cell-type-specific marker expression. (Scheme was created with BioRender.com and figure was modified from Allgöwer et al.[203] under CC BY 4.0, https://creativecommons.org/licenses/by/4.0/)

3.5.1 PDLOs in mono- and bi-culture

The PDLOs used for the co-culture scRNA-seq data set were generated with a different KRAS line (KRAS PDLO 2) than the one used for the time-series data set (KRAS PDLO 1). After annotating the PDLOs of the co-culture data set with the corresponding KRAS groups, it was therefore crucial to compare KRAS^{high}, KRAS^{intermediate} and KRAS^{low} cells of both data sets. Indeed, the KRAS groups clustered as expected, ensuring robustness of the model (**Figure 28A**). KRAS^{high} and KRAS^{intermediate} cells were equally distributed between the +Dox and +Dox +infliximab conditions (**Figure 28B-C**). Fewer PDLO cells were captured for the monoculture conditions, as these samples were included in only one of two sequencing runs (**Figure 28C**).

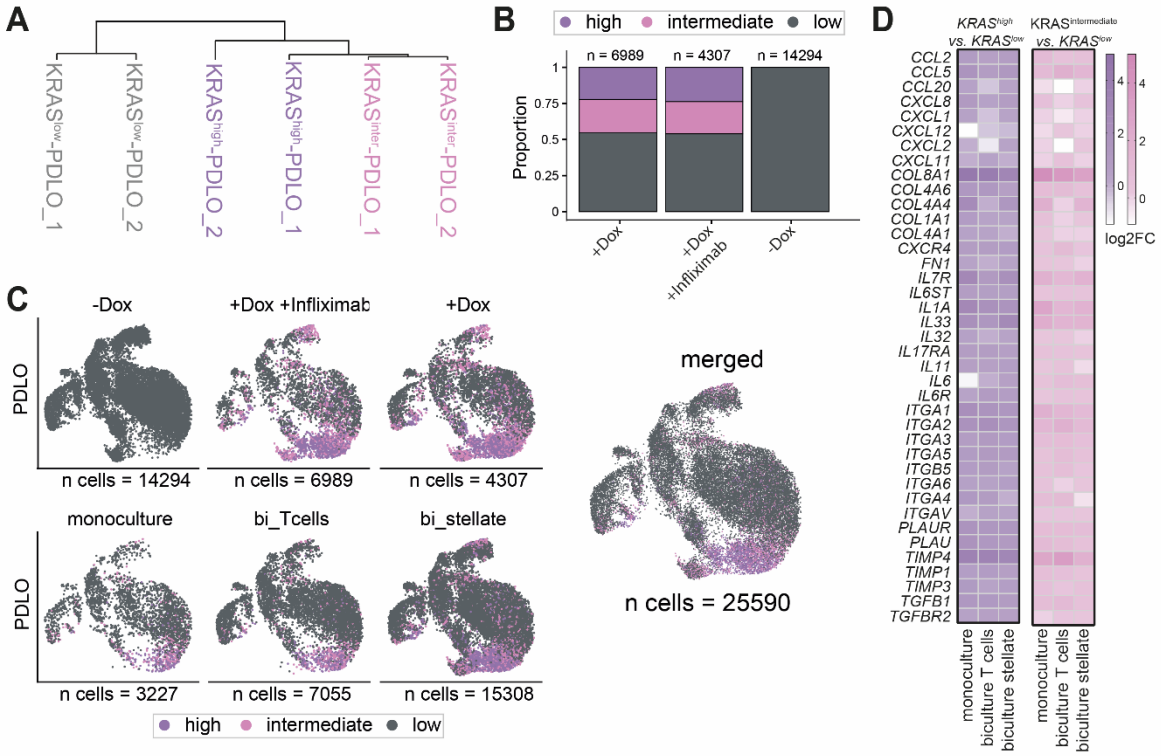

Figure 28 | PDLOs in mono- and bi-culture. (**A**) Cluster tree showing similarity of KRAS^{high}, KRAS^{intermediate}, and KRAS^{low} clusters from time-series scRNA-seq data set (KRAS PDLO 1) and co-culture scRNA-seq data set (KRAS PDLO 2). (B) Proportions of KRAS^{high}, KRAS^{intermediate}, and KRAS^{low} cells per treatment condition within the PDLOs of the co-culture scRNA-seq data set. (**C**) UMAPs of PDLOs split by treatment conditions (top) and culture conditions (bottom) and colored by KRAS groups. (**D**) Log2FC values of selectively chosen ECM- and inflammation-related DEGs when comparing KRAS^{high} and KRAS^{intermediate} to KRAS^{low}. (Figure was modified from Allgöwer et al.[203] under CC BY 4.0, https://creativecommons.org/licenses/by/4.0/)

As shown for the time-series scRNA-seq data set, the KRAS^{high} and KRAS^{intermediate} cells of the co-culture data set overexpressed several genes related to ECM

remodeling and inflammation (**Figure 28C**). Interestingly, the log2FC values for the individual genes remained within a similar range across the culture conditions.

3.5.2 T cells in co-culture with PDLOs

For the T cell subset, fewer cells were captured within the Dox-treated cultures (**Figure 29A**). The cells were annotated based on CD8 and CD4 expression of the Louvain clusters (**Figure 29B-D**), revealing that slightly more CD8+ cells are present in the Dox-treated condition, whereas fewer $CD8^+$ cells are present if infliximab is added (**Figure 29E**). The Louvain cluster 5 (44 cells) did not show a relevant CD3 expression and was therefore excluded from further downstream analysis.

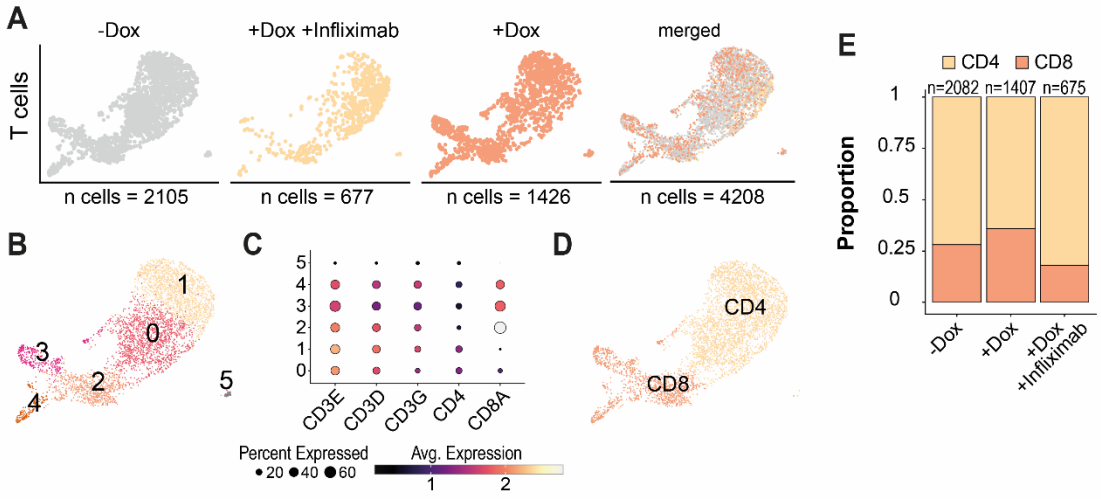

Figure 29 | T cells are differently distributed between treatment conditions. (**A**) UMAPs of T cells co-cultured with PDLOs in the different treatment conditions. (**B**) UMAP of T cells colored by Louvain clusters. (**C**) Gene expression of T cell-specific marker genes within the Louvain clusters. (**D**) UMAP showing CD4 and CD8 T cell subpopulations. (**E**) Proportions of CD4 and CD8 cells within the different treatment conditions. (Figure was modified from Allgöwer et al.[203] under CC BY 4.0, https://creativecommons.org/licenses/by/4.0/)

Within the CD8 subset, T cells from the Dox-treated cultures showed reduced expression of genes associated with T cell activation and migration, which was reversed upon TNFα neutralization (**Figure 30A**). Moreover, CD8 cells from the Dox-treated cultures exhibited increased expression of T cell exhaustion markers.

When comparing all T cells (CD8 and CD4) of the Dox-treated cultures to those of the untreated cultures, DEGs were enriched for HALLMARK gene sets related to proliferation (mTORC1 signaling, Myc targets, E2F targets and G2-M Checkpoint) and stress response (ROS pathway and oxidative phosphorylation) as well as IFNG

signaling (Figure 30B). A similar enrichment was observed when comparing Dox-treated cultures without infliximab to those with infliximab, indicating that these pathways rely on the KRAS^{G12D}-TNF axis. Several genes, such as *DHCR24, RRM2, WARS1, MTHFD2, EBP, DHCR7, PRDX1, SLC25A5, CYCS,* and *ALAS1*, are upregulated in a KRAS^{G12D}-TNF-dependent manner, suggesting an overstimulated and metabolically impaired T cell state (Figure 30C).

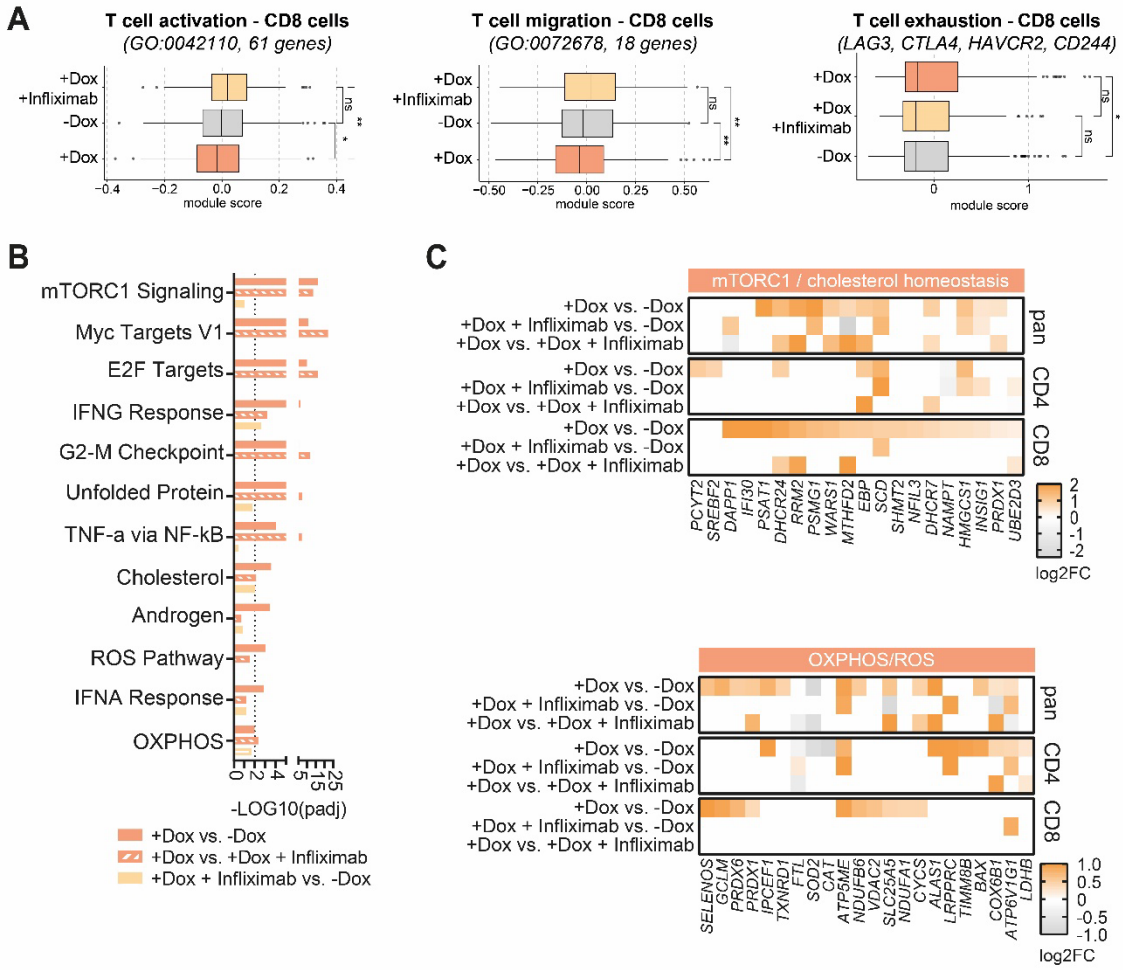

Figure 30 | T cells show overstimulated growth signaling and stress response. (**A**) Module scores of CD8 subset for T cell activation (right), T cell migration (middle), and T cell exhaustion (right). Median with corresponding extremes. Wilcoxon test **, p<0.01; ns, p>0.05. (**B**) Top terms (p<0.05) of HALLMARK gene set enrichment for all T cells. (IFNG Response = Interferon Gamma Response, Unfolded Protein = Unfolded Protein Response, TNF-α via NF-κB = TNF-α Signaling via NF-κB, Cholesterol = Cholesterol Homeostasis, Androgen = Androgen Response, ROS Pathway = Reactive Oxygen Species Pathway, IFNA = Interferon Alpha Response, OXPHOS = Oxidative Phosphorylation). (C) Log2FC values for DEGs related to mTORC1 Signaling, Cholesterol Homeostasis, ROS and OXPHOS. (Figure was modified from Allgöwer et al.[203] under CC BY 4.0, https://creativecommons.org/licenses/by/4.0/)

3.5.3 PaSCs in co-culture with PDLOs

The highest amount of PaSCs was captured within the Dox-treated condition, and cell numbers were slightly decreased when infliximab was added (**Figure 31A**). Louvain clusters were attempted to be annotated using gene signatures from Tao et al.[200] for different CAF subpopulations (**Figure 31B-C**). However, the individual clusters could not be assigned to specific subtypes, as multiple signatures were co-expressed within the same clusters (**Figure 31C**). Instead, annotation was performed on a single-cell level, revealing higher proportions of iCAFs, nCAFs (normal-like CAFs), and pCAFs (proliferative CAFs) in Dox-treated cultures (**Figure 31D**).

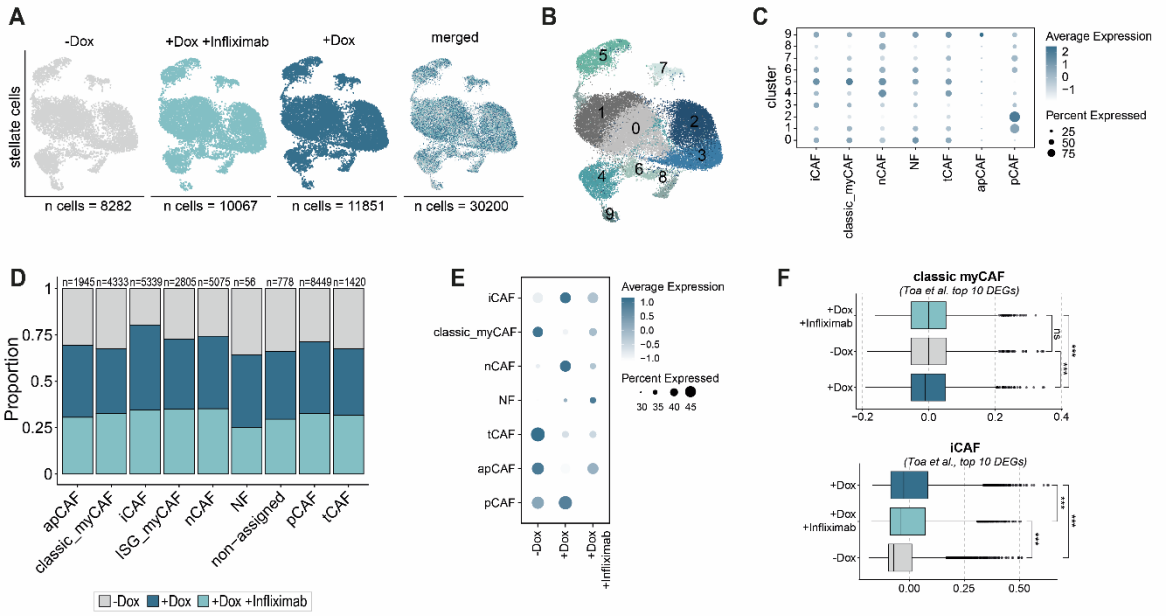

Figure 31 | *KRAS*^{G12D}-expressing PDLOs induce a shift of CAF populations in PaSCs. (**A**) UMAP of PaSCs for the individual treatment conditions. (**B**) UMAP of PaSCs colored by Louvain clusters. (**C**) Module scores of Louvain clusters for the top 100 CAF signature genes derived from Tao et al.[200] (**D**) Proportions of PaSCs by treatment for the different CAF subpopulations.[200] (**E**) Module scores of PaSCs for the individual treatment conditions using the top 100 CAF signature genes derived from Tao et al.[200]. (**F**) Module scores for the PaSCs using the top 10 DEGs for classical myCAFs and iCAFs from Tao et al.[200]. Median with corresponding extremes. Wilcoxon test ***, p<0.001; ns, p>0.05. (Figure was modified from Allgöwer et al.[203] under CC BY 4.0, https://creativecommons.org/licenses/by/4.0/)

The averaged expression of the CAF signatures within the treatment conditions confirmed enrichment of iCAF-, nCAF- and pCAF-related genes in the Dox-treated cultures, which was reduced upon addition of infliximab (**Figure 31E**). In contrast, the PaSCs of the untreated cultures showed higher expression of genes defining the classical myCAF, tCAFs (transitional CAFs), and apCAF subtypes. Using only the top

10 signature genes for classical myCAFs and iCAFs from Tao et al.[200] could capture the shift towards iCAFs in the Dox-treated condition, highlighting a robust change in CAF polarization (**Figure 31F**). When comparing PaSCs of one treatment condition to the cells of both other conditions, several genes related to cell cycle and inflammation were found to be dysregulated (**Figure 32A**). PaSCs co-cultured with *KRAS*^{G12D}-expressing PDLOs displayed increased expression of genes promoting proliferation, such as *MCM2*, *MCM5*, and *CDK1*, while PaSCs from the untreated cultures exhibited the upregulation of genes involved in cell-cycle arrest, such as *CDKN2A* and *CDKN2B*. The expression of these genes was not altered in the Dox-treated cultures upon TNFα neutralization, underpinning the relevance of TNF signaling in this context. Moreover, PaSCs from Dox-treated cultures showed upregulated expression of inflammatory genes, including *IL6* and *CXCL2*, which are considered key markers of the iCAF phenotype.

Additionally, the averaged expression of the top 100 DEGs of PaSCs from each treatment condition was analyzed in the pancreatic stromal cells from Peng et al.[201], revealing that only the DEGs from the Dox-treated culture were enriched in human tissue, especially in the tumor-derived fibroblasts (**Figure 32B**).

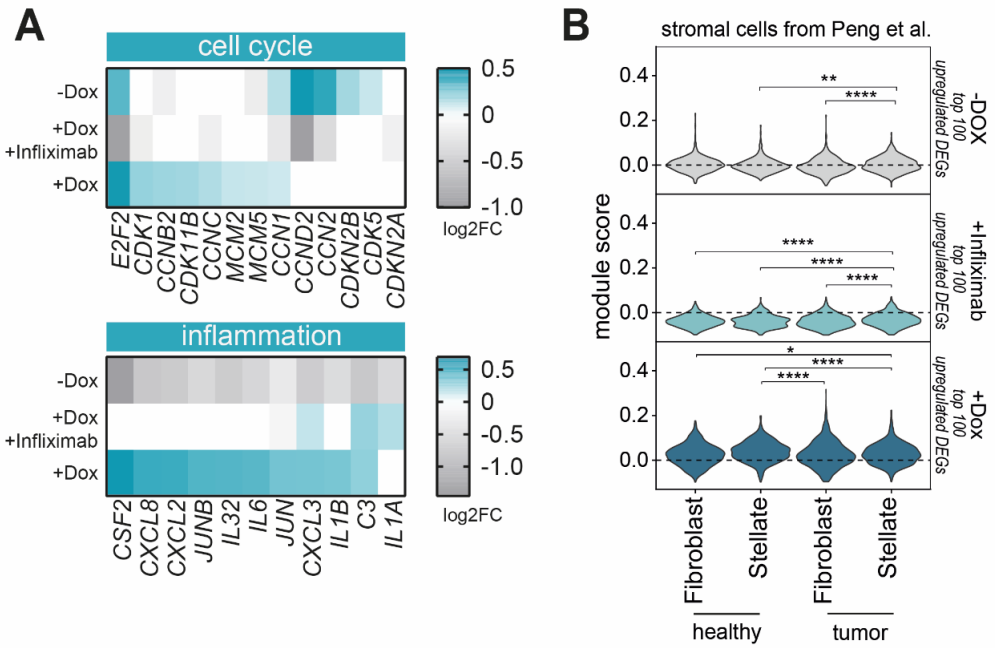

Figure 32 | Differently expressed genes of PaSCs. (**A**) Log2FC values of selectively chosen DEGs related to cell cycle and inflammation when comparing PaSCs of one treatment condition to both other treatment conditions. (**B**) Module scores in stromal cells from Peng et al.[201] using the top 100 DEGs when comparing PaSCs of one treatment condition to both other treatment conditions. Unpaired t-test: ****, p<0.0001; **, p<0.01; *, p<0.05. (Figure was modified from Allgöwer et al.[203] under CC BY 4.0, https://creativecommons.org/licenses/by/4.0/)

3.5.4 Cell-cell communication analysis within PDLO co-cultures

Cell-cell communication analysis within the bi-cultures of PDLOs and T cells or PaSCs revealed that interaction strengths are predicted to be overall stronger within *KRAS*^{G12D}-expressing PDLO cultures, independent of TNF neutralization (**Figure 33A**). Interestingly, this was also true for PDLO cells annotated as KRAS^{low}.

When investigating TNF signaling between the cells, the primary ligand source is predicted to be KRAS^{high} cells, especially from bi-cultures with stellate cells (**Figure 33B**). As expected, the interaction strength is distinctly weaker within infliximab cultures. While PaSCs are predicted to receive TNF signaling via both the *TNFRSF1A* and *TNFRSF1B* receptors, interaction with T cells is expected to be restricted to the *TNFRSF1B* receptor. In contrast to the previous cell-cell communication analysis with healthy pancreatic or PDAC cells, the KRAS^{intermediate} cells show an overall weak interaction strength of the TNF pathway.

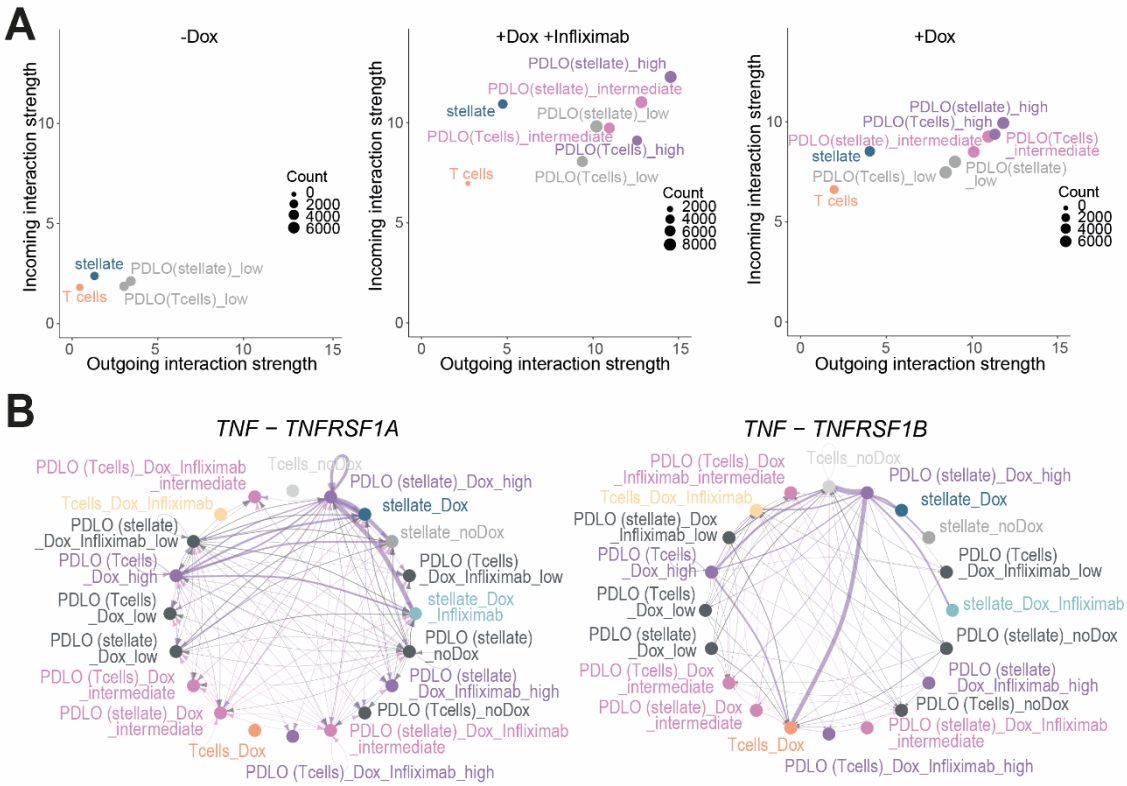

Figure 33 | Cell-cell communication analysis of PDLO bi-cultures. (**A**) Predicted interaction strength of different cell types of the PDLO bi-cultures. (**B**) Predicted interaction strength and directionality of PDLOs, T cells, and PaSCs within the TNF signaling network. (Figure was modified from Allgöwer et al.[203] under CC BY 4.0, https://creativecommons.org/licenses/by/4.0/)

4. Discussion

4.1 KRAS^{G12D} expression in PDLOs

The PDLO model used within the framework of this thesis is based on genetically engineered stem cells, transduced with an inducible *KRAS^{G12D}* construct by employing the PiggyBac transposon system. The PiggyBac transposon system combines transfection with a transposon plasmid, harboring a mobile DNA element, in the presence of a transposase plasmid, allowing the transposition from the vector into the genome by "cut-and-paste".[205] It outperforms viral transduction methods in terms of technical efforts, cargo capacity, and safety with respect to integration into gene-coding regions.[205,206] Thus, the PiggyBac system is a widely applied technique, especially suited for the genetic modification of stem cells.[205,206]

The transposon sequence is integrated throughout the genome, predominantly at TTAA sites with a high affinity for intronic regions.[205–207] Hence, integration is not entirely random but rather occurs in a semi-stochastic manner. For the KRAS lines used in this thesis, cells showed an average gain of 4 *KRAS^{G12D}* copies. In PDAC tumors, several forms of mutated KRAS (*KRAS^{mut}*) copy-number alterations were observed. KRAS mutations occur either as heterozygous (balanced) or as copy-number-neutral loss of *KRAS^{wt}* (copy-number-neutral loss of heterozygosity, CN-LOH), resulting in either 1 or 2 *KRAS^{mut}* copies, respectively.[111,208,209] This was also reflected in the TaqMan copy number analysis of PDAC cell lines and PDOs. However, PDAC tumors can also show amplification of *KRAS^{mut}* copy numbers, induced, for example, by focal gain, hence acquiring three or more *KRAS^{mut}* copies.[111,208,209] The majority of PanINs harbor *KRAS* mutations, and a gain in *KRAS^{mut}* alleles of at least two copies was also observed in human low-grade PanINs.[111,208,210,211] Nevertheless, it is described that *KRAS^{mut}* cells accumulate due to clonal expansion and that KRAS allelic imbalance is acquired over time of tumor progression, initially harboring only one mutated *KRAS* copy.[208,210,211] This places the KRAS^{G12D}-PDLO model genotypically closer to advanced stages rather than early dysplastic states.

Moreover, *KRAS* copy numbers closely correlate with *KRAS* expression[208] and KRAS^{G12D} expression in the PDLO model was approximately 3-fold higher compared to *KRAS^{wt}* levels. Despite increased copy numbers and enhanced mRNA expression, protein levels of phospho-ERK in *KRAS^{G12D}*-expressing PDLOs were comparable to

those of PDAC cell lines and PDOs, thereby demonstrating that KRAS downstream signaling remains within a physiological range.

$KRAS^{G12D}$ expression within the PDLOs is mediated by a reverse tetracycline transactivator (rtTA). The rtTA undergoes conformational changes upon binding with doxycycline, which then enables binding of the rtTA to the tet operon, thereby initiating transcription of the downstream gene of interest ($KRAS^{G12D}$).[212] This TetON system allows stem cell differentiation towards KRAS-wildtype PDLOs, initiating oncogene expression only once healthy ductal structures have formed. The Dox concentration was chosen based on previous work demonstrating robust transgene expression in PDLOs upon treatment with 3 µg/ml Dox.[34,196] Importantly, expression of $KRAS^{G12D}$ was not observed in untreated PiggyBac-engineered PDLOs, excluding leaky transgene expression within the controls. Moreover, Dox treatment of parental PDLOs, not harboring the inducible $KRAS^{G12D}$ construct, did not reproduce key findings, thereby eliminating potential effects of the Dox treatment itself.

A polyclonal hESC line was used to generate PDLOs, meaning that no clonal selection was performed after transduction of stem cells with the PiggyBac system. Thus, cells harbor varying copy numbers of the transgene, while some cells lack the integrated $KRAS^{G12D}$ construct. This was nicely reflected in the *KRAS*^{G12D}-dependent grouping of cells from the time-series scRNA-seq data set, showing that $KRAS^{high}$ and $KRAS^{intermediate}$ cells are distributed across different time points of Dox treatment, and the $KRAS^{low}$ group includes cells from both untreated and treated conditions. Velocity analysis further confirmed that $KRAS^{high}$ and $KRAS^{intermediate}$ cells are predicted to arise independently, supporting the notion that these two populations mirror cell-to-cell variability in transgene copy number rather than distinct states along a trajectory.

Interestingly, the transcriptome of $KRAS^{high}$ and $KRAS^{intermediate}$ was shown to be very similar, and no striking differences were observed based on $KRAS^{G12D}$ levels. Müller et al. demonstrated that gain of the *KRAS*^{mut} allele *in vivo*, resulting in higher mRNA levels of *KRAS*^{mut}, was associated with a more mesenchymal morphology and dedifferentiated tumors, resulting in a higher metastatic potential.[111] This seems to be contradictory to the subtle differences of the KRAS-expressing groups identified in the PDLO model. However, within the *in vivo* study, allelic balanced tumors

(heterozygous mutation) were compared to tumors with allelic imbalances (≥ 2 *KRAS*^{mut} alleles), without further decrypting differences between the different imbalanced states.[111] The KRAS^{high} and KRAS^{intermediate} cells yet both represent imbalanced states. The analog comparison within the PDLO model would be the grouping of cells expressing equal levels of *KRAS*^{wt} and *KRAS*^{G12D}, implying a balanced/heterozygous state, and compare those to cells overexpressing *KRAS*^{G12D}.

Allelic imbalances of the *KRAS* gene were also correlated with worse survival of PDAC patients.[209] This could also be shown for the early *KRAS*^{G12D}-induced transcriptome derived from the PDLO model, highlighting the substantial impact and clinical relevance of oncogenic KRAS signaling throughout tumor evolution.

Another *in vivo* study used a tamoxifen-dependent system to drive Cre-mediated recombination of the KRAS allele in pancreatic ducts.[213] Increasing doses of tamoxifen correlated with enhanced recombination, generating ducts with different percentages of KRAS-expressing cells (cKras^{Low}, cKras^{Mod}, cKras^{High}). While the individual cells of the different groups expressed the same levels of *KRAS*^{mut}, accumulation of *KRAS*^{mut}-positive cells gradually increased tumor progression from healthy duct (cKRAS^{Low}) to PanINs (cKRAS^{Mod} and cKRAS^{High}) and PDAC (cKRAS^{High}). In line with other studies, this highlights that both the magnitude of KRAS signaling per cell and the expanding population of KRAS-expressing cells cooperate to drive pancreatic tumorigenesis.[210,211,213] Regarding the amount of *KRAS*^{G12D}-expressing cells, the PDLO model can most closely be associated with the cKRAS^{Mod} group.

Although transcriptomic differences between KRAS^{high} and KRAS^{intermediate} cells were subtle, the deep learning approach confirmed that distinct cell identity can be predicted with high accuracy. Moreover, grouping of patient samples based on the PDLO-derived KRAS signatures showed a shift in tissue composition, indicating that *KRAS*^{G12D} levels might be relevant in more advanced stages. In summary, overexpression of *KRAS*^{G12D} outside its endogenous locus is a major limitation of the PDLO model. Nevertheless, this platform allows modelling of initial KRAS signaling without interference of other genetic alterations, and enables comparison to matched controls. Despite dominant oncogene expression, PDLOs transcriptionally bridged healthy and malignant ducts of human pancreatic tissue, underscoring the pre-cancer state of *KRAS*^{G12D}-expressing cells within the model.

4.1 *KRAS*^{G12D}-dependent senescence & EMT

During tumor progression, it is described that PanINs acquire features of senescence, also due to oncogenic KRAS signaling, which induces overstimulated growth and thereby forces cells into cell cycle arrest (oncogene-induced senescence, OIS).[214–216] This was nicely reflected in the time-series scRNA-seq data set and the time-resolved EdU-based cell cycle analysis, where cells initially showed a substantial increase in proliferation at day 1 of Dox treatment, which then declined over time as *KRAS*^{G12D} was further expressed until day 7. Previous work showed that proliferation is further reduced in *KRAS*^{G12D}-expressing PDLOs after 9 days of Dox treatment, while enhanced senescence is observed.[34,196]

For PanINs to further progress towards PDAC, cells must overcome senescence, and proliferative rates in tumors are higher than in precursor lesions. Several bypass mechanisms have been described, including loss-of-function mutations in tumor suppressors (e.g., *CDKN2A* and *TP53*) and EMT-mediated dedifferentiation.[214–216] EMT was previously observed in *KRAS*^{G12D}-expressing PDLOs[34,196], and correlation of *KRAS*^{G12D} expression with an EMT signature gene set was also shown in the time-series scRNA-seq data set. Moreover, *KRAS*^{G12D}-expressing PDLOs better correlated with genes related to the basal PDAC subtype compared to genes associated with classical tumors. The basal subtype acquires a mesenchymal-like phenotype and could be linked to ductal-derived tumors, while acinar-derived tumors better correlate with the classical subtype. Hence, the PDLO model is able to capture key mechanisms described *in vivo*.

4.2 *KRAS*^{G12D}-induced ECM- and inflammation-related gene signatures

When comparing the *KRAS*^{G12D}-overexpressing PDLO cells (KRAS^{high} and KRAS^{intermediate}) to KRAS^{low} cells, a variety of cytokines, chemokines, interleukins, collagens, and integrins were shown to be dysregulated in both the time-series as well as the co-culture scRNA-seq data set. Within the co-culture scRNA-seq data set, the expression of most of these genes did not change, neither when co-cultured with T cells nor with PaSCs. Hence, KRAS^{G12D} seems to induce these ECM- and inflammation-related signatures independent of paracrine signaling from other cell types.

Among the dysregulated genes, several genes encoding for ECM components such as fibronectin, collagens, and laminins were identified to be overexpressed in a *KRAS*^{G12D}-dependent manner, along with the upregulation of multiple integrins. This could be further confirmed at the protein level. The ECM not only forms a physical barrier around the tumor, thereby hindering immune infiltration and effective chemotherapeutic treatment, but also directly modulates tumor and TME cells.[217,218] Integrins are, for example, found to be overexpressed in PDAC and, upon binding of fibronectin, collagens, or laminins, influence cell-adhesion and actin polymerization and therefore contribute to tumor cell migration.[217] Type I collagens are the most abundant collagens in PDAC; however, type 4 collagen was also found to increase tumor cell proliferation and migration, most likely through interaction with integrin α2 and β1.[217,219]

Fibronectin (*FN1*) serves as a scaffold for other ECM components and plays a pivotal role in cell proliferation and infiltration of the basal membrane.[217,218] Additionally, fibronectin triggers TGFβ secretion in cancer cells.[217,218] TGFB1 was also found to be upregulated in *KRAS*^{G12D}-expressing PDLOs, and TGFβ is described as a key modulator of CAFs. Furthermore, *PLAU* was upregulated in a *KRAS*^{G12D}-dependent manner, encoding for the urokinase-plasmin activator (uPA). *PLAU* was also found to be overexpressed in PDAC tissue and correlated with enhanced TGFβ signaling along with increased levels of matrix metalloproteinase-14 (*MMP14*, also upregulated in the time-series scRNA-seq data set and proteome of PDLOs), which resulted in more EMT.[220]

In conclusion, the ECM-related gene signatures and protein expression captured by the PDLO model are consistent with previously described ECM remodeling mechanisms in PanINs and PDAC, underscoring the rapid onset of niche-related programs under KRAS^{G12D} signaling in epithelial cells.

KRAS^{G12D}-expressing PDLOs also displayed an upregulation of several cytokines, chemokines, and interleukins. These, however, were not found in the proteomics analysis. This might be explained by the fact that cytokines are generally expressed at lower concentrations and were therefore most likely masked by the high abundance of other proteins (such as ECM proteins).[221] Moreover, cytokines and other small signaling proteins are described to be rapidly secreted, often within

hours, and therefore might not be captured when analyzing the intracellular proteome.[222,223]

In the PDLO transcriptome, *CXCL1* and *CXCL8* were upregulated in both the time-series and co-culture scRNA-seq data sets. These chemokines were also identified to be overexpressed in PDAC tissue, and their secretion is mainly linked to neutrophil recruitment and angiogenesis.[224–226] These chemokines are both target genes of the NFκB pathway[226], in line with increased NFκB signaling observed in *KRAS*^{G12D}-expressing PDLOs. Moreover, *CXCL1* was described as an essential mediator of KRAS-induced senescence via the NFκB subunit RelA in murine preneoplastic lesions.[227] The chemokine *CCL20*, which was also upregulated in the *KRAS*^{G12D}-expressing PDLOs, is likewise overexpressed in PDAC and described as an NF-κB/RelA target.[226,228]

Furthermore, *CXCR4* was upregulated in KRAS^{high} and KRAS^{intermediate} cells. A gradual increase of *CXCR4* expression over time of PDAC development was also described previously, showing that *CXCR4* triggers MAPK and mTOR/AKT signaling and therefore promotes proliferation of PanINs and tumors.[229–232] Moreover, KPC mice with Cxcr4 knock-out showed fewer high-grade PanIN lesions.[233] While KPC-Cxcr4-KO mice did not show altered frequency of PDAC, tumors were less differentiated while presenting decreased desmoplastic reaction compared to mice expressing Cxcr4.[233] *CXCR4* is a chemokine receptor, and downstream signaling is initiated by the binding of its ligand *CXCL12*.[229,231,232] Interestingly, *CXCL12* was downregulated in *KRAS*^{G12D}-expressing PDLOs when cultured alone, KRAS^{high} cells however showed increased *CXCL12* expression when T cells or PaSCs were present. Within the PDAC TME, activated stellate cells and CAFs were identified to be a primary source of *CXCL12* secretion[234,235], which might explain a paracrine feedback loop within the PDLO co-cultures. Overall, the inflammation signatures upon KRAS signaling in the PDLOs recapitulate findings from PanINs and PDAC *in vivo*.

4.3 *KRAS*^{G12D}-dependent effects on T cells

Co-culture with *KRAS*^{G12D}-expressing PDLOs demonstrated reduced T cell migration/infiltration across different experimental platforms. This contradicts observations in the early stages of carcinogenesis. Initially, T cells infiltrate PanINs in response to lesion development, and T cell exclusion is then established in

advanced stages.[93,95,96] However, for *in vitro* experiments, healthy but unmatched (non-autologous) T cells were added to PDLOs, which will most likely induce a "host-versus-graft" reaction and infiltration of PDLOs is therefore expected. Moreover, *in vivo*, T cell recruitment to the PDAC TME is modulated by other cell types, such as TAMs and MDSCs,[93,95,96] which were not included in the bi-culture experiments. The PDLO co-culture set-ups thereby represent an artificial system and cannot fully recapitulate the true pathophysiology observed *in vivo*. Nevertheless, it could be established that KRAS signaling shields PDLOs from T cell infiltration, despite the use of non-autologous T cells and absence of other important players of immune modulation.

T cell migration is a tightly orchestrated process, and multiple factors can impact T cell motility. Mechanisms involved in T cell migration include interaction with antigen-presenting cells (APCs), chemotaxis, and composition of the ECM.[236,237] As decreased migration was also overserved towards the *KRAS^{G12D}*-induced secretome of PDLOs, the shielding impact of KRAS signaling cannot be limited to receptor interaction induced by cell-cell contact, but must, at least in parts, be regulated by chemoattractants and/or chemorepellents. Within PDAC tumors, stellate cells and CAFs for example secrete *CXCL12*, thereby attracting cytotoxic T cells and trapping them in the stromal tissue.[95,96] This is in line the cell-cell communication analysis of PDLOs and the PDAC tissue from Peng et al.[201], showing that T cells have an increased incoming signaling strength of the CXCL pathway, while fibroblasts and KRAS^{low} cells were identified as major senders. As *CXCL12* is downregulated in the *KRAS^{G12D}*-expressing PDLOs, T cells might be less prone to migrate towards those cells and their secretome.

However, to overcome the immune reaction induced by non-autologous mismatch of T cells and PDLOs, the *KRAS^{G12D}*-derived secretome must additionally include factors that actively prevent T cell infiltration. Among these factors, TNFα was identified to play a central role and will be discussed separately (section 4.5). Besides TNFα, cell-cell communication analysis *in silico* revealed interaction of *KRAS^{G12D}*-expressing PDLOs with T cells via the *PTN-SDC2/4* axis. *SDC2* and *SCD4* have both been described to inhibit T cell activation[238], which might therefore contribute to reduced T cell migration/infiltration. Furthermore, *SPP1-CD44* signaling was predicted to be enhanced between KRAS^{high}/KRAS^{intermediate} PDLOs and T cells. While *SPP1* is mainly described to be sourced from TAMs in other cancer entities,

SPP1-CD44 interaction was shown to induce a stress response of T cells and reduce T cell infiltration.[239,240]

During tumor progression of PDAC, several cell types, including neoplastic epithelial cells, TAMs and Tregs, induce exhaustion of cytotoxic T cells by expressing immune checkpoint modulators (e.g. *PD-L1* and *CTLA4*).[95] T cells exposed to PDLO-derived secretome, however, did not display *KRAS*^{G12D}-dependent changes in exhaustion or activation. In contrast, scRNA-seq of bi-cultures showed increased expression of genes related to exhaustion in the presence of *KRAS*^{G12D}-PDLOs, while also giving hints to a metabolically altered phenotype. As this was in parts TNF-dependent, this will be discussed in more detail in the designated section (section 4.5).

4.4 KRAS^{G12D}-dependent effects on stellate cells

KRAS^{G12D} expression in PDLOs induced increased proliferation of PaSCs. This is also observed *in vivo* during tumor progression, where bidirectional signaling promotes the growth of both epithelial and stellate cells.[77–79,241] Quiescent stellate cells are, for example, activated by TGFβ, IL6, and IL1, all of which were upregulated in the transcriptome of *KRAS*^{G12D}-expressing PDLOs.

Furthermore, *KRAS*^{G12D}-expressing PDLOs and their secretome triggered the upregulation of canonical CAF markers in PaSCs. However, marker expression was not uniform between experimental setups. Indirect co-culture showed a significant increase in *ACTA2* and *CXCL2* expression, whereas conditioned media treatment specifically enhanced IL6 mRNA levels. Overall, the range of fold-change values was notably higher for indirect co-culture. The PDLO-derived conditioned medium is known to have a low total protein concentration (compared to complete media containing FBS, for example), and bidirectional cross-talk within the indirect co-culture might therefore have a more substantial impact. In addition, the immortalized PaSC line displays a high baseline activation, which is reduced when culturing the cells in Matrigel.[242] Therefore, PaSCs grown in Matrigel domes, as done for the indirect co-culture, will most likely be less activated, and differences between treatment conditions (no Dox vs. Dox) will become more apparent. Here, pre-treatment of PaSCs with all trans-retinoic acid could be applied for future experiments, to reduce baseline activation prior to exposure with conditioned medium.[243,244]

Moreover, it has been established that direct cell-cell contacts promote myCAF polarization, while differentiation towards the iCAF phenotype is mainly induced by paracrine signaling.[245] Interestingly, the transcriptome of PaSCs in direct co-culture with *KRAS*^{G12D}-expressing PDLOs showed a shift towards iCAF-related gene expression. This further underpins the dominance of the *KRAS*^{G12D}-induced secretome. However, PaSCs within the scRNA-seq data set showed ambiguous marker expression and could not be assigned to a specific CAF subtype.

In general, stellate cells and CAFs are described as highly plastic cells, which can reversibly switch between different subtypes, and it should be assumed that not all CAF subtypes have been described in full detail yet.[200,246] Taken together, data from the PDLO model suggest that early epithelial *KRAS*^{G12D} signaling promotes a general activation of stellate cells with the potential to induce different CAF subtype polarization. However, longer exposure time or triggers from other cell types might be necessary to fully manifest CAF identity. Additionally, further dissection of the co-culture scRNA-seq data set could be a starting point to identify novel intermediate states of stromal cells in the pre-cancer context.

4.5 The role of TNFα in the pre-cancer niche

Cell-cell communication predicted that *KRAS*^{G12D}-dependent TNF signaling may play a central role in T cell and PaSCs interaction. TNFα is an inflammatory cytokine that can exist in membrane-bound form or as soluble factor.[247] Besides its crucial role in regulating cell death, TNFα triggers NFκB signaling, which results in the expression of other cytokines and chemokines, thereby inducing inflammation and contributing to immune cell recruitment.[247] Hence, anti-TNFa therapy, using neutralizing antibodies such as infliximab, is used for treatment of autoimmune diseases, including Crohn's disease and rheumatoid arthritis.[248]

In the context of PDAC, TNFα is described to be mainly sourced from TAMs. TAM-derived TNFα is linked to tumor growth and promotes an aggressive basal-like subtype.[249,250] Additionally, TNFα is involved in desmoplasia and triggers proliferation of stromal cells.[251,252] Interestingly, TNFα secreted by cytotoxic T cells induces tumor cell killing, highlighting the context-specific dual role of TNFα.[253] While evidence exists that tumors cells also overexpress *TNF*[251], the impact of the epithelial-derived KRAS/TNF axis on niche cells at earliest stage before cancer onset has not been described yet. PDLOs secreted elevated levels of TNFα in a *KRAS*^{G12D}-

dependent manner, and neutralization of TNFα in the PDLO-derived secretome resulted in increased T cell migration. Within the PDAC TME, TNFα induces dysfunctionality of T cells, promoting exhaustion.[254,255] While the *KRAS*^{G12D}-derived PDLO secretome did not manifest T cell exhaustion on protein level, transcriptome of T cells after bi-culture showed increased expression of exhaustion-related genes. This was not observed upon additional infliximab treatment, indicating involvement of TNFα.

Further analysis of the T cell transcriptome showed that exposure to *KRAS*^{G12D}-expressing PDLOs leads to an increased growth signature (mTORC1, Myc, E2F) accompanied by enriched metabolism-related signaling (cholesterol, oxidative phosphorylation, and ROS). Interestingly, these pathways were also enriched when comparing Dox-treated cultures to Dox-treated cultures with additional infliximab treatment. Therefore, these signaling pathways must be, at least in parts, TNF-dependent. In summary, the presence of these signatures suggests that T cells are exposed to an overstimulating growth signal, resulting in a metabolically impaired and dysfunctional state, while not yet fully exhausted.[256,257]

Neutralization of TNFα furthermore reduced the *KRAS*^{G12D}-dependent shift towards iCAF polarization of PaSCs. This has also been previously described in the context of end-stage PDAC, demonstrating that IL1α and TNFα are both capable of promoting the iCAF fate *in vitro* and *in vivo*.[82] Moreover, TNFα was shown to induce proliferation of pancreatic stellate cells[258], which could also be established within the PDLO model, where PaSCs displayed decreased expression of cell cycle-related genes.

4.6 Conclusion and outlook

The PDLO model mirrored key events described in pancreatic tumorigenesis, including canonical KRAS signaling pathways, such as senescence, and EMT. While *KRAS*^{G12D} overexpression represents a limitation of the study, PDLOs could be correlated to signatures of early neoplasia and transcriptionally bridged healthy and malignant duct. However, to enable *KRAS*^{G12D} expression in a more physiological range, alternative gene-editing techniques could be applied, such as targeting the safe harbor AAVS1 locus, thereby reducing *KRAS* copy numbers.[259,260]

Strikingly, PDLOs displayed ECM- and inflammation-related signatures after only a few days of *KRAS*^{G12D} expression, without additional stimulation of any other cell types. This strongly indicates that epithelial KRAS^{G12D} signaling induces a niche preparatory program, thereby generating a favorable environment for the upcoming tumor evolution. Furthermore, *KRAS*^{G12D}-expressing PDLOs induced T cell shielding while activating PaSCs. Extending the time of co-culturing may allow further dissection of the cross-talk between epithelial cells and niche cells. Moreover, multicellular systems, for example, tri-cultures with PDLOs, T cells, and stellate cells, are needed to capture synergistic/antagonistic effects between the different cell types.

TNFα could be identified as a crucial player involved in niche remodeling, as TNF neutralization rescued T cell migration and reduced *KRAS*^{G12D}-induced iCAF polarization and expression of proliferation marker in PaSCs. Therefore, it would be of interest to assess the impact of infliximab treatment *in vivo*. Exploiting available patient data sets could, for example, further elucidate current knowledge on the role of epithelial-derived TNFα.

Although TNF signaling was found to have a pivotal role in *KRAS*^{G12D}-dependent niche preparation, it is most likely not the sole modulator. Several other candidates may be involved, as predicted by the cell-cell communication analysis. Therefore, screening of other potential candidates might further dissect the mechanisms involved in generating a pre-cancer niche.

5. Summary

PDAC is a highly aggressive and lethal disease. Diagnosis often occurs in advanced stages, and currently available therapeutic options fail to provide the necessary cure. Although crucial breakthroughs in PDAC research have been made over the past decades, the underlying pathological mechanisms are by far not understood in their full complexity. Somatic mutations of the KRAS gene have been established as key drivers of the disease. However, the impact of oncogenic KRAS signaling on early dysplasia and niche remodeling remains elusive. The availability of human material before PDAC onset is extremely limited. Hence, molecular events that precede the development of invasive states in the human context are poorly explored.

To address this gap, human pluripotent stem cells were equipped with an inducible *KRAS*^{G12D} construct. These genetically modified stem cells were then directed towards the pancreatic lineage, allowing oncogenic *KRAS* expression in healthy pancreatic duct-like organoids. In-depth global analysis of these PDLOs was performed, including time-resolved transcriptome analysis at cellular resolution, as well as chromatin accessibility and proteomic data.

KRAS^{G12D}-dependent signaling in PDLOs mirrored key events of tumorigenesis, such as senescence and epithelial-to-mesenchymal transition, and transcriptomically bridged healthy and malignant ductal tissue of human pancreatic samples. Strikingly, a few days of *KRAS*^{G12D} expression induced signatures related to extracellular matrix remodeling and inflammation. Further *in vitro* validation, employing various co-culture platforms, revealed that the *KRAS*^{G12D}-induced secretome activates human pancreatic stellate cells while reducing T cell infiltration. *In silico* cell-cell communication analysis identified TNFα as a central ligand involved in potential cross-talk of *KRAS*^{G12D}-expressing PDLOs with stromal and T cells. *KRAS*^{G12D}-expressing PDLOs secreted increased levels of TNFα, and TNFα neutralization *in vitro* resulted in increased T cell migration. Analysis of the T cell transcriptome after co-culture with PDLOs implied that *KRAS*^{G12D}-TNF signaling induces a dysfunctional T cell state through overstimulation and metabolic impairment. Moreover, the *KRAS*^{G12D}-TNFα signaling axis was shown to direct stellate cells towards the iCAF subtype.

In conclusion, the PDLO model could demonstrate that *KRAS*^{G12D} signaling orchestrates niche remodeling prior to cancer onset, thereby giving new insights into the earliest states of pancreatic tumorigenesis.

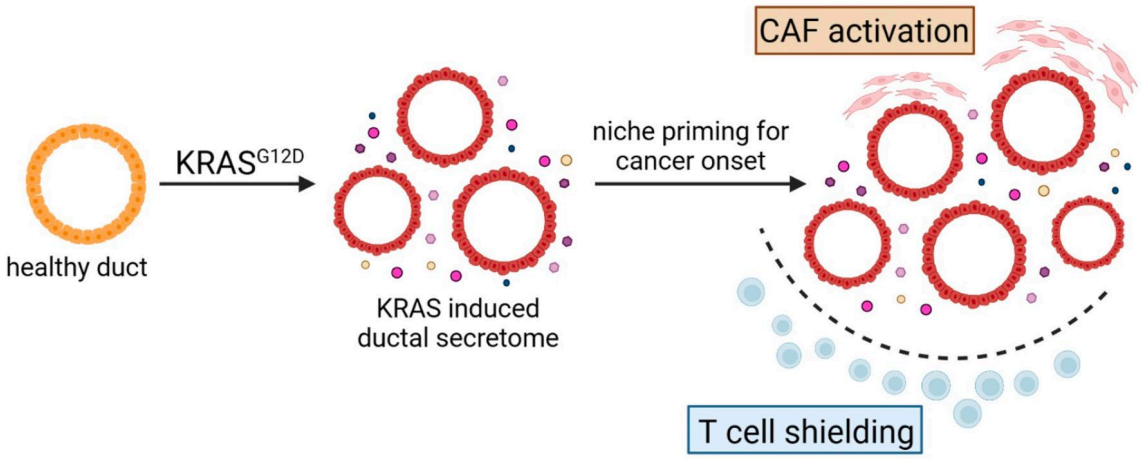

Figure 34 | Schematic summary. Genetically engineered human pluripotent stem cells were directed towards the pancreatic lineage, enabling oncogenic *KRAS*^{G12D} expression in healthy pancreatic duct-like organoids (PDLOs). *KRAS*^{G12D}-expression in healthy PDLO induced secretion of several factors, including TNFα. The *KRAS*^{G12D}-induced secretome promoted T cell shielding and activated pancreatic stellate cells. (Scheme was created with BioRender.com).

6. References

(1) Howard, J. M.; Hess, W. *History of the Pancreas: Mysteries of a Hidden Organ*; Springer Science & Business Media, 2012.

(2) Tsuchiya, R.; Fujisawa, N. On the Etymology of "Pancreas." *Int J Gastrointest Canc* **1997**, *21* (3), 269–272. https://doi.org/10.1007/BF02821615.

(3) Williams, J. A. The Nobel Pancreas: A Historical Perspective. *Gastroenterology* **2013**, *144* (6), 1166–1169. https://doi.org/10.1053/j.gastro.2012.10.056.

(4) Beger, H. G.; Buchler, M. W.; Kozarek, R.; Lerch, M. M.; Neoptolemos, J. P.; Warshaw, A. L.; Whitcomb, D. C.; Shiratori, K. *The Pancreas: An Integrated Textbook of Basic Science, Medicine, and Surgery*; John Wiley & Sons, 2009.

(5) Henry, B. M.; Skinningsrud, B.; Saganiak, K.; Pękala, P. A.; Walocha, J. A.; Tomaszewski, K. A. Development of the Human Pancreas and Its Vasculature — An Integrated Review Covering Anatomical, Embryological, Histological, and Molecular Aspects. *Annals of Anatomy - Anatomischer Anzeiger* **2019**, *221*, 115–124. https://doi.org/10.1016/j.aanat.2018.09.008.

(6) Atkinson, M. A.; Campbell-Thompson, M.; Kusmartseva, I.; Kaestner, KlausH. Organisation of the Human Pancreas in Health and in Diabetes. *Diabetologia* **2020**, No. 63, 1966–1973. https://doi.org/10.1007/s00125-020-05203-7.

(7) Karpinska, M.; Czauderna, M. Pancreas—Its Functions, Disorders, and Physiological Impact on the Mammals' Organism. *Frontiers in Physiology* **2022**, *13*.

(8) Lim, P. S.; Patil, A.; Sashankar, A. The Pancreas. *Anaesthesia & Intensive Care Medicine* **2023**, *24* (10), 644–649. https://doi.org/10.1016/j.mpaic.2023.07.006.

(9) Li, S.; Xie, K. Ductal Metaplasia in Pancreas. *Biochimica et Biophysica Acta (BBA) - Reviews on Cancer* **2022**, *1877* (2), 188698. https://doi.org/10.1016/j.bbcan.2022.188698.

(10) Hegyi, P.; Petersen, O. H. The Exocrine Pancreas: The Acinar-Ductal Tango in Physiology and Pathophysiology. In *Reviews of Physiology, Biochemistry and Pharmacology, Vol. 165*; Nilius, B., Amara, S. G., Gudermann, T., Jahn, R., Lill, R., Offermanns, S., Petersen, O. H., Eds.; Reviews of Physiology, Biochemistry and Pharmacology; Springer International Publishing: Cham, 2013; Vol. 165, pp 1–30. https://doi.org/10.1007/112_2013_14.

(11) Williams, J. A. Regulation of Acinar Cell Function in The Pancreas. *Curr Opin Gastroenterol* **2010**, *26* (5), 478–483. https://doi.org/10.1097/MOG.0b013e32833d11c6.

(12) Gorelick, F. S.; Pandol, S.; Jamieson, J. D. Structure-Function Relationships in the Pancreatic Acinar Cell. In *Physiology of the Gastrointestinal Tract*; Elsevier, 2018; pp 869–894. https://doi.org/10.1016/B978-0-12-809954-4.00039-6.

(13) Dolenšek, J.; Pohorec, V.; Rupnik, M. S.; Stožer, A.; Dolenšek, J.; Pohorec, V.; Rupnik, M. S.; Stožer, A. Pancreas Physiology. In *Challenges in Pancreatic Pathology*; IntechOpen, 2017. https://doi.org/10.5772/65895.

(14) Pallagi, P.; Hegyi, P.; Rakonczay, Z. The Physiology and Pathophysiology of Pancreatic Ductal Secretion: The Background for Clinicians. *Pancreas* **2015**, *44* (8), 1211–1233. https://doi.org/10.1097/MPA.0000000000000421.

(15) Angyal, D.; Bijvelds, M. J. C.; Bruno, M. J.; Peppelenbosch, M. P.; De Jonge, H. R. Bicarbonate Transport in Cystic Fibrosis and Pancreatitis. *Cells* **2021**, *11* (1), 54. https://doi.org/10.3390/cells11010054.

(16) Angyal, D.; Groeneweg, T. A.; Leung, A.; Desain, M.; Dulla, K.; De Jonge, H. R.; Bijvelds, M. J. C. Pro-Inflammatory Cytokines Stimulate CFTR-Dependent Anion Secretion in Pancreatic Ductal Epithelium. *Cell Mol Biol Lett* **2024**, *29* (1), 18. https://doi.org/10.1186/s11658-024-00537-1.

(17) Walkowska, J.; Zielinska, N.; Karauda, P.; Tubbs, R. S.; Kurtys, K.; Olewnik, Ł. The Pancreas and Known Factors of Acute Pancreatitis. *Journal of Clinical Medicine* **2022**, *11* (19), 5565. https://doi.org/10.3390/jcm11195565.

(18) Talathi, S. S.; Zimmerman, R.; Young, M. Anatomy, Abdomen and Pelvis, Pancreas. In *StatPearls [Internet]*; StatPearls Publishing, 2023.

(19) Jia, Y.; Liu, Y.; Feng, L.; Sun, S.; Sun, G. Role of Glucagon and Its Receptor in the Pathogenesis of Diabetes. *Front. Endocrinol.* **2022**, *13*. https://doi.org/10.3389/fendo.2022.928016.

(20) Napolitano, T.; Silvano, S.; Vieira, A.; Balaji, S.; Garrido-Utrilla, A.; Friano, M. E.; Atlija, J.; Collombat, P. Role of Ghrelin in Pancreatic Development and Function. *Diabetes, Obesity and Metabolism* **2018**, *20* (S2), 3–10. https://doi.org/10.1111/dom.13385.

(21) Malinova, A.; Veghini, L.; Real, F. X.; Corbo, V. Cell Lineage Infidelity in PDAC Progression and Therapy Resistance. *Front. Cell Dev. Biol.* **2021**, *9*. https://doi.org/10.3389/fcell.2021.795251.

(22) Jennings, R. E.; Berry, A. A.; Strutt, J. P.; Gerrard, D. T.; Hanley, N. A. Human Pancreas Development. *Development* **2015**, *142* (18), 3126–3137. https://doi.org/10.1242/dev.120063.

(23) Benitez, C. M.; Goodyer, W. R.; Kim, S. K. Deconstructing Pancreas Developmental Biology. *Cold Spring Harb Perspect Biol* **2012**, *4* (6), a012401. https://doi.org/10.1101/cshperspect.a012401.

(24) Hogrebe, N. J.; Maxwell, K. G.; Augsornworawat, P.; Millman, J. R. Generation of Insulin-Producing Pancreatic β Cells from Multiple Human Stem Cell Lines. *Nat Protoc* **2021**, *16* (9), 4109–4143. https://doi.org/10.1038/s41596-021-00560-y.

(25) Liu, H.; Li, R.; Liao, H.-K.; Min, Z.; Wang, C.; Yu, Y.; Shi, L.; Dan, J.; Hayek, A.; Martinez Martinez, L.; Nuñez Delicado, E.; Izpisua Belmonte, J. C. Chemical Combinations Potentiate Human Pluripotent Stem Cell-Derived 3D Pancreatic Progenitor Clusters toward Functional β Cells. *Nat Commun* **2021**, *12* (1), 3330. https://doi.org/10.1038/s41467-021-23525-x.

(26) Ma, X.; Lu, Y.; Zhou, Z.; Li, Q.; Chen, X.; Wang, W.; Jin, Y.; Hu, Z.; Chen, G.; Deng, Q.; Shang, W.; Wang, H.; Fu, H.; He, X.; Feng, X.-H.; Zhu, S. Human Expandable Pancreatic Progenitor–Derived β Cells Ameliorate Diabetes. *Sci. Adv.* **2022**, *8* (8), eabk1826. https://doi.org/10.1126/sciadv.abk1826.

(27) Rosado-Olivieri, E. A.; Anderson, K.; Kenty, J. H.; Melton, D. A. YAP Inhibition Enhances the Differentiation of Functional Stem Cell-Derived Insulin-Producing β Cells. *Nat Commun* **2019**, *10* (1), 1464. https://doi.org/10.1038/s41467-019-09404-6.

(28) Zhang, D.; Jiang, W.; Liu, M.; Sui, X.; Yin, X.; Chen, S.; Shi, Y.; Deng, H. Highly Efficient Differentiation of Human ES Cells and iPS Cells into Mature Pancreatic Insulin-Producing Cells. *Cell Res* **2009**, *19* (4), 429–438. https://doi.org/10.1038/cr.2009.28.

(29) Ida, H.; Akiyama, T.; Ishiguro, K.; Goparaju, S. K.; Nakatake, Y.; Chikazawa-Nohtomi, N.; Sato, S.; Kimura, H.; Yokoyama, Y.; Nagino, M.; Ko, M. S. H.; Ko, S. B. H. Establishment of a Rapid and Footprint-Free Protocol for Differentiation of Human Embryonic Stem Cells into Pancreatic Endocrine Cells with Synthetic mRNAs Encoding Transcription Factors. *Stem Cell Res Ther* **2018**, *9* (1), 277. https://doi.org/10.1186/s13287-018-1038-3.

(30) Huang, L.; Holtzinger, A.; Jagan, I.; BeGora, M.; Lohse, I.; Ngai, N.; Nostro, C.; Wang, R.; Muthuswamy, L. B.; Crawford, H. C.; Arrowsmith, C.; Kalloger, S. E.; Renouf, D. J.; Connor, A. A.; Cleary, S.; Schaeffer, D. F.; Roehrl, M.; Tsao, M.-S.; Gallinger, S.; Keller, G.; Muthuswamy, S. K. Ductal Pancreatic Cancer Modeling and Drug Screening Using Human Pluripotent Stem Cell and Patient-Derived Tumor Organoids. *Nat Med* **2015**, *21* (11), 1364–1371. https://doi.org/10.1038/nm.3973.

(31) Simsek, S.; Zhou, T.; Robinson, C. L.; Tsai, S.-Y.; Crespo, M.; Amin, S.; Lin, X.; Hon, J.; Evans, T.; Chen, S. Modeling Cystic Fibrosis Using Pluripotent Stem Cell-Derived Human Pancreatic Ductal Epithelial Cells. *Stem Cells Translational Medicine* **2016**, *5* (5), 572–579. https://doi.org/10.5966/sctm.2015-0276.

(32) Ito, K.; Matsuura, K.; Mihara, Y.; Sakamoto, Y.; Hasegawa, K.; Kokudo, N.; Shimizu, T. Delivery of Pancreatic Digestive Enzymes into the Gastrointestinal Tract by Pancreatic Exocrine Tissue Transplant. *Sci Rep* **2019**, *9* (1), 5922. https://doi.org/10.1038/s41598-019-42362-z.

(33) Hohwieler, M.; Illing, A.; Hermann, P. C.; Mayer, T.; Stockmann, M.; Perkhofer, L.; Eiseler, T.; Antony, J. S.; Müller, M.; Renz, S.; Kuo, C.-C.; Lin, Q.; Sendler, M.; Breunig, M.; Kleiderman, S. M.; Lechel, A.; Zenker, M.; Leichsenring, M.; Rosendahl, J.; Zenke, M.; Sainz, B.; Mayerle, J.; Costa, I. G.; Seufferlein, T.; Kormann, M.; Wagner, M.; Liebau, S.; Kleger, A. Human Pluripotent Stem Cell-Derived Acinar/Ductal Organoids Generate Human Pancreas upon Orthotopic Transplantation and Allow Disease Modelling. *Gut* **2017**, *66* (3), 473–486. https://doi.org/10.1136/gutjnl-2016-312423.

(34) Breunig, M.; Merkle, J.; Wagner, M.; Melzer, M. K.; Barth, T. F. E.; Engleitner, T.; Krumm, J.; Wiedenmann, S.; Cohrs, C. M.; Perkhofer, L.; Jain, G.; Krüger, J.; Hermann, P. C.; Schmid, M.; Madácsy, T.; Varga, Á.; Griger, J.; Azoitei, N.; Müller, M.; Wessely, O.; Robey, P. G.; Heller, S.; Dantes, Z.; Reichert, M.; Günes, C.; Bolenz, C.; Kuhn, F.; Maléth, J.; Speier, S.; Liebau, S.; Sipos, B.; Kuster, B.; Seufferlein, T.; Rad, R.; Meier, M.; Hohwieler, M.; Kleger, A. Modeling Plasticity and Dysplasia of Pancreatic Ductal Organoids Derived from Human Pluripotent Stem Cells. *Cell Stem Cell* **2021**, *28* (6), 1105-1124.e19. https://doi.org/10.1016/j.stem.2021.03.005.

(35) Merz, S.; Breunig, M.; Melzer, M. K.; Heller, S.; Wiedenmann, S.; Seufferlein, T.; Meier, M.; Krüger, J.; Mulaw, M. A.; Hohwieler, M.; Kleger, A. Single-Cell Profiling of GP2-Enriched Pancreatic Progenitors to Simultaneously Create Acinar, Ductal,

and Endocrine Organoids. *Theranostics* **2023**, *13* (6), 1949–1973. https://doi.org/10.7150/thno.78323.

(36) Huang, L.; Desai, R.; Conrad, D. N.; Leite, N. C.; Akshinthala, D.; Lim, C. M.; Gonzalez, R.; Muthuswamy, L. B.; Gartner, Z.; Muthuswamy, S. K. Commitment and Oncogene-Induced Plasticity of Human Stem Cell-Derived Pancreatic Acinar and Ductal Organoids. *Cell Stem Cell* **2021**, *28* (6), 1090-1104.e6. https://doi.org/10.1016/j.stem.2021.03.022.

(37) Fetal and Neonatal Physiology. *Development of the Endocrine and Exocrine Pancreas*. Clinical Tree. https://clinicalpub.com/development-of-the-endocrine-and-exocrine-pancreas/ (accessed 2025-04-03).

(38) Rovira, M.; Delaspre, F.; Massumi, M.; Serra, S. A.; Valverde, M. A.; Lloreta, J.; Dufresne, M.; Payré, B.; Konieczny, S. F.; Savatier, P.; Real, F. X.; Skoudy, A. Murine Embryonic Stem Cell–Derived Pancreatic Acinar Cells Recapitulate Features of Early Pancreatic Differentiation. *Gastroenterology* **2008**, *135* (4), 1301-1310.e5. https://doi.org/10.1053/j.gastro.2008.06.049.

(39) Means, A. L.; Meszoely, I. M.; Suzuki, K.; Miyamoto, Y.; Rustgi, A. K.; Coffey, R. J.; Wright, C. V. E.; Stoffers, D. A.; Leach, S. D. Pancreatic Epithelial Plasticity Mediated by Acinar Cell Transdifferentiation and Generation of Nestin-Positive Intermediates. *Development* **2005**, *132* (16), 3767–3776. https://doi.org/10.1242/dev.01925.

(40) Mfopou, J. K.; Houbracken, I.; Wauters, E.; Mathijs, I.; Song, I.; Himpe, E.; Baldan, J.; Heimberg, H.; Bouwens, L. Acinar Phenotype Is Preserved in Human Exocrine Pancreas Cells Cultured at Low Temperature: Implications for Lineage-Tracing of β-Cell Neogenesis. *Bioscience Reports* **2016**, *36* (3), e00329. https://doi.org/10.1042/BSR20150259.

(41) Yadav, S.; Sharma, P.; Zakalik, D. Comparison of Demographics, Tumor Characteristics, and Survival Between Pancreatic Adenocarcinomas and Pancreatic Neuroendocrine Tumors: A Population-Based Study. *American Journal of Clinical Oncology* **2018**, *41* (5), 485–491. https://doi.org/10.1097/COC.0000000000000305.

(42) Dioguardi Burgio, M.; Ronot, M.; Vilgrain, V. Rare Solid Tumor of the Exocrine Pancreas: A Pictorial Review. *Seminars in Ultrasound, CT and MRI* **2019**, *40* (6), 483–499. https://doi.org/10.1053/j.sult.2019.04.007.

(43) Lei, S.; Mao, Y.; Yang, Q.; Yan, H.; Wang, J. Trends in Pancreatic Cancer Incidence, Prevalence, and Survival Outcomes by Histological Subtypes: A Retrospective Cohort Study. *Gastroenterology Report* **2025**, *13*, goaf030. https://doi.org/10.1093/gastro/goaf030.

(44) Bray, F.; Laversanne, M.; Sung, H.; Ferlay, J.; Siegel, R. L.; Soerjomataram, I.; Jemal, A. Global Cancer Statistics 2022: GLOBOCAN Estimates of Incidence and Mortality Worldwide for 36 Cancers in 185 Countries. *CA: A Cancer Journal for Clinicians* **2024**, *74* (3), 229–263. https://doi.org/10.3322/caac.21834.

(45) Ferlay, J.; Ervik, M.; Lam, F.; Laversanne, M.; Colombet, M.; Mery, L.; Piñeros, M.; Znaor, A.; Soerjomataram, I.; Bray, F. Global Cancer Observatory: Cancer Today, 2024. https://gco.iarc.who.int/today.

(46) Filho, A. M.; Laversanne, M.; Ferlay, J.; Colombet, M.; Piñeros, M.; Znaor, A.; Parkin, D. M.; Soerjomataram, I.; Bray, F. The GLOBOCAN 2022 Cancer Estimates: Data

Sources, Methods, and a Snapshot of the Cancer Burden Worldwide. *International Journal of Cancer* **2025**, *156* (7), 1336–1346. https://doi.org/10.1002/ijc.35278.

(47) Jacobs, M. F.; Stoffel, E. M. Genetic and Other Risk Factors for Pancreatic Ductal Adenocarcinoma (PDAC). *Familial Cancer* **2024**, *23* (3), 221–232. https://doi.org/10.1007/s10689-024-00372-5.

(48) Michalak, N.; Małecka-Wojciesko, E. Modifiable Pancreatic Ductal Adenocarcinoma (PDAC) Risk Factors. *JCM* **2023**, *12* (13), 4318. https://doi.org/10.3390/jcm12134318.

(49) Hu, J.-X.; Zhao, C.-F.; Chen, W.-B.; Liu, Q.-C.; Li, Q.-W.; Lin, Y.-Y.; Gao, F. Pancreatic Cancer: A Review of Epidemiology, Trend, and Risk Factors. *World J Gastroenterol* **2021**, *27* (27), 4298–4321. https://doi.org/10.3748/wjg.v27.i27.4298.

(50) Casolino, R.; Corbo, V.; Beer, P.; Hwang, C.; Paiella, S.; Silvestri, V.; Ottini, L.; Biankin, A. V. Germline Aberrations in Pancreatic Cancer: Implications for Clinical Care. *Cancers* **2022**, *14* (13), 3239. https://doi.org/10.3390/cancers14133239.

(51) Willingham, F.; Raphael, K. Hereditary Pancreatitis: Current Perspectives. *CEG* **2016**, *Volume 9*, 197–207. https://doi.org/10.2147/CEG.S84358.

(52) Beyer, G.; Habtezion, A.; Werner, J.; Lerch, M. M.; Mayerle, J. Chronic Pancreatitis. *The Lancet* **2020**, *396* (10249), 499–512. https://doi.org/10.1016/S0140-6736(20)31318-0.

(53) Eibl, G.; Cruz-Monserrate, Z.; Korc, M.; Petrov, M. S.; Goodarzi, M. O.; Fisher, W. E.; Habtezion, A.; Lugea, A.; Pandol, S. J.; Hart, P. A.; Andersen, D. K. Diabetes Mellitus and Obesity as Risk Factors for Pancreatic Cancer. *J Acad Nutr Diet* **2018**, *118* (4), 555–567. https://doi.org/10.1016/j.jand.2017.07.005.

(54) Mayerle, J. Pancreatic Cancer: Why the Cell of Origin Matters. *Nat Rev Gastroenterol Hepatol* **2022**, *19* (5), 279–279. https://doi.org/10.1038/s41575-022-00595-w.

(55) Guerra, C.; Schuhmacher, A. J.; Cañamero, M.; Grippo, P. J.; Verdaguer, L.; Pérez-Gallego, L.; Dubus, P.; Sandgren, E. P.; Barbacid, M. Chronic Pancreatitis Is Essential for Induction of Pancreatic Ductal Adenocarcinoma by K-Ras Oncogenes in Adult Mice. *Cancer Cell* **2007**, *11* (3), 291–302. https://doi.org/10.1016/j.ccr.2007.01.012.

(56) Habbe, N.; Shi, G.; Meguid, R. A.; Fendrich, V.; Esni, F.; Chen, H.; Feldmann, G.; Stoffers, D. A.; Konieczny, S. F.; Leach, S. D.; Maitra, A. Spontaneous Induction of Murine Pancreatic Intraepithelial Neoplasia (mPanIN) by Acinar Cell Targeting of Oncogenic Kras in Adult Mice. *Proceedings of the National Academy of Sciences* **2008**, *105* (48), 18913–18918. https://doi.org/10.1073/pnas.0810097105.

(57) Ferreira, R. M. M.; Sancho, R.; Messal, H. A.; Nye, E.; Spencer-Dene, B.; Stone, R. K.; Stamp, G.; Rosewell, I.; Quaglia, A.; Behrens, A. Duct- and Acinar-Derived Pancreatic Ductal Adenocarcinomas Show Distinct Tumor Progression and Marker Expression. *Cell Rep* **2017**, *21* (4), 966–978. https://doi.org/10.1016/j.celrep.2017.09.093.

(58) Flowers, B. M.; Xu, H.; Mulligan, A. S.; Hanson, K. J.; Seoane, J. A.; Vogel, H.; Curtis, C.; Wood, L. D.; Attardi, L. D. Cell-of-Origin Influences Pancreatic Cancer Subtype. *Cancer Discov* **2021**, *11* (3), 660–677. https://doi.org/10.1158/2159-8290.CD-20-0633.

(59) Bailey, J. M.; Hendley, A. M.; Lafaro, K. J.; Pruski, M. A.; Jones, N. C.; Alsina, J.; Younes, M.; Maitra, A.; McAllister, F.; Iacobuzio-Donahue, C. A.; Leach, S. D. P53 Mutations Cooperate with Oncogenic Kras to Promote Adenocarcinoma from Pancreatic Ductal Cells. *Oncogene* **2016**, *35* (32), 4282–4288. https://doi.org/10.1038/onc.2015.441.

(60) Lee, A. Y. L.; Dubois, C. L.; Sarai, K.; Zarei, S.; Schaeffer, D. F.; Sander, M.; Kopp, J. L. Cell of Origin Affects Tumor Development and Phenotype in Pancreatic Ductal Adenocarcinoma. *Gut* **2019**, *68* (3), 487–498. https://doi.org/10.1136/gutjnl-2017-314426.

(61) Fischer, C. G.; Wood, L. D. From Somatic Mutation to Early Detection: Insights from Molecular Characterization of Pancreatic Cancer Precursor Lesions. *J Pathol* **2018**, *246* (4), 395–404. https://doi.org/10.1002/path.5154.

(62) Pian, L.; Song, M.; Wang, T.; Qi, L.; Peng, T.; Xie, K. Identification and Analysis of Pancreatic Intraepithelial Neoplasia: Opportunities and Challenges. *Front. Endocrinol.* **2025**, *15*, 1401829. https://doi.org/10.3389/fendo.2024.1401829.

(63) Sagami, R.; Yamao, K.; Nakahodo, J.; Minami, R.; Tsurusaki, M.; Murakami, K.; Amano, Y. Pre-Operative Imaging and Pathological Diagnosis of Localized High-Grade Pancreatic Intra-Epithelial Neoplasia without Invasive Carcinoma. *Cancers* **2021**, *13* (5), 945. https://doi.org/10.3390/cancers13050945.

(64) Andea, A.; Sarkar, F.; Adsay, V. N. Clinicopathological Correlates of Pancreatic Intraepithelial Neoplasia: A Comparative Analysis of 82 Cases with and 152 Cases without Pancreatic Ductal Adenocarcinoma. *Mod Pathol* **2003**, *16* (10), 996–1006. https://doi.org/10.1097/01.MP.0000087422.24733.62.

(65) Carpenter, E. S.; Elhossiny, A. M.; Kadiyala, P.; Li, J.; McGue, J.; Griffith, B. D.; Zhang, Y.; Edwards, J.; Nelson, S.; Lima, F.; Donahue, K. L.; Du, W.; Bischoff, A. C.; Alomari, D.; Watkoske, H. R.; Mattea, M.; The, S.; Espinoza, C. E.; Barrett, M.; Sonnenday, C. J.; Olden, N.; Chen, C.-T.; Peterson, N.; Gunchick, V.; Sahai, V.; Rao, A.; Bednar, F.; Shi, J.; Frankel, T. L.; Pasca di Magliano, M. Analysis of Donor Pancreata Defines the Transcriptomic Signature and Microenvironment of Early Neoplastic Lesions. *Cancer Discovery* **2023**, *13* (6), 1324–1345. https://doi.org/10.1158/2159-8290.CD-23-0013.

(66) Marstrand-Daucé, L.; Lorenzo, D.; Chassac, A.; Nicole, P.; Couvelard, A.; Haumaitre, C. Acinar-to-Ductal Metaplasia (ADM): On the Road to Pancreatic Intraepithelial Neoplasia (PanIN) and Pancreatic Cancer. *IJMS* **2023**, *24* (12), 9946. https://doi.org/10.3390/ijms24129946.

(67) Storz, P. Acinar Cell Plasticity and Development of Pancreatic Ductal Adenocarcinoma. *Nat Rev Gastroenterol Hepatol* **2017**, *14* (5), 296–304. https://doi.org/10.1038/nrgastro.2017.12.

(68) Seidel, T.; Ohri, N.; Glaß, M.; Sunami, Y.; Müller, L. P.; Kleeff, J. Stromal Cells in Early Inflammation-Related Pancreatic Carcinogenesis—Biology and Its Potential Role in Therapeutic Targeting. *Cancers* **2025**, *17* (9), 1541. https://doi.org/10.3390/cancers17091541.

(69) Esposito, I. Pathology of Pancreatic Ductal Adenocarcinoma: Facts, Challenges and Future Developments. *WJG* **2014**, *20* (38), 13833. https://doi.org/10.3748/wjg.v20.i38.13833.

(70) Haeberle, L.; Esposito, I. Pathology of Pancreatic Cancer. *Transl Gastroenterol Hepatol* **2019**, *4*, 50. https://doi.org/10.21037/tgh.2019.06.02.

(71) Wood, L. D.; Adsay, N. V.; Basturk, O.; Brosens, L. A. A.; Fukushima, N.; Hong, S.-M.; Kim, S.-J.; Lee, J. W.; Luchini, C.; Noë, M.; Pitman, M. B.; Scarpa, A.; Singhi, A. D.; Tanaka, M.; Furukawa, T. Systematic Review of Challenging Issues in Pathology of Intraductal Papillary Mucinous Neoplasms. *Pancreatology* **2023**, *23* (7), 878–891. https://doi.org/10.1016/j.pan.2023.08.002.

(72) Li, J.; Wei, T.; Zhang, J.; Liang, T. Intraductal Papillary Mucinous Neoplasms of the Pancreas: A Review of Their Genetic Characteristics and Mouse Models. *Cancers* **2021**, *13* (21), 5296. https://doi.org/10.3390/cancers13215296.

(73) Triantopoulou, C.; Gourtsoyianni, S.; Karakaxas, D.; Delis, S. Intraductal Papillary Mucinous Neoplasm of the Pancreas: A Challenging Diagnosis. *Diagnostics* **2023**, *13* (12), 2015. https://doi.org/10.3390/diagnostics13122015.

(74) Nilsson, L. N.; Keane, M. G.; Shamali, A.; Millastre Bocos, J.; Marijinissen van Zanten, M.; Antila, A.; Verdejo Gil, C.; Del Chiaro, M.; Laukkarinen, J. Nature and Management of Pancreatic Mucinous Cystic Neoplasm (MCN): A Systematic Review of the Literature. *Pancreatology* **2016**, *16* (6), 1028–1036. https://doi.org/10.1016/j.pan.2016.09.011.

(75) Xie, W.; Liang, H.; Guo, Y.; Xiao, S.-Y. Update on Mucinous Cystic Neoplasm of the Pancreas: A Narrative Review. *Journal of Pancreatology* **2021**, *4* (3), 115–121. https://doi.org/10.1097/JP9.0000000000000074.

(76) Vitorakis, N.; Gargalionis, A. N.; Papavassiliou, K. A.; Adamopoulos, C.; Papavassiliou, A. G. Precision Targeting Strategies in Pancreatic Cancer: The Role of Tumor Microenvironment. *Cancers* **2024**, *16* (16), 2876. https://doi.org/10.3390/cancers16162876.

(77) Masugi, Y. The Desmoplastic Stroma of Pancreatic Cancer: Multilayered Levels of Heterogeneity, Clinical Significance, and Therapeutic Opportunities. *Cancers* **2022**, *14* (13), 3293. https://doi.org/10.3390/cancers14133293.

(78) Mercanti, L.; Sindaco, M.; Mazzone, M.; Di Marcantonio, M. C.; Piscione, M.; Muraro, R.; Mincione, G. PDAC, the Influencer Cancer: Cross-Talk with Tumor Microenvironment and Connected Potential Therapy Strategies. *Cancers* **2023**, *15* (11), 2923. https://doi.org/10.3390/cancers15112923.

(79) Opitz, F. V.; Haeberle, L.; Daum, A.; Esposito, I. Tumor Microenvironment in Pancreatic Intraepithelial Neoplasia. *Cancers* **2021**, *13* (24), 6188. https://doi.org/10.3390/cancers13246188.

(80) Elyada, E.; Bolisetty, M.; Laise, P.; Flynn, W. F.; Courtois, E. T.; Burkhart, R. A.; Teinor, J. A.; Belleau, P.; Biffi, G.; Lucito, M. S.; Sivajothi, S.; Armstrong, T. D.; Engle, D. D.; Yu, K. H.; Hao, Y.; Wolfgang, C. L.; Park, Y.; Preall, J.; Jaffee, E. M.; Califano, A.; Robson, P.; Tuveson, D. A. Cross-Species Single-Cell Analysis of Pancreatic Ductal Adenocarcinoma Reveals Antigen-Presenting Cancer-Associated Fibroblasts. *Cancer Discovery* **2019**, *9* (8), 1102–1123. https://doi.org/10.1158/2159-8290.cd-19-0094.

(81) Öhlund, D.; Handly-Santana, A.; Biffi, G.; Elyada, E.; Almeida, A. S.; Ponz-Sarvise, M.; Corbo, V.; Oni, T. E.; Hearn, S. A.; Lee, E. J.; Chio, I. I. C.; Hwang, C.-I.; Tiriac, H.; Baker, L. A.; Engle, D. D.; Feig, C.; Kultti, A.; Egeblad, M.; Fearon, D. T.; Crawford, J. M.; Clevers, H.; Park, Y.; Tuveson, D. A. Distinct Populations of

Inflammatory Fibroblasts and Myofibroblasts in Pancreatic Cancer. *J Exp Med* **2017**, *214* (3), 579–596. https://doi.org/10.1084/jem.20162024.

(82) Biffi, G.; Oni, T. E.; Spielman, B.; Hao, Y.; Elyada, E.; Park, Y.; Preall, J.; Tuveson, D. A. IL1-Induced JAK/STAT Signaling Is Antagonized by TGFβ to Shape CAF Heterogeneity in Pancreatic Ductal Adenocarcinoma. *Cancer Discov* **2019**, *9* (2), 282–301. https://doi.org/10.1158/2159-8290.CD-18-0710.

(83) Bell, A. T. F.; Mitchell, J. T.; Kiemen, A. L.; Lyman, M.; Fujikura, K.; Lee, J. W.; Coyne, E.; Shin, S. M.; Nagaraj, S.; Deshpande, A.; Wu, P.-H.; Sidiropoulos, D. N.; Erbe, R.; Stern, J.; Chan, R.; Williams, S.; Chell, J. M.; Ciotti, L.; Zimmerman, J. W.; Wirtz, D.; Ho, W. J.; Zaidi, N.; Thompson, E.; Jaffee, E. M.; Wood, L. D.; Fertig, E. J.; Kagohara, L. T. PanIN and CAF Transitions in Pancreatic Carcinogenesis Revealed with Spatial Data Integration. *cels* **2024**, *15* (8), 753-769.e5. https://doi.org/10.1016/j.cels.2024.07.001.

(84) Bernard, V.; Semaan, A.; Huang, J.; San Lucas, F. A.; Mulu, F. C.; Stephens, B. M.; Guerrero, P. A.; Huang, Y.; Zhao, J.; Kamyabi, N.; Sen, S.; Scheet, P. A.; Taniguchi, C. M.; Kim, M. P.; Tzeng, C.-W.; Katz, M. H.; Singhi, A. D.; Maitra, A.; Alvarez, H. A. Single Cell Transcriptomics of Pancreatic Cancer Precursors Demonstrates Epithelial and Microenvironmental Heterogeneity as an Early Event in Neoplastic Progression. *Clin Cancer Res* **2019**, *25* (7), 2194–2205. https://doi.org/10.1158/1078-0432.CCR-18-1955.

(85) Garg, B.; Giri, B.; Modi, S.; Sethi, V.; Castro, I.; Umland, O.; Ban, Y.; Lavania, S.; Dawra, R.; Banerjee, S.; Vickers, S.; Merchant, N. B.; Chen, S. X.; Gilboa, E.; Ramakrishnan, S.; Saluja, A.; Dudeja, V. NFκB in Pancreatic Stellate Cells Reduces Infiltration of Tumors by Cytotoxic T Cells and Killing of Cancer Cells, via Up-Regulation of CXCL12. *Gastroenterology* **2018**, *155* (3), 880-891.e8. https://doi.org/10.1053/j.gastro.2018.05.051.

(86) Qin, Q.; Yu, R.; Eriksson, J. E.; Tsai, H.; Zhu, H. Cancer-Associated Fibroblasts in Pancreatic Ductal Adenocarcinoma Therapy: Challenges and Opportunities. *Cancer Letters* **2024**, *591*, 216859. https://doi.org/10.1016/j.canlet.2024.216859.

(87) Özdemir, B. C.; Pentcheva-Hoang, T.; Carstens, J. L.; Zheng, X.; Wu, C.-C.; Simpson, T.; Laklai, H.; Sugimoto, H.; Kahlert, C.; Novitskiy, S. V.; Acosta, A. D.; Sharma, P.; Heidari, P.; Mahmood, U.; Chin, L.; Moses, H.; Weaver, V.; Maitra, A.; Allison, J. P.; LeBleu, V. S.; Kalluri, R. Depletion of Carcinoma-Associated Fibroblasts and Fibrosis Induces Immunosuppression and Accelerates Pancreas Cancer with Diminished Survival. *Cancer Cell* **2014**, *25* (6), 719–734. https://doi.org/10.1016/j.ccr.2014.04.005.

(88) Mizutani, Y.; Kobayashi, H.; Iida, T.; Asai, N.; Masamune, A.; Hara, A.; Esaki, N.; Ushida, K.; Mii, S.; Shiraki, Y.; Ando, K.; Weng, L.; Ishihara, S.; Ponik, S. M.; Conklin, M. W.; Haga, H.; Nagasaka, A.; Miyata, T.; Matsuyama, M.; Kobayashi, T.; Fujii, T.; Yamada, S.; Yamaguchi, J.; Wang, T.; Woods, S. L.; Worthley, D.; Shimamura, T.; Fujishiro, M.; Hirooka, Y.; Enomoto, A.; Takahashi, M. Meflin-Positive Cancer-Associated Fibroblasts Inhibit Pancreatic Carcinogenesis. *Cancer Res* **2019**, *79* (20), 5367–5381. https://doi.org/10.1158/0008-5472.CAN-19-0454.

(89) Yang, S.; Liu, Q.; Liao, Q. Tumor-Associated Macrophages in Pancreatic Ductal Adenocarcinoma: Origin, Polarization, Function, and Reprogramming. *Front. Cell Dev. Biol.* **2021**, *8*, 607209. https://doi.org/10.3389/fcell.2020.607209.

(90) Poh, A. R.; Ernst, M. Tumor-Associated Macrophages in Pancreatic Ductal Adenocarcinoma: Therapeutic Opportunities and Clinical Challenges. *Cancers* **2021**, *13* (12), 2860. https://doi.org/10.3390/cancers13122860.

(91) Ho, W. J.; Jaffee, E. M.; Zheng, L. The Tumour Microenvironment in Pancreatic Cancer — Clinical Challenges and Opportunities | Nature Reviews Clinical Oncology. *Nature Reviews Clinical Oncology* **2020**, No. 17, 527–540. https://doi.org/10.1038/s41571-020-0363-5.

(92) Kiemen, A. L.; Almagro-Pérez, C.; Matos, V.; Forjaz, A.; Braxton, A. M.; Dequiedt, L.; Parksong, J.; Cannon, C. D.; Yuan, X.; Shin, S. M.; Babu, J. M.; Thompson, E. D.; Cornish, T. C.; Ho, W. J.; Wood, L. D.; Wu, P.-H.; Barrutia, A. M.; Hruban, R. H.; Wirtz, D. 3D Histology Reveals That Immune Response to Pancreatic Precancers Is Heterogeneous and Depends on Global Pancreas Structure. bioRxiv 2024. https://doi.org/10.1101/2024.08.03.606493.

(93) Enzler, T.; Shi, J.; McGue, J.; Griffith, B. D.; Sun, L.; Sahai, V.; Nathan, H.; Frankel, T. L. A Comparison of Spatial and Phenotypic Immune Profiles of Pancreatic Ductal Adenocarcinoma and Its Precursor Lesions. *Int J Mol Sci* **2024**, *25* (5), 2953. https://doi.org/10.3390/ijms25052953.

(94) Raskov, H.; Orhan, A.; Christensen, J. P.; Gögenur, I. Cytotoxic CD8+ T Cells in Cancer and Cancer Immunotherapy. *Br J Cancer* **2021**, *124* (2), 359–367. https://doi.org/10.1038/s41416-020-01048-4.

(95) Goulart, M. R.; Stasinos, K.; Fincham, R. E. A.; Delvecchio, F. R.; Kocher, H. M. T Cells in Pancreatic Cancer Stroma. *World J Gastroenterol* **2021**, *27* (46), 7956–7968. https://doi.org/10.3748/wjg.v27.i46.7956.

(96) Ajina, R.; Weiner, L. M. T-Cell Immunity in Pancreatic Cancer. *Pancreas* **2020**, *49* (8), 1014. https://doi.org/10.1097/MPA.0000000000001621.

(97) Hiraoka, N.; Onozato, K.; Kosuge, T.; Hirohashi, S. Prevalence of FOXP3+ Regulatory T Cells Increases during the Progression of Pancreatic Ductal Adenocarcinoma and Its Premalignant Lesions. *Clin Cancer Res* **2006**, *12* (18), 5423–5434. https://doi.org/10.1158/1078-0432.CCR-06-0369.

(98) Zhang, Y.; Lazarus, J.; Steele, N. G.; Yan, W.; Lee, H.-J.; Nwosu, Z. C.; Halbrook, C. J.; Menjivar, R. E.; Kemp, S. B.; Sirihorachai, V. R.; Velez-Delgado, A.; Donahue, K.; Carpenter, E. S.; Brown, K. L.; Irizarry-Negron, V.; Nevison, A. C.; Vinta, A.; Anderson, M. A.; Crawford, H. C.; Lyssiotis, C. A.; Frankel, T. L.; Bednar, F.; Pasca di Magliano, M. Regulatory T-Cell Depletion Alters the Tumor Microenvironment and Accelerates Pancreatic Carcinogenesis. *Cancer Discov* **2020**, *10* (3), 422–439. https://doi.org/10.1158/2159-8290.CD-19-0958.

(99) Dong, P.; Yan, Y.; Fan, Y.; Wang, H.; Wu, D.; Yang, L.; Zhang, J.; Yin, X.; Lv, Y.; Zhang, J.; Hou, Y.; Liu, F.; Yu, X. The Role of Myeloid-Derived Suppressor Cells in the Treatment of Pancreatic Cancer. *Technol Cancer Res Treat* **2022**, *21*, 15330338221142472. https://doi.org/10.1177/15330338221142472.

(100) Kemp, S. B.; Pasca di Magliano, M.; Crawford, H. C. Myeloid Cell Mediated Immune Suppression in Pancreatic Cancer. *Cellular and Molecular Gastroenterology and Hepatology* **2021**, *12* (5), 1531–1542. https://doi.org/10.1016/j.jcmgh.2021.07.006.

(101) Robertson, F. P.; Cameron, A.; Spiers, H. V. M.; Joseph, N.; Taylor, E.; Ratnayake, B.; Jamieson, N. B.; Pandanaboyana, S. Evidence for Molecular Subtyping in

Pancreatic Ductal Adenocarcinoma: A Systematic Review. *HPB* **2024**, *26* (5), 609–617. https://doi.org/10.1016/j.hpb.2024.02.001.

(102) Moffitt, R. A.; Marayati, R.; Flate, E. L.; Volmar, K. E.; Loeza, S. G. H.; Hoadley, K. A.; Rashid, N. U.; Williams, L. A.; Eaton, S. C.; Chung, A. H.; Smyla, J. K.; Anderson, J. M.; Kim, H. J.; Bentrem, D. J.; Talamonti, M. S.; Iacobuzio-Donahue, C. A.; Hollingsworth, M. A.; Yeh, J. J. Virtual Microdissection Identifies Distinct Tumor- and Stroma-Specific Subtypes of Pancreatic Ductal Adenocarcinoma. *Nat Genet* **2015**, *47* (10), 1168–1178. https://doi.org/10.1038/ng.3398.

(103) Collisson, E. A.; Sadanandam, A.; Olson, P.; Gibb, W. J.; Truitt, M.; Gu, S.; Cooc, J.; Weinkle, J.; Kim, G. E.; Jakkula, L.; Feiler, H. S.; Ko, A. H.; Olshen, A. B.; Danenberg, K. L.; Tempero, M. A.; Spellman, P. T.; Hanahan, D.; Gray, J. W. Subtypes of Pancreatic Ductal Adenocarcinoma and Their Differing Responses to Therapy. *Nat Med* **2011**, *17* (4), 500–503. https://doi.org/10.1038/nm.2344.

(104) Collisson, E. A.; Bailey, P.; Chang, D. K.; Biankin, A. V. Molecular Subtypes of Pancreatic Cancer. *Nat Rev Gastroenterol Hepatol* **2019**, *16* (4), 207–220. https://doi.org/10.1038/s41575-019-0109-y.

(105) Puleo, F.; Nicolle, R.; Blum, Y.; Cros, J.; Marisa, L.; Demetter, P.; Quertinmont, E.; Svrcek, M.; Elarouci, N.; Iovanna, J.; Franchimont, D.; Verset, L.; Galdon, M. G.; Devière, J.; de Reyniès, A.; Laurent-Puig, P.; Van Laethem, J.-L.; Bachet, J.-B.; Maréchal, R. Stratification of Pancreatic Ductal Adenocarcinomas Based on Tumor and Microenvironment Features. *Gastroenterology* **2018**, *155* (6), 1999-2013.e3. https://doi.org/10.1053/j.gastro.2018.08.033.

(106) Bailey, P.; Chang, D. K.; Nones, K.; Johns, A. L.; Patch, A.-M.; Gingras, M.-C.; Miller, D. K.; Christ, A. N.; Bruxner, T. J. C.; Quinn, M. C.; Nourse, C.; Murtaugh, L. C.; Harliwong, I.; Idrisoglu, S.; Manning, S.; Nourbakhsh, E.; Wani, S.; Fink, L.; Holmes, O.; Chin, V.; Anderson, M. J.; Kazakoff, S.; Leonard, C.; Newell, F.; Waddell, N.; Wood, S.; Xu, Q.; Wilson, P. J.; Cloonan, N.; Kassahn, K. S.; Taylor, D.; Quek, K.; Robertson, A.; Pantano, L.; Mincarelli, L.; Sanchez, L. N.; Evers, L.; Wu, J.; Pinese, M.; Cowley, M. J.; Jones, M. D.; Colvin, E. K.; Nagrial, A. M.; Humphrey, E. S.; Chantrill, L. A.; Mawson, A.; Humphris, J.; Chou, A.; Pajic, M.; Scarlett, C. J.; Pinho, A. V.; Giry-Laterriere, M.; Rooman, I.; Samra, J. S.; Kench, J. G.; Lovell, J. A.; Merrett, N. D.; Toon, C. W.; Epari, K.; Nguyen, N. Q.; Barbour, A.; Zeps, N.; Moran-Jones, K.; Jamieson, N. B.; Graham, J. S.; Duthie, F.; Oien, K.; Hair, J.; Grützmann, R.; Maitra, A.; Iacobuzio-Donahue, C. A.; Wolfgang, C. L.; Morgan, R. A.; Lawlor, R. T.; Corbo, V.; Bassi, C.; Rusev, B.; Capelli, P.; Salvia, R.; Tortora, G.; Mukhopadhyay, D.; Petersen, G. M.; Munzy, D. M.; Fisher, W. E.; Karim, S. A.; Eshleman, J. R.; Hruban, R. H.; Pilarsky, C.; Morton, J. P.; Sansom, O. J.; Scarpa, A.; Musgrove, E. A.; Bailey, U.-M. H.; Hofmann, O.; Sutherland, R. L.; Wheeler, D. A.; Gill, A. J.; Gibbs, R. A.; Pearson, J. V.; Waddell, N.; Biankin, A. V.; Grimmond, S. M. Genomic Analyses Identify Molecular Subtypes of Pancreatic Cancer. *Nature* **2016**, *531* (7592), 47–52. https://doi.org/10.1038/nature16965.

(107) Zhang, Z.; Zhang, H.; Liao, X.; Tsai, H. KRAS Mutation: The Booster of Pancreatic Ductal Adenocarcinoma Transformation and Progression. *Front. Cell Dev. Biol.* **2023**, *11*, 1147676. https://doi.org/10.3389/fcell.2023.1147676.

(108) Dai, M.; Chen, S.; Teng, X.; Chen, K.; Cheng, W. KRAS as a Key Oncogene in the Clinical Precision Diagnosis and Treatment of Pancreatic Cancer. *J Cancer* **2022**, *13* (11), 3209–3220. https://doi.org/10.7150/jca.76695.

(109) Luo, J. KRAS Mutation in Pancreatic Cancer. *Semin Oncol* **2021**, *48* (1), 10–18. https://doi.org/10.1053/j.seminoncol.2021.02.003.

(110) Collins, M. A.; Bednar, F.; Zhang, Y.; Brisset, J.-C.; Galbán, S.; Galbán, C. J.; Rakshit, S.; Flannagan, K. S.; Adsay, N. V.; Pasca di Magliano, M. Oncogenic Kras Is Required for Both the Initiation and Maintenance of Pancreatic Cancer in Mice. *J Clin Invest* **2012**, *122* (2), 639–653. https://doi.org/10.1172/JCI59227.

(111) Mueller, S.; Engleitner, T.; Maresch, R.; Zukowska, M.; Lange, S.; Kaltenbacher, T.; Konukiewitz, B.; Öllinger, R.; Zwiebel, M.; Strong, A.; Yen, H.-Y.; Banerjee, R.; Louzada, S.; Fu, B.; Seidler, B.; Götzfried, J.; Schuck, K.; Hassan, Z.; Arbeiter, A.; Schönhuber, N.; Klein, S.; Veltkamp, C.; Friedrich, M.; Rad, L.; Barenboim, M.; Ziegenhain, C.; Hess, J.; Dovey, O. M.; Eser, S.; Parekh, S.; Constantino-Casas, F.; de la Rosa, J.; Sierra, M. I.; Fraga, M.; Mayerle, J.; Klöppel, G.; Cadiñanos, J.; Liu, P.; Vassiliou, G.; Weichert, W.; Steiger, K.; Enard, W.; Schmid, R. M.; Yang, F.; Unger, K.; Schneider, G.; Varela, I.; Bradley, A.; Saur, D.; Rad, R. Evolutionary Routes and KRAS Dosage Define Pancreatic Cancer Phenotypes. *Nature* **2018**, *554* (7690), 62–68. https://doi.org/10.1038/nature25459.

(112) Shen, X.; Niu, N.; Xue, J. Oncogenic KRAS Triggers Metabolic Reprogramming in Pancreatic Ductal Adenocarcinoma. *J Transl Int Med* **2022**, *11* (4), 322–329. https://doi.org/10.2478/jtim-2022-0022.

(113) Liu, Y.-H.; Hu, C.-M.; Hsu, Y.-S.; Lee, W.-H. Interplays of Glucose Metabolism and KRAS Mutation in Pancreatic Ductal Adenocarcinoma. *Cell Death Dis* **2022**, *13* (9), 817. https://doi.org/10.1038/s41419-022-05259-w.

(114) Ma, Q.; Zhang, W.; Wu, K.; Shi, L. The Roles of KRAS in Cancer Metabolism, Tumor Microenvironment and Clinical Therapy. *Molecular Cancer* **2025**, *24* (1), 14. https://doi.org/10.1186/s12943-024-02218-1.

(115) Rozeveld, C. N.; Johnson, K. M.; Zhang, L.; Razidlo, G. L. KRAS Controls Pancreatic Cancer Cell Lipid Metabolism and Invasive Potential through the Lipase HSL. *Cancer Res* **2020**, *80* (22), 4932–4945. https://doi.org/10.1158/0008-5472.CAN-20-1255.

(116) Kawada, K.; Toda, K.; Sakai, Y. Targeting Metabolic Reprogramming in KRAS-Driven Cancers. *Int J Clin Oncol* **2017**, *22* (4), 651–659. https://doi.org/10.1007/s10147-017-1156-4.

(117) Hafezi, S.; Saber-Ayad, M.; Abdel-Rahman, W. M. Highlights on the Role of KRAS Mutations in Reshaping the Microenvironment of Pancreatic Adenocarcinoma. *International Journal of Molecular Sciences* **2021**, *22* (19), 10219. https://doi.org/10.3390/ijms221910219.

(118) Linehan, A.; O'Reilly, M.; McDermott, R.; O'Kane, G. M. Targeting KRAS Mutations in Pancreatic Cancer: Opportunities for Future Strategies. *Front. Med.* **2024**, *11*. https://doi.org/10.3389/fmed.2024.1369136.

(119) Kung, H.-C.; Zheng, K. W.; Zimmerman, J. W.; Zheng, L. The Tumour Microenvironment in Pancreatic Cancer — New Clinical Challenges, but More Opportunities. *Nat Rev Clin Oncol* **2025**, 1–27. https://doi.org/10.1038/s41571-025-01077-z.

(120) Caban, M.; Małecka-Wojciesko, E. Gaps and Opportunities in the Diagnosis and Treatment of Pancreatic Cancer. *Cancers* **2023**, *15* (23), 5577. https://doi.org/10.3390/cancers15235577.

(121) Conroy, T.; Pfeiffer, P.; Vilgrain, V.; Lamarca, A.; Seufferlein, T.; O'Reilly, E. M.; Hackert, T.; Golan, T.; Prager, G.; Haustermans, K.; Vogel, A.; Ducreux, M. Pancreatic Cancer: ESMO Clinical Practice Guideline for Diagnosis, Treatment and Follow-Up -. *Annals of Oncology* **2023**, *34* (11), 987–1002.

(122) Pekarek, L.; Fraile-Martinez, O.; Garcia-Montero, C.; Alvarez-Mon, M.; Acero, J.; Ruiz-Llorente, L.; García-Honduvilla, N.; Albillos, A.; Buján, J.; Alvarez-Mon, M.; Guijarro, L.; Ortega, M. Towards an Updated View on the Clinical Management of Pancreatic Adenocarcinoma: Current and Future Perspectives (Review). *Oncol Lett* **2021**, *22* (5), 809. https://doi.org/10.3892/ol.2021.13070.

(123) Cao, K.; Xia, Y.; Yao, J.; Han, X.; Lambert, L.; Zhang, T.; Tang, W.; Jin, G.; Jiang, H.; Fang, X.; Nogues, I.; Li, X.; Guo, W.; Wang, Y.; Fang, W.; Qiu, M.; Hou, Y.; Kovarnik, T.; Vocka, M.; Lu, Y.; Chen, Y.; Chen, X.; Liu, Z.; Zhou, J.; Xie, C.; Zhang, R.; Lu, H.; Hager, G. D.; Yuille, A. L.; Lu, L.; Shao, C.; Shi, Y.; Zhang, Q.; Liang, T.; Zhang, L.; Lu, J. Large-Scale Pancreatic Cancer Detection via Non-Contrast CT and Deep Learning. *Nat Med* **2023**, *29* (12), 3033–3043. https://doi.org/10.1038/s41591-023-02640-w.

(124) Tarasiuk, A.; Mackiewicz, T.; Małecka-Panas, E.; Fichna, J. Biomarkers for Early Detection of Pancreatic Cancer – miRNAs as a Potential Diagnostic and Therapeutic Tool? *Cancer Biology & Therapy* **2021**, *22* (5–6), 347–356. https://doi.org/10.1080/15384047.2021.1941584.

(125) Guo, S.; Fesler, A.; Wang, H.; Ju, J. microRNA Based Prognostic Biomarkers in Pancreatic Cancer. *Biomark Res* **2018**, *6* (1), 18. https://doi.org/10.1186/s40364-018-0131-1.

(126) Edland, K. H.; Tjensvoll, K.; Oltedal, S.; Dalen, I.; Lapin, M.; Garresori, H.; Glenjen, N.; Gilje, B.; Nordgård, O. Monitoring of Circulating Tumour DNA in Advanced Pancreatic Ductal Adenocarcinoma Predicts Clinical Outcome and Reveals Disease Progression Earlier than Radiological Imaging. *Mol Oncol* **2023**, *17* (9), 1857–1870. https://doi.org/10.1002/1878-0261.13472.

(127) Zhang, X.-P.; Xu, S.; Gao, Y.-X.; Zhao, Z.-M.; Zhao, G.-D.; Hu, M.-G.; Tan, X.-L.; Lau, W. Y.; Liu, R. Early and Late Recurrence Patterns of Pancreatic Ductal Adenocarcinoma after Pancreaticoduodenectomy: A Multicenter Study. *Int J Surg* **2023**, *109* (4), 785–793. https://doi.org/10.1097/JS9.0000000000000296.

(128) Koltai, T.; Reshkin, S. J.; Carvalho, T. M. A.; Di Molfetta, D.; Greco, M. R.; Alfarouk, K. O.; Cardone, R. A. Resistance to Gemcitabine in Pancreatic Ductal Adenocarcinoma: A Physiopathologic and Pharmacologic Review. *Cancers* **2022**, *14* (10), 2486. https://doi.org/10.3390/cancers14102486.

(129) Oettle, H.; Post, S.; Neuhaus, P.; Gellert, K.; Langrehr, J. Adjuvant Chemotherapy With Gemcitabine vs Observation in Patients Undergoing Curative-Intent Resection of Pancreatic Cancer. *JAMA* **2007**, *3* (297), 267–277. https://doi.org/doi: 10.1001/jama.297.3.267.

(130) Burris, H. A.; Moore, M. J.; Andersen, J.; Green, M. R.; Rothenberg, M. L.; Modiano, M. R.; Cripps, M. C.; Portenoy, R. K.; Storniolo, A. M.; Nelson, P. T., R.; Dorr, F. A.; Stephens, C. D.; von Hoff, D. D. Improvements in Survival and Clinical Benefit with Gemcitabine as First-Line Therapy for Patients with Advanced Pancreas Cancer: A Randomized Trial. *Journal of Clinical Oncology* **1997**, *15* (6). https://doi.org/10.1200/JCO.1997.15.6.240.

(131) Zhang, X.-W.; Ma, Y.-X.; Sun, Y.; Cao, Y.-B.; Li, Q.; Xu, C.-A. Gemcitabine in Combination with a Second Cytotoxic Agent in the First-Line Treatment of Locally Advanced or Metastatic Pancreatic Cancer: A Systematic Review and Meta-Analysis. *Targ Oncol* **2017**, *12* (3), 309–321. https://doi.org/10.1007/s11523-017-0486-5.

(132) Von Hoff, D. D.; Ervin, T.; Arena, F. P.; Chiorean, E. G.; Infante, J.; Moore, M.; Seay, T.; Tjulandin, S. A.; Ma, W. W.; Saleh, M. N.; Harris, M.; Reni, M.; Dowden, S.; Laheru, D.; Bahary, N.; Ramanathan, R. K.; Tabernero, J.; Hidalgo, M.; Goldstein, D.; Van Cutsem, E.; Wei, X.; Iglesias, J.; Renschler, M. F. Increased Survival in Pancreatic Cancer with Nab-Paclitaxel plus Gemcitabine. *N Engl J Med* **2013**, *369* (18), 1691–1703. https://doi.org/10.1056/NEJMoa1304369.

(133) Conroy, T.; Castan, F.; Lopez, A.; Turpin, A.; Ben Abdelghani, M.; Wei, A. C.; Mitry, E.; Biagi, J. J.; Evesque, L.; Artru, P.; Lecomte, T.; Assenat, E.; Bauguion, L.; Ychou, M.; Bouché, O.; Monard, L.; Lambert, A.; Hammel, P.; Canadian Cancer Trials Group and the Unicancer-GI–PRODIGE Group. Five-Year Outcomes of FOLFIRINOX vs Gemcitabine as Adjuvant Therapy for Pancreatic Cancer: A Randomized Clinical Trial. *JAMA Oncol* **2022**, *8* (11), 1571–1578. https://doi.org/10.1001/jamaoncol.2022.3829.

(134) Conroy, T.; Hammel, P.; Hebbar, M.; Abdelghani, M. B.; Wei, A. C.; Raoul, J.-L.; Choné, L.; Francois, E.; Artru, P.; Biagi, J. J.; Lecomte, T.; Assenat, E.; Faroux, R.; Ychou, M.; Volet, J.; Sauvanet, A.; Breysacher, G.; Fiore, F. D.; Cripps, C.; Kavan, P.; Texereau, P.; Bouhier-Leporrier, K.; Khemissa-Akouz, F.; Legoux, J.-L.; Juzyna, B.; Gourgou, S.; O'Callaghan, C. J.; Jouffroy-Zeller, C.; Rat, P.; Malka, D.; Castan, F.; Bachet, J.-B. FOLFIRINOX or Gemcitabine as Adjuvant Therapy for Pancreatic Cancer. *New England Journal of Medicine* **2018**. https://doi.org/10.1056/NEJMoa1809775.

(135) Zeng, S.; Pöttler, M.; Lan, B.; Grützmann, R.; Pilarsky, C.; Yang, H. Chemoresistance in Pancreatic Cancer. *Int J Mol Sci* **2019**, *20* (18), 4504. https://doi.org/10.3390/ijms20184504.

(136) Zhao, X.; Li, Z.; Gu, Z. A New Era: Tumor Microenvironment in Chemoresistance of Pancreatic Cancer. *J Cancer Sci Clin Ther* **2022**, *6* (1), 61–86. https://doi.org/10.26502/jcsct.5079146.

(137) Bhoopathi, P.; Mannangatti, P.; Das, S. K.; Fisher, P. B.; Emdad, L. Chapter Nine - Chemoresistance in Pancreatic Ductal Adenocarcinoma: Overcoming Resistance to Therapy. In *Advances in Cancer Research*; Emdad, L., Atfi, A., Gogna, R., Trevino, J. G., Fisher, P. B., Eds.; Pancreatic Cancer: Basic Mechanisms and Therapies; Academic Press, 2023; Vol. 159, pp 285–341. https://doi.org/10.1016/bs.acr.2023.02.010.

(138) Long, S.-A.; Amparo, A. M.; Goodhart, G.; Ahmad, S. A.; Waters, A. M. Evaluation of KRAS Inhibitor-Directed Therapies for Pancreatic Cancer Treatment. *Front. Oncol.* **2024**, *14*, 1402128. https://doi.org/10.3389/fonc.2024.1402128.

(139) Bannoura, S. F.; Uddin, Md. H.; Nagasaka, M.; Fazili, F.; Al-Hallak, M. N.; Philip, P. A.; El-Rayes, B.; Azmi, A. S. Targeting KRAS in Pancreatic Cancer: New Drugs on the Horizon. *Cancer Metastasis Rev* **2021**, *40* (3), 819–835. https://doi.org/10.1007/s10555-021-09990-2.

(140) Ostrem, J. M.; Peters, U.; Sos, M. L.; Wells, J. A.; Shokat, K. M. K-Ras(G12C) Inhibitors Allosterically Control GTP Affinity and Effector Interactions. *Nature* **2013**, *503* (7477), 548–551. https://doi.org/10.1038/nature12796.

(141) Wang, X.; Allen, S.; Blake, J. F.; Bowcut, V.; Briere, D. M.; Calinisan, A.; Dahlke, J. R.; Fell, J. B.; Fischer, J. P.; Gunn, R. J.; Hallin, J.; Laguer, J.; Lawson, J. D.; Medwid, J.; Newhouse, B.; Nguyen, P.; O'Leary, J. M.; Olson, P.; Pajk, S.; Rahbaek, L.; Rodriguez, M.; Smith, C. R.; Tang, T. P.; Thomas, N. C.; Vanderpool, D.; Vigers, G. P.; Christensen, J. G.; Marx, M. A. Identification of MRTX1133, a Noncovalent, Potent, and Selective KRASG12D Inhibitor. *J. Med. Chem.* **2022**, *65* (4), 3123–3133. https://doi.org/10.1021/acs.jmedchem.1c01688.

(142) Kemp, S. B.; Cheng, N.; Markosyan, N.; Sor, R.; Kim, I.-K.; Hallin, J.; Shoush, J.; Quinones, L.; Brown, N. V.; Bassett, J. B.; Joshi, N.; Yuan, S.; Smith, M.; Vostrejs, W. P.; Perez-Vale, K. Z.; Kahn, B.; Mo, F.; Donahue, T. R.; Radu, C. G.; Clendenin, C.; Christensen, J. G.; Vonderheide, R. H.; Stanger, B. Z. Efficacy of a Small-Molecule Inhibitor of KrasG12D in Immunocompetent Models of Pancreatic Cancer. *Cancer Discov* **2023**, *13* (2), 298–311. https://doi.org/10.1158/2159-8290.CD-22-1066.

(143) Mirati Therapeutics Inc. *A Phase 1/2 Multiple Expansion Cohort Trial of MRTX1133 in Patients With Advanced Solid Tumors Harboring a KRAS G12D Mutation*; Clinical trial registration NCT05737706; clinicaltrials.gov, 2025. https://clinicaltrials.gov/study/NCT05737706 (accessed 2025-11-05).

(144) Revolution Medicines, Inc. *Phase 1/1b, Multicenter, Open-Label, Study of RMC 9805 in Participants With Advanced KRASG 12D-Mutant Solid Tumors*; Clinical trial registration NCT06040541; clinicaltrials.gov, 2025. https://clinicaltrials.gov/study/NCT06040541 (accessed 2025-11-05).

(145) Jiang, L.; Menard, M.; Weller, C.; Wang, Z.; Burnett, L.; Aronchik, I.; Steele, S.; Flagella, M.; Zhao, R.; Evans, J. W. W.; Chin, S.; Chou, K.-J.; Mu, Y.; Longhi, M.; McDowell, L.; Knox, J. E.; Gill, A.; Smith, J. A.; Singh, M.; Quintana, E.; Jiang, J. Abstract 526: RMC-9805, a First-in-Class, Mutant-Selective, Covalent and Oral KRASG12D(ON) Inhibitor That Induces Apoptosis and Drives Tumor Regression in Preclinical Models of KRASG12D Cancers. *Cancer Res* **2023**, *83* (7_Supplement), 526. https://doi.org/10.1158/1538-7445.AM2023-526.

(146) Holderfield, M.; Lee, B. J.; Jiang, J.; Tomlinson, A.; Seamon, K. J.; Mira, A.; Patrucco, E.; Goodhart, G.; Dilly, J.; Gindin, Y.; Dinglasan, N.; Wang, Y.; Lai, L. P.; Cai, S.; Jiang, L.; Nasholm, N.; Shifrin, N.; Blaj, C.; Shah, H.; Evans, J. W.; Montazer, N.; Lai, O.; Shi, J.; Ahler, E.; Quintana, E.; Chang, S.; Salvador, A.; Marquez, A.; Cregg, J.; Liu, Y.; Milin, A.; Chen, A.; Ziv, T. B.; Parsons, D.; Knox, J. E.; Klomp, J. E.; Roth, J.; Rees, M.; Ronan, M.; Cuevas-Navarro, A.; Hu, F.; Lito, P.; Santamaria, D.; Aguirre, A. J.; Waters, A. M.; Der, C. J.; Ambrogio, C.; Wang, Z.; Gill, A. L.; Koltun, E. S.; Smith, J. A. M.; Wildes, D.; Singh, M. Concurrent Inhibition of Oncogenic and Wild-Type RAS-GTP for Cancer Therapy. *Nature* **2024**, *629* (8013), 919–926. https://doi.org/10.1038/s41586-024-07205-6.

(147) Jiang, J.; Jiang, L.; Maldonato, B. J.; Wang, Y.; Holderfield, M.; Aronchik, I.; Winters, I. P.; Salman, Z.; Blaj, C.; Menard, M.; Brodbeck, J.; Chen, Z.; Wei, X.; Rosen, M. J.; Gindin, Y.; Lee, B. J.; Evans, J. W.; Chang, S.; Wang, Z.; Seamon, K. J.; Parsons, D.; Cregg, J.; Marquez, A.; Tomlinson, A. C. A.; Yano, J. K.; Knox, J. E.; Quintana, E.; Aguirre, A. J.; Arbour, K. C.; Reed, A.; Gustafson, W. C.; Gill, A. L.; Koltun, E. S.; Wildes, D.; Smith, J. A. M.; Wang, Z.; Singh, M. Translational and Therapeutic Evaluation of RAS-GTP Inhibition by RMC-6236 in RAS-Driven Cancers. *Cancer Discov* **2024**, *14* (6), 994–1017. https://doi.org/10.1158/2159-8290.CD-24-0027.

(148) Isermann, T.; Sers, C.; Der, C. J.; Papke, B. KRAS Inhibitors: Resistance Drivers and Combinatorial Strategies. *Trends in Cancer* **2025**, *11* (2), 91–116. https://doi.org/10.1016/j.trecan.2024.11.009.

(149) Dilly, J.; Hoffman, M. T.; Abbassi, L.; Li, Z.; Paradiso, F.; Parent, B. D.; Hennessey, C. J.; Jordan, A. C.; Morgado, M.; Dasgupta, S.; Uribe, G. A.; Yang, A.; Kapner, K. S.; Hambitzer, F. P.; Qiang, L.; Feng, H.; Geisberg, J.; Wang, J.; Evans, K. E.; Lyu, H.; Schalck, A.; Feng, N.; Lopez, A. M.; Bristow, C. A.; Kim, M. P.; Rajapakshe, K. I.; Bahrambeigi, V.; Roth, J. A.; Garg, K.; Guerrero, P. A.; Stanger, B. Z.; Cristea, S.; Lowe, S. W.; Baslan, T.; Van Allen, E. M.; Mancias, J. D.; Chan, E.; Anderson, A.; Katlinskaya, Y. V.; Shalek, A. K.; Hong, D. S.; Pant, S.; Hallin, J.; Anderes, K.; Olson, P.; Heffernan, T. P.; Chugh, S.; Christensen, J. G.; Maitra, A.; Wolpin, B. M.; Raghavan, S.; Nowak, J. A.; Winter, P. S.; Dougan, S. K.; Aguirre, A. J. Mechanisms of Resistance to Oncogenic KRAS Inhibition in Pancreatic Cancer. *Cancer Discov* **2024**, *14* (11), 2135–2161. https://doi.org/10.1158/2159-8290.CD-24-0177.

(150) Krempley, B. D.; Yu, K. H. Preclinical Models of Pancreatic Ductal Adenocarcinoma. *Chinese Clinical Oncology* **2017**, *6* (3), 25–25. https://doi.org/10.21037/cco.2017.06.15.

(151) Suri, R.; Zimmerman, J. W.; Burkhart, R. A. Modeling Human Pancreatic Ductal Adenocarcinoma for Translational Research: Current Options, Challenges, and Prospective Directions. *Ann Pancreat Cancer* **2020**, *3*, 17. https://doi.org/10.21037/apc-20-29.

(152) Dobrynin, Y. V. Establishment and Characteristics of Cell Strains From Some Epithelial Tumors of Human Origin. *J Natl Cancer Inst* **1963**, *31* (5), 1173–1195. https://doi.org/10.1093/jnci/31.5.1173.

(153) Garcia, P. L.; Miller, A. L.; Yoon, K. J. Patient-Derived Xenograft Models of Pancreatic Cancer: Overview and Comparison with Other Types of Models. *Cancers (Basel)* **2020**, *12* (5), 1327. https://doi.org/10.3390/cancers12051327.

(154) Miquel, M.; Zhang, S.; Pilarsky, C. Pre-Clinical Models of Metastasis in Pancreatic Cancer. *Front. Cell Dev. Biol.* **2021**, *9*, 748631. https://doi.org/10.3389/fcell.2021.748631.

(155) Hingorani, S. R.; Wang, L.; Multani, A. S.; Combs, C.; Deramaudt, T. B.; Hruban, R. H.; Rustgi, A. K.; Chang, S.; Tuveson, D. A. Trp53R172H and KrasG12D Cooperate to Promote Chromosomal Instability and Widely Metastatic Pancreatic Ductal Adenocarcinoma in Mice. *Cancer Cell* **2005**, *7* (5), 469–483. https://doi.org/10.1016/j.ccr.2005.04.023.

(156) Dennaoui, R.; Shrestha, H.; Wagner, K.-U. Models of Pancreatic Ductal Adenocarcinoma. *Cancer Metastasis Rev* **2021**, *40* (3), 803–818. https://doi.org/10.1007/s10555-021-09989-9.

(157) Pitter, K. L.; Grbovic-Huezo, O.; Joost, S.; Singhal, A.; Blum, M.; Wu, K.; Holm, M.; Ferrena, A.; Bhutkar, A.; Hudson, A.; Lecomte, N.; de Stanchina, E.; Chaligne, R.; Iacobuzio-Donahue, C. A.; Pe'er, D.; Tammela, T. Systematic Comparison of Pancreatic Ductal Adenocarcinoma Models Identifies a Conserved Highly Plastic Basal Cell State. *Cancer Res* **2022**, *82* (19), 3549–3560. https://doi.org/10.1158/0008-5472.CAN-22-1742.

(158) Gopinathan, A.; Morton, J. P.; Jodrell, D. I.; Sansom, O. J. GEMMs as Preclinical Models for Testing Pancreatic Cancer Therapies. *Disease Models & Mechanisms* **2015**, *8* (10), 1185–1200. https://doi.org/10.1242/dmm.021055.

(159) Yu, Y.; Yang, G.; Huang, H.; Fu, Z.; Cao, Z.; Zheng, L.; You, L.; Zhang, T. Preclinical Models of Pancreatic Ductal Adenocarcinoma: Challenges and Opportunities in the Era of Precision Medicine. *Journal of Experimental & Clinical Cancer Research* **2021**, *40* (1), 8. https://doi.org/10.1186/s13046-020-01787-5.

(160) Poh, W. T.; Stanslas, J. The New Paradigm in Animal Testing – "3Rs Alternatives." *Regulatory Toxicology and Pharmacology* **2024**, *153*, 105705. https://doi.org/10.1016/j.yrtph.2024.105705.

(161) Zhao, Z.; Chen, X.; Dowbaj, A. M.; Sljukic, A.; Bratlie, K.; Lin, L.; Fong, E. L. S.; Balachander, G. M.; Chen, Z.; Soragni, A.; Huch, M.; Zeng, Y. A.; Wang, Q.; Yu, H. Organoids. *Nat Rev Methods Primers* **2022**, *2* (1), 94. https://doi.org/10.1038/s43586-022-00174-y.

(162) Hofer, M.; Lutolf, M. P. Engineering Organoids. *Nat Rev Mater* **2021**, *6* (5), 402–420. https://doi.org/10.1038/s41578-021-00279-y.

(163) Piro, G.; Agostini, A.; Larghi, A.; Quero, G.; Carbone, C.; Esposito, A.; Rizzatti, G.; Attili, F.; Alfieri, S.; Costamagna, G.; Tortora, G. Pancreatic Cancer Patient-Derived Organoid Platforms: A Clinical Tool to Study Cell- and Non-Cell-Autonomous Mechanisms of Treatment Response. *Front. Med.* **2021**, *8*. https://doi.org/10.3389/fmed.2021.793144.

(164) Boj, S. F.; Hwang, C.-I.; Baker, L. A.; Chio, I. I. C.; Engle, D. D.; Corbo, V.; Jager, M.; Ponz-Sarvise, M.; Tiriac, H.; Spector, M. S.; Gracanin, A.; Oni, T.; Yu, K. H.; van Boxtel, R.; Huch, M.; Rivera, K. D.; Wilson, J. P.; Feigin, M. E.; Öhlund, D.; Handly-Santana, A.; Ardito-Abraham, C. M.; Ludwig, M.; Elyada, E.; Alagesan, B.; Biffi, G.; Yordanov, G. N.; Delcuze, B.; Creighton, B.; Wright, K.; Park, Y.; Morsink, F. H. M.; Molenaar, I. Q.; Borel Rinkes, I. H.; Cuppen, E.; Hao, Y.; Jin, Y.; Nijman, I. J.; Iacobuzio-Donahue, C.; Leach, S. D.; Pappin, D. J.; Hammell, M.; Klimstra, D. S.; Basturk, O.; Hruban, R. H.; Offerhaus, G. J.; Vries, R. G. J.; Clevers, H.; Tuveson, D. A. Organoid Models of Human and Mouse Ductal Pancreatic Cancer. *Cell* **2015**, *160* (1), 324–338. https://doi.org/10.1016/j.cell.2014.12.021.

(165) Knoblauch, M.; Ma, T.; Beirith, I.; Koch, D.; Hofmann, F.; Heinrich, K.; Aghamaliev, U.; Sirtl, S.; Westphalen, C. B.; Nieß, H.; Reichert, M.; Angele, M. K.; Regel, I.; Bazhin, A. V.; Werner, J.; Ilmer, M.; Renz, B. W. In-Vitro Model to Mimic T Cell Subset Change in Human PDAC Organoid Co-Culture. *J Cancer Res Clin Oncol* **2023**, *149* (14), 13051–13064. https://doi.org/10.1007/s00432-023-05100-7.

(166) Osuna de la Peña, D.; Trabulo, S. M. D.; Collin, E.; Liu, Y.; Sharma, S.; Tatari, M.; Behrens, D.; Erkan, M.; Lawlor, R. T.; Scarpa, A.; Heeschen, C.; Mata, A.; Loessner, D. Bioengineered 3D Models of Human Pancreatic Cancer Recapitulate in Vivo Tumour Biology. *Nat Commun* **2021**, *12* (1), 5623. https://doi.org/10.1038/s41467-021-25921-9.

(167) Godier, C.; Baka, Z.; Lamy, L.; Gribova, V.; Marchal, P.; Lavalle, P.; Gaffet, E.; Bezdetnaya, L.; Alem, H. A 3D Bio-Printed-Based Model for Pancreatic Ductal Adenocarcinoma. *Diseases* **2024**, *12* (9), 206. https://doi.org/10.3390/diseases12090206.

(168) Tabe, S.; Takeuchi, K.; Aoshima, K.; Okumura, A.; Yamamoto, Y.; Yanagisawa, K.; Eto, R.; Matsuo, M.; Ueno, Y.; Konishi, T.; Furukawa, Y.; Yamaguchi, K.; Morinaga, S.; Miyagi, Y.; Ohtsuka, M.; Tanimizu, N.; Taniguchi, H. A Pancreatic Cancer Organoid Incorporating Macrophages Reveals the Correlation between the Diversity of Tumor-Associated Macrophages and Cancer Cell Survival. *Biomaterials* **2025**, *314*, 122838. https://doi.org/10.1016/j.biomaterials.2024.122838.

(169) Geyer, M.; Schreyer, D.; Gaul, L.-M.; Pfeffer, S.; Pilarsky, C.; Queiroz, K. A Microfluidic-Based PDAC Organoid System Reveals the Impact of Hypoxia in Response to Treatment. *Cell Death Discov.* **2023**, *9* (1), 20. https://doi.org/10.1038/s41420-023-01334-z.

(170) Haque, M. R.; Wessel, C. R.; Leary, D. D.; Wang, C.; Bhushan, A.; Bishehsari, F. Patient-Derived Pancreatic Cancer-on-a-Chip Recapitulates the Tumor Microenvironment. *Microsyst Nanoeng* **2022**, *8* (1), 36. https://doi.org/10.1038/s41378-022-00370-6.

(171) Goluba, K.; Parfejevs, V.; Rostoka, E.; Jekabsons, K.; Blake, I.; Neimane, A.; Ule, A. A.; Rimsa, R.; Vangravs, R.; Pcolkins, A.; Riekstina, U. Personalized PDAC Chip with Functional Endothelial Barrier for Tumour Biomarker Detection: A Platform for Precision Medicine Applications. *Materials Today Bio* **2024**, *29*, 101262. https://doi.org/10.1016/j.mtbio.2024.101262.

(172) Merkle, J.; Breunig, M.; Schmid, M.; Allgöwer, C.; Krüger, J.; Melzer, M. K.; Bens, S.; Siebert, R.; Perkhofer, L.; Azoitei, N.; Seufferlein, T.; Heller, S.; Meier, M.; Müller, M.; Kleger, A.; Hohwieler, M. CDKN2A-Mutated Pancreatic Ductal Organoids from Induced Pluripotent Stem Cells to Model a Cancer Predisposition Syndrome. *Cancers (Basel)* **2021**, *13* (20), 5139. https://doi.org/10.3390/cancers13205139.

(173) Jin, S.; Guerrero-Juarez, C. F.; Zhang, L.; Chang, I.; Ramos, R.; Kuan, C.-H.; Myung, P.; Plikus, M. V.; Nie, Q. Inference and Analysis of Cell-Cell Communication Using CellChat. *Nat Commun* **2021**, *12* (1), 1088. https://doi.org/10.1038/s41467-021-21246-9.

(174) Yu, G.; Wang, L.-G.; He, Q.-Y. ChIPseeker: An R/Bioconductor Package for ChIP Peak Annotation, Comparison and Visualization. *Bioinformatics* **2015**, *31* (14), 2382–2383. https://doi.org/10.1093/bioinformatics/btv145.

(175) Yu, G.; Wang, L.-G.; Han, Y.; He, Q.-Y. clusterProfiler: An R Package for Comparing Biological Themes among Gene Clusters. *OMICS* **2012**, *16* (5), 284–287. https://doi.org/10.1089/omi.2011.0118.

(176) Love, M. I.; Huber, W.; Anders, S. Moderated Estimation of Fold Change and Dispersion for RNA-Seq Data with DESeq2. *Genome Biol* **2014**, *15* (12), 550. https://doi.org/10.1186/s13059-014-0550-8.

(177) Wickham, H.; François, R.; Henry, L.; Müller, K.; Vaughan, D. *dplyr: A Grammar of Data Manipulation*. https://dplyr.tidyverse.org (accessed 2025-11-13).

(178) Lawrence, M.; Huber, W.; Pagès, H.; Aboyoun, P.; Carlson, M.; Gentleman, R.; Morgan, M. T.; Carey, V. J. Software for Computing and Annotating Genomic Ranges. *PLoS Comput Biol* **2013**, *9* (8), e1003118. https://doi.org/10.1371/journal.pcbi.1003118.

(179) Wickham, H. *Ggplot2*; Use R!; Springer International Publishing: Cham, 2016. https://doi.org/10.1007/978-3-319-24277-4.

(180) Hänzelmann, S.; Castelo, R.; Guinney, J. GSVA: Gene Set Variation Analysis for Microarray and RNA-Seq Data. *BMC Bioinformatics* **2013**, *14* (1), 7. https://doi.org/10.1186/1471-2105-14-7.

(181) Bates, D.; Maechler, M.; Jagan, M. Matrix: Sparse and Dense Matrix Classes and Methods, 2025, 1.7-4. https://doi.org/10.32614/CRAN.package.Matrix.

(182) Liao, Y.; Smyth, G. K.; Shi, W. The R Package Rsubread Is Easier, Faster, Cheaper and Better for Alignment and Quantification of RNA Sequencing Reads. *Nucleic Acids Res* **2019**, *47* (8), e47. https://doi.org/10.1093/nar/gkz114.

(183) Wolf, F. A.; Angerer, P.; Theis, F. J. SCANPY: Large-Scale Single-Cell Gene Expression Data Analysis. *Genome Biology* **2018**, *19* (1), 15. https://doi.org/10.1186/s13059-017-1382-0.

(184) Blanco-Carmona, E. Generating Publication Ready Visualizations for Single Cell Transcriptomics Using SCpubr. bioRxiv March 1, 2022, p 2022.02.28.482303. https://doi.org/10.1101/2022.02.28.482303.

(185) Hafemeister, C.; Satija, R. Normalization and Variance Stabilization of Single-Cell RNA-Seq Data Using Regularized Negative Binomial Regression. *Genome Biology* **2019**, *20* (1), 296. https://doi.org/10.1186/s13059-019-1874-1.

(186) Bergen, V.; Lange, M.; Peidli, S.; Wolf, F. A.; Theis, F. J. Generalizing RNA Velocity to Transient Cell States through Dynamical Modeling. *Nat Biotechnol* **2020**, *38* (12), 1408–1414. https://doi.org/10.1038/s41587-020-0591-3.

(187) Satija, R.; Farrell, J. A.; Gennert, D.; Schier, A. F.; Regev, A. Spatial Reconstruction of Single-Cell Gene Expression Data. *Nat Biotechnol* **2015**, *33* (5), 495–502. https://doi.org/10.1038/nbt.3192.

(188) Butler, A.; Hoffman, P.; Smibert, P.; Papalexi, E.; Satija, R. Integrating Single-Cell Transcriptomic Data across Different Conditions, Technologies, and Species. *Nat Biotechnol* **2018**, *36* (5), 411–420. https://doi.org/10.1038/nbt.4096.

(189) Hao, Y.; Hao, S.; Andersen-Nissen, E.; Mauck, W.; Zheng, S.; Butler, A.; Lee, M.; Wilk, A.; Darby, C.; Zagar, M.; Hoffman, P.; Stoeckius, M.; Papalexi, E.; Mimitou, E.; Jain, J.; Srivastava, A.; Stuart, T.; Fleming, L.; Yeung, B.; Rogers, A.; McElrath, J.; Blish, C.; Gottardo, R.; Smibert, P.; Satija, R. Integrated Analysis of Multimodal Single-Cell Data. *Cell* **2020**, *184* (13). https://doi.org/10.1101/2020.10.12.335331.

(190) Hao, Y.; Stuart, T.; Kowalski, M. H.; Choudhary, S.; Hoffman, P.; Hartman, A.; Srivastava, A.; Molla, G.; Madad, S.; Fernandez-Granda, C.; Satija, R. Dictionary Learning for Integrative, Multimodal and Scalable Single-Cell Analysis. *Nat Biotechnol* **2024**, *42* (2), 293–304. https://doi.org/10.1038/s41587-023-01767-y.

(191) Hoffman, P. *SeuratDisk: Interfaces for HDF5-Based Single Cell File Formats — SeuratDisk-package*. https://mojaveazure.github.io/seurat-disk/reference/SeuratDisk-package.html (accessed 2025-11-13).

(192) Wickham, H. *stringr: Simple, Consistent Wrappers for Common String Operations*. https://stringr.tidyverse.org (accessed 2025-11-13).

(193) Kassambara, A.; Kosinski, M.; Biecek, P. *survminer: Drawing Survival Curves using "ggplot2."* https://rpkgs.datanovia.com/survminer/authors.html (accessed 2025-11-13).

(194) Colaprico, A.; Silva, T. C.; Olsen, C.; Garofano, L.; Cava, C.; Garolini, D.; Sabedot, T. S.; Malta, T. M.; Pagnotta, S. M.; Castiglioni, I.; Ceccarelli, M.; Bontempi, G.; Noushmehr, H. TCGAbiolinks: An R/Bioconductor Package for Integrative Analysis of TCGA Data. *Nucleic Acids Res* **2016**, *44* (8), e71. https://doi.org/10.1093/nar/gkv1507.

(195) Mounir, M.; Lucchetta, M.; Silva, T. C.; Olsen, C.; Bontempi, G.; Chen, X.; Noushmehr, H.; Colaprico, A.; Papaleo, E. New Functionalities in the TCGAbiolinks Package for the Study and Integration of Cancer Data from GDC and GTEx. *PLoS Comput Biol* **2019**, *15* (3), e1006701. https://doi.org/10.1371/journal.pcbi.1006701.

(196) Merkle, J. Modeling Familial Pancreatic Cancer Using Ductal Organoids Derived from Genetically Engineered Pluripotent Stem Cells. PhD Thesis, Ulm University, 2021.

(197) *Differentiation of human pluripotent stem cells into pancreatic duct-like organoids*. https://star-protocols.cell.com/protocols/1219 (accessed 2025-11-10).

(198) Wiedenmann, S.; Breunig, M.; Merkle, J.; von Toerne, C.; Georgiev, T.; Moussus, M.; Schulte, L.; Seufferlein, T.; Sterr, M.; Lickert, H.; Weissinger, S. E.; Möller, P.; Hauck, S. M.; Hohwieler, M.; Kleger, A.; Meier, M. Single-Cell-Resolved Differentiation of Human Induced Pluripotent Stem Cells into Pancreatic Duct-like Organoids on a Microwell Chip. *Nat Biomed Eng* **2021**, *5* (8), 897–913. https://doi.org/10.1038/s41551-021-00757-2.

(199) Saçma, M.; Pospiech, J.; Bogeska, R.; de Back, W.; Mallm, J.-P.; Sakk, V.; Soller, K.; Marka, G.; Vollmer, A.; Karns, R.; Cabezas-Wallscheid, N.; Trumpp, A.; Méndez-Ferrer, S.; Milsom, M. D.; Mulaw, M. A.; Geiger, H.; Florian, M. C. Haematopoietic Stem Cells in Perisinusoidal Niches Are Protected from Ageing. *Nat Cell Biol* **2019**, *21* (11), 1309–1320. https://doi.org/10.1038/s41556-019-0418-y.

(200) Tao, M.; Liu, W.; Chen, J.; Liu, R.; Zou, J.; Yu, B.; Wang, C.; Huang, M.; Chen, Q.; Zhang, Z.; Chen, Z.; Sun, H.; Zhou, C.; Tan, S.; Zheng, Y.; Wang, H. Transcriptome Landscape of Cancer-Associated Fibroblasts in Human PDAC. *Adv Sci (Weinh)* **2025**, *12* (20), e2415196. https://doi.org/10.1002/advs.202415196.

(201) Peng, J.; Sun, B.-F.; Chen, C.-Y.; Zhou, J.-Y.; Chen, Y.-S.; Chen, H.; Liu, L.; Huang, D.; Jiang, J.; Cui, G.-S.; Yang, Y.; Wang, W.; Guo, D.; Dai, M.; Guo, J.; Zhang, T.; Liao, Q.; Liu, Y.; Zhao, Y.-L.; Han, D.-L.; Zhao, Y.; Yang, Y.-G.; Wu, W. Single-Cell RNA-Seq Highlights Intra-Tumoral Heterogeneity and Malignant Progression in Pancreatic Ductal Adenocarcinoma. *Cell Res* **2019**, *29* (9), 725–738. https://doi.org/10.1038/s41422-019-0195-y.

(202) Lahusen, A.; Cai, J.; Schirmbeck, R.; Wellstein, A.; Kleger, A.; Seufferlein, T.; Eiseler, T.; Lin, Y.-N. A Pancreatic Cancer Organoid-in-Matrix Platform Shows Distinct Sensitivities to T Cell Killing. *Sci Rep* **2024**, *14* (1), 9377. https://doi.org/10.1038/s41598-024-60107-5.

(203) Allgöwer, C.; Mulaw, M. A.; Nagai, J.; Wiedenmann, S.; Ringel, E. A.; Ferrara, B.; Piemonti, L.; Maulana, T. I.; Ferreira, L. T.; Flinders, A.; Teufel, C.; Reichardt, L.; Lopatta, P. B.; Srinivasan, D.; Lahusen, A.; Seufferlein, T.; Gaisa, N. T.; Beck, A.; Lindenmayer, J.; Melzer, M. K.; Zimmer, E.; Roger, E.; Heller, S.; Löhr, J.-M.; Liebau, S.; Loskill, P.; Lin, Y.-N.; Camisa, P. R.; Jorgensen, C.; Crippa, S.; Meier, M.; Hohwieler, M.; Costa, I. G.; Breunig, M.; Kleger, A. An Oncogenic KRAS-Driven Secretome Involving TNFα Promotes Niche Preparation Prior to Pancreatic Cancer Onset. *Mol Cancer* **2026**, *25*, 29. https://doi.org/10.1186/s12943-025-02541-1.

(204) Maulana, T. I.; Teufel, C.; Cipriano, M.; Roosz, J.; Lazarevski, L.; Hil, F. E. van den; Scheller, L.; Orlova, V.; Koch, A.; Hudecek, M.; Alb, M.; Loskill, P. Breast Cancer-on-Chip for Patient-Specific Efficacy and Safety Testing of CAR-T Cells. *Cell Stem Cell* **2024**, *31* (7), 989-1002.e9. https://doi.org/10.1016/j.stem.2024.04.018.

(205) Ae Park, M.; Sun Jung, H.; Slukvin, I. Genetic Engineering of Human Pluripotent Stem Cells Using PiggyBac Transposon System. *Curr Protoc Stem Cell Biol* **2018**, *47* (1), e63. https://doi.org/10.1002/cpsc.63.

(206) Kim, S.-I.; Oceguera-Yanez, F.; Sakurai, C.; Nakagawa, M.; Yamanaka, S.; Woltjen, K. Inducible Transgene Expression in Human iPS Cells Using Versatile All-in-One piggyBac Transposons. In *Induced Pluripotent Stem (iPS) Cells: Methods and Protocols*; Turksen, K., Nagy, A., Eds.; Springer: New York, NY, 2016; pp 111–131. https://doi.org/10.1007/7651_2015_251.

(207) Rostovskaya, M.; Fu, J.; Obst, M.; Baer, I.; Weidlich, S.; Wang, H.; Smith, A. J. H.; Anastassiadis, K.; Stewart, A. F. Transposon-Mediated BAC Transgenesis in Human ES Cells. *Nucleic Acids Res* **2012**, *40* (19), e150. https://doi.org/10.1093/nar/gks643.

(208) Müller, S. Evolutionary Trajectories and KRAS Dosage Define Pancreatic Cancer Phenotypes, Technische Universität München, München, 2019.

(209) Varghese, A. M.; Perry, M. A.; Chou, J. F.; Nandakumar, S.; Muldoon, D.; Erakky, A.; Zucker, A.; Fong, C.; Mehine, M.; Nguyen, B.; Basturk, O.; Balogun, F.; Kelsen, D. P.; Brannon, A. R.; Mandelker, D.; Vakiani, E.; Park, W.; Yu, K. H.; Stadler, Z. K.; Schattner, M. A.; Jarnagin, W. R.; Wei, A. C.; Chakravarty, D.; Capanu, M.; Schultz, N.; Berger, M. F.; Iacobuzio-Donahue, C. A.; Bandlamudi, C.; O'Reilly, E. M. Clinicogenomic Landscape of Pancreatic Adenocarcinoma Identifies KRAS Mutant Dosage as Prognostic of Overall Survival. *Nat Med* **2025**, *31* (2), 466–477. https://doi.org/10.1038/s41591-024-03362-3.

(210) Braxton, A. M.; Kiemen, A. L.; Grahn, M. P.; Forjaz, A.; Parksong, J.; Mahesh Babu, J.; Lai, J.; Zheng, L.; Niknafs, N.; Jiang, L.; Cheng, H.; Song, Q.; Reichel, R.; Graham, S.; Damanakis, A. I.; Fischer, C. G.; Mou, S.; Metz, C.; Granger, J.; Liu, X.-D.; Bachmann, N.; Zhu, Y.; Liu, Y.; Almagro-Pérez, C.; Jiang, A. C.; Yoo, J.; Kim, B.; Du, S.; Foster, E.; Hsu, J. Y.; Rivera, P. A.; Chu, L. C.; Liu, F.; Fishman, E. K.; Yuille, A.; Roberts, N. J.; Thompson, E. D.; Scharpf, R. B.; Cornish, T. C.; Jiao, Y.; Karchin, R.; Hruban, R. H.; Wu, P.-H.; Wirtz, D.; Wood, L. D. 3D Genomic Mapping Reveals Multifocality of Human Pancreatic Precancers. *Nature* **2024**, *629* (8012), 679–687. https://doi.org/10.1038/s41586-024-07359-3.

(211) Kanda, M.; Matthaei, H.; Wu, J.; Hong, S.-M.; Yu, J.; Borges, M.; Hruban, R. H.; Maitra, A.; Kinzler, K.; Vogelstein, B.; Goggins, M. Presence of Somatic Mutations in Most Early-Stage Pancreatic Intraepithelial Neoplasia. *Gastroenterology* **2012**, *142* (4), 730-733.e9. https://doi.org/10.1053/j.gastro.2011.12.042.

(212) Das, A. T.; Tenenbaum, L.; Berkhout, B. Tet-On Systems For Doxycycline-Inducible Gene Expression. *Curr Gene Ther* **2016**, *16* (3), 156–167. https://doi.org/10.2174/1566523216666160524144041.

(213) Singh, K.; Pruski, M.; Bland, R.; Younes, M.; Guha, S.; Thosani, N.; Maitra, A.; Cash, B. D.; McAllister, F.; Logsdon, C. D.; Chang, J. T.; Bailey-Lundberg, J. M. Kras Mutation Rate Precisely Orchestrates Ductal Derived Pancreatic Intraepithelial Neoplasia and Pancreatic Cancer. *Lab Invest* **2021**, *101* (2), 177–192. https://doi.org/10.1038/s41374-020-00490-5.

(214) Deschênes-Simard, X.; Parisotto, M.; Rowell, M.-C.; Le Calvé, B.; Igelmann, S.; Moineau-Vallée, K.; Saint-Germain, E.; Kalegari, P.; Bourdeau, V.; Kottakis, F.; Bardeesy, N.; Ferbeyre, G. Circumventing Senescence Is Associated with Stem Cell Properties and Metformin Sensitivity. *Aging Cell* **2019**, *18* (2), e12889. https://doi.org/10.1111/acel.12889.

(215) Yang, K.; Li, X.; Xie, K. Senescence Program and Its Reprogramming in Pancreatic Premalignancy. *Cell Death Dis* **2023**, *14* (8), 528. https://doi.org/10.1038/s41419-023-06040-3.

(216) Caldwell, M. E.; DeNicola, G. M.; Martins, C. P.; Jacobetz, M. A.; Maitra, A.; Hruban, R. H.; Tuveson, D. A. Cellular Features of Senescence during the Evolution of Human and Murine Ductal Pancreatic Cancer. *Oncogene* **2012**, *31* (12), 1599–1608. https://doi.org/10.1038/onc.2011.350.

(217) Perez, V. M.; Kearney, J. F.; Yeh, J. J. The PDAC Extracellular Matrix: A Review of the ECM Protein Composition, Tumor Cell Interaction, and Therapeutic Strategies. *Front. Oncol.* **2021**, *11*. https://doi.org/10.3389/fonc.2021.751311.

(218) Wu, C.; Weis, S. M.; Cheresh, D. A. Tumor-Initiating Cells Establish a Niche to Overcome Isolation Stress. *Trends in Cell Biology* **2024**, *34* (5), 380–387. https://doi.org/10.1016/j.tcb.2023.08.001.

(219) Öhlund, D.; Franklin, O.; Lundberg, E.; Lundin, C.; Sund, M. Type IV Collagen Stimulates Pancreatic Cancer Cell Proliferation, Migration, and Inhibits Apoptosis through an Autocrine Loop. *BMC Cancer* **2013**, *13*, 154. https://doi.org/10.1186/1471-2407-13-154.

(220) Wu, C.-Z.; Chu, Y. C.; Lai, S.-W.; Hsieh, M.-S.; Yadav, V. K.; Fong, I.-H.; Deng, L.; Huang, C.-C.; Tzeng, Y.-M.; Yeh, C.-T.; Chen, J.-S. Urokinase Plasminogen Activator Induces Epithelial-Mesenchymal and Metastasis of Pancreatic Cancer through Plasmin/MMP14/TGF-β Axis, Which Is Inhibited by 4-Acetyl-Antroquinonol B Treatment. *Phytomedicine* **2022**, *100*, 154062. https://doi.org/10.1016/j.phymed.2022.154062.

(221) Ahn, S.-B.; Khan, A. Detection and Quantitation of Twenty-Seven Cytokines, Chemokines and Growth Factors Pre- and Post-High Abundance Protein Depletion in Human Plasma. *EuPA Open Proteomics* **2014**, *3*, 78–84. https://doi.org/10.1016/j.euprot.2014.02.012.

(222) Blank, U.; Madera-Salcedo, I. K.; Danelli, L.; Claver, J.; Tiwari, N.; Sánchez-Miranda, E.; Vázquez-Victorio, G.; Ramírez-Valadez, K. A.; Macias-Silva, M.; González-Espinosa, C. Vesicular Trafficking and Signaling for Cytokine and Chemokine Secretion in Mast Cells. *Front Immunol* **2014**, *5*, 453. https://doi.org/10.3389/fimmu.2014.00453.

(223) Stanley, A. C.; Lacy, P. Pathways for Cytokine Secretion. *Physiology* **2010**, *25* (4), 218–229. https://doi.org/10.1152/physiol.00017.2010.

(224) Saxena, S.; Molczyk, C.; Purohit, A.; Ehrhorn, E.; Goel, P.; Prajapati, D. R.; Atri, P.; Kaur, S.; Grandgenett, P. M.; Hollingsworth, M. A.; Batra, S. K.; Singh, R. K. Differential Expression Profile of CXC-Receptor-2 Ligands as Potential Biomarkers in Pancreatic Ductal Adenocarcinoma. *Am J Cancer Res* **2022**, *12* (1), 68–90.

(225) Huang, J.; Chen, Z.; Ding, C.; Lin, S.; Wan, D.; Ren, K. Prognostic Biomarkers and Immunotherapeutic Targets Among CXC Chemokines in Pancreatic Adenocarcinoma. *Front. Oncol.* **2021**, *11*. https://doi.org/10.3389/fonc.2021.711402.

(226) Geismann, C.; Schäfer, H.; Gundlach, J.-P.; Hauser, C.; Egberts, J.-H.; Schneider, G.; Arlt, A. NF-κB Dependent Chemokine Signaling in Pancreatic Cancer. *Cancers* **2019**, *11* (10), 1445. https://doi.org/10.3390/cancers11101445.

(227) Lesina, M.; Wörmann, S. M.; Morton, J.; Diakopoulos, K. N.; Korneeva, O.; Wimmer, M.; Einwächter, H.; Sperveslage, J.; Demir, I. E.; Kehl, T.; Saur, D.; Sipos, B.; Heikenwälder, M.; Steiner, J. M.; Wang, T. C.; Sansom, O. J.; Schmid, R. M.; Algül, H. RelA Regulates CXCL1/CXCR2-Dependent Oncogene-Induced Senescence in Murine Kras-Driven Pancreatic Carcinogenesis. *J Clin Invest* **2016**, *126* (8), 2919–2932. https://doi.org/10.1172/JCI86477.

(228) Geismann, C.; Grohmann, F.; Dreher, A.; Häsler, R.; Rosenstiel, P.; Legler, K.; Hauser, C.; Egberts, J. H.; Sipos, B.; Schreiber, S.; Linkermann, A.; Hassan, Z.; Schneider, G.; Schäfer, H.; Arlt, A. Role of CCL20 Mediated Immune Cell Recruitment in NF-κB Mediated TRAIL Resistance of Pancreatic Cancer. *Biochimica et Biophysica Acta (BBA) - Molecular Cell Research* **2017**, *1864* (5), 782–796. https://doi.org/10.1016/j.bbamcr.2017.02.005.

(229) Shakir, M.; Tang, D.; Zeh, H. J.; Tang, S. W.; Anderson, C. J.; Bahary, N.; Lotze, M. T. The Chemokine Receptors CXCR4/CXCR7 and Their Primary Heterodimeric Ligands CXCL12 and CXCL12/High Mobility Group Box 1 in Pancreatic Cancer Growth and Development: Finding Flow. *Pancreas* **2015**, *44* (4), 528. https://doi.org/10.1097/MPA.0000000000000298.

(230) Thomas, R. M.; Kim, J.; Revelo-Penafiel, M. P.; Angel, R.; Dawson, D. W.; Lowy, A. M. The Chemokine Receptor CXCR4 Is Expressed in Pancreatic Intraepithelial Neoplasia. **2008**. https://doi.org/10.1136/gut.2007.143941.

(231) Shen, X.; Artinyan, A.; Jackson, D.; Thomas, R. M.; Lowy, A. M.; Kim, J. Chemokine Receptor CXCR4 Enhances Proliferation in Pancreatic Cancer Cells Through AKT and ERK Dependent Pathways. *Pancreas* **2010**, *39* (1), 81. https://doi.org/10.1097/MPA.0b013e3181bb2ab7.

(232) Roy, I.; Zimmerman, N. P.; Mackinnon, A. C.; Tsai, S.; Evans, D. B.; Dwinell, M. B. CXCL12 Chemokine Expression Suppresses Human Pancreatic Cancer Growth and Metastasis. *PLoS ONE* **2014**, *9* (3), e90400. https://doi.org/10.1371/journal.pone.0090400.

(233) Morita, T.; Kodama, Y.; Shiokawa, M.; Kuriyama, K.; Marui, S.; Kuwada, T.; Sogabe, Y.; Matsumori, T.; Kakiuchi, N.; Tomono, T.; Mima, A.; Ueda, T.; Tsuda, M.; Yamauchi, Y.; Nishikawa, Y.; Sakuma, Y.; Ota, Y.; Maruno, T.; Uza, N.; Nagasawa, T.; Chiba, T.; Seno, H. CXCR4 in Tumor Epithelial Cells Mediates Desmoplastic Reaction in Pancreatic Ductal Adenocarcinoma. *Cancer Res* **2020**, *80* (19), 4058–4070. https://doi.org/10.1158/0008-5472.CAN-19-2745.

(234) Malik, S.; Westcott, J. M.; Brekken, R. A.; Burrows, F. J. CXCL12 in Pancreatic Cancer: Its Function and Potential as a Therapeutic Drug Target. *Cancers (Basel)* **2021**, *14* (1), 86. https://doi.org/10.3390/cancers14010086.

(235) Roberto, M.; Arrivi, G.; Di Civita, M. A.; Barchiesi, G.; Pilozzi, E.; Marchetti, P.; Santini, D.; Mazzuca, F.; Tomao, S. The Role of CXCL12 Axis in Pancreatic Cancer: New Biomarkers and Potential Targets. *Front. Oncol.* **2023**, *13*. https://doi.org/10.3389/fonc.2023.1154581.

(236) Sundqvist, K.-G. T Cell Motility—How Is It Regulated? *Front. Immunol.* **2020**, *11*. https://doi.org/10.3389/fimmu.2020.588642.

(237) Fowell, D. J.; Kim, M. The Spatiotemporal Control of Effector T Cell Migration. *Nat Rev Immunol* **2021**, *21* (9), 582–596. https://doi.org/10.1038/s41577-021-00507-0.

(238) Teixé, T.; Nieto-Blanco, P.; Vilella, R.; Engel, P.; Reina, M.; Espel, E. Syndecan-2 and -4 Expressed on Activated Primary Human CD4+ Lymphocytes Can Regulate T Cell Activation. *Mol Immunol* **2008**, *45* (10), 2905–2919. https://doi.org/10.1016/j.molimm.2008.01.033.

(239) Almgrami, R. T.; Zhang, T.; Zhao, Q.; You, M.; Liu, J.; Zhang, Y. Single-Cell Transcriptomic Analyses Provide Insights into SPP1+ TAM-Mediated Immune Suppression and CD8+ T Cell Dysfunction in Lung Cancer. *Cancer Immunol Immunother* **2025**, *74* (10), 319. https://doi.org/10.1007/s00262-025-04180-3.

(240) Ding, D.; Li, W.; Ren, J.; Li, Y.; Jiang, G.; Liang, R.; Huang, H.; You, J.; Wang, Y.; Wei, B. SPP1high Macrophage-Induced T-Cell Stress Promotes Colon Cancer Liver Metastasis through SPP1/CD44/PI3K/AKT Signaling. *J Immunother Cancer* **2025**, *13* (10), e012330. https://doi.org/10.1136/jitc-2025-012330.

(241) Pandol, S.; Gukovskaya, A.; Edderkoui, M.; Dawson, D.; Eibl, G.; Lugea, A. Epidemiology, Risk Factors, and the Promotion of Pancreatic Cancer: Role of the Stellate Cell. *Journal of Gastroenterology and Hepatology* **2012**, *27* (s2), 127–134. https://doi.org/10.1111/j.1440-1746.2011.07013.x.

(242) Jesnowski, R.; Fürst, D.; Ringel, J.; Chen, Y.; Schrödel, A.; Kleeff, J.; Kolb, A.; Schareck, W. D.; Löhr, M. Immortalization of Pancreatic Stellate Cells as an in Vitro Model of Pancreatic Fibrosis: Deactivation Is Induced by Matrigel and N-Acetylcysteine. *Lab Invest* **2005**, *85* (10), 1276–1291. https://doi.org/10.1038/labinvest.3700329.

(243) Sarper, M.; Cortes, E.; Lieberthal, T. J.; del Río Hernández, A. ATRA Modulates Mechanical Activation of TGF-β by Pancreatic Stellate Cells. *Sci Rep* **2016**, *6* (1), 27639. https://doi.org/10.1038/srep27639.

(244) Chronopoulos, A.; Robinson, B.; Sarper, M.; Cortes, E.; Auernheimer, V.; Lachowski, D.; Attwood, S.; García, R.; Ghassemi, S.; Fabry, B.; del Río Hernández, A. ATRA Mechanically Reprograms Pancreatic Stellate Cells to Suppress Matrix Remodelling and Inhibit Cancer Cell Invasion. *Nat Commun* **2016**, *7* (1), 12630. https://doi.org/10.1038/ncomms12630.

(245) Öhlund, D.; Handly-Santana, A.; Biffi, G.; Elyada, E.; Almeida, A. S.; Ponz-Sarvise, M.; Corbo, V.; Oni, T. E.; Hearn, S. A.; Lee, E. J.; Chio, I. I. C.; Hwang, C.-I.; Tiriac, H.; Baker, L. A.; Engle, D. D.; Feig, C.; Kultti, A.; Egeblad, M.; Fearon, D. T.; Crawford, J. M.; Clevers, H.; Park, Y.; Tuveson, D. A. Distinct Populations of Inflammatory Fibroblasts and Myofibroblasts in Pancreatic Cancer. *J Exp Med* **2017**, *214* (3), 579–596. https://doi.org/10.1084/jem.20162024.

(246) Sunami, Y.; Häußler, J.; Kleeff, J. Cellular Heterogeneity of Pancreatic Stellate Cells, Mesenchymal Stem Cells, and Cancer-Associated Fibroblasts in Pancreatic Cancer. *Cancers* **2020**, *12* (12), 3770. https://doi.org/10.3390/cancers12123770.

(247) van Loo, G.; Bertrand, M. J. M. Death by TNF: A Road to Inflammation. *Nat Rev Immunol* **2023**, *23* (5), 289–303. https://doi.org/10.1038/s41577-022-00792-3.

(248) Leone, G. M.; Mangano, K.; Petralia, M. C.; Nicoletti, F.; Fagone, P. Past, Present and (Foreseeable) Future of Biological Anti-TNF Alpha Therapy. *Journal of Clinical Medicine* **2023**, *12* (4), 1630. https://doi.org/10.3390/jcm12041630.

(249) Tu, M.; Klein, L.; Espinet, E.; Georgomanolis, T.; Wegwitz, F.; Li, X.; Urbach, L.; Danieli-Mackay, A.; Küffer, S.; Bojarczuk, K.; Mizi, A.; Günesdogan, U.; Chapuy, B.; Gu, Z.; Neesse, A.; Kishore, U.; Ströbel, P.; Hessmann, E.; Hahn, S. A.; Trumpp, A.;

Papantonis, A.; Ellenrieder, V.; Singh, S. K. TNF-α-Producing Macrophages Determine Subtype Identity and Prognosis via AP1 Enhancer Reprogramming in Pancreatic Cancer. *Nat Cancer* **2021**, *2* (11), 1185–1203. https://doi.org/10.1038/s43018-021-00258-w.

(250) Tekin, C.; Aberson, H. L.; Bijlsma, M. F.; Spek, C. A. Early Macrophage Infiltrates Impair Pancreatic Cancer Cell Growth by TNF-α Secretion. *BMC Cancer* **2020**, *20* (1), 1183. https://doi.org/10.1186/s12885-020-07697-1.

(251) Zhao, X.; Fan, W.; Xu, Z.; Chen, H.; He, Y.; Yang, G.; Yang, G.; Hu, H.; Tang, S.; Wang, P.; Zhang, Z.; Xu, P.; Yu, M. Inhibiting Tumor Necrosis Factor-Alpha Diminishes Desmoplasia and Inflammation to Overcome Chemoresistance in Pancreatic Ductal Adenocarcinoma. *Oncotarget* **2016**, *7* (49), 81110–81122. https://doi.org/10.18632/oncotarget.13212.

(252) Adjuto-Saccone, M.; Soubeyran, P.; Garcia, J.; Audebert, S.; Camoin, L.; Rubis, M.; Roques, J.; Binétruy, B.; Iovanna, J. L.; Tournaire, R. TNF-α Induces Endothelial–Mesenchymal Transition Promoting Stromal Development of Pancreatic Adenocarcinoma. *Cell Death Dis* **2021**, *12* (7), 649. https://doi.org/10.1038/s41419-021-03920-4.

(253) Lianyuan, T.; Dianrong, X.; Chunhui, Y.; Zhaolai, M.; Bin, J. The Predictive Value and Role of Stromal Tumor-Infiltrating Lymphocytes in Pancreatic Ductal Adenocarcinoma (PDAC). *Cancer Biology & Therapy* **2018**, *19* (4), 296–305. https://doi.org/10.1080/15384047.2017.1416932.

(254) Bianchi, A.; De Castro Silva, I.; Deshpande, N. U.; Singh, S.; Mehra, S.; Garrido, V. T.; Guo, X.; Nivelo, L. A.; Kolonias, D. S.; Saigh, S. J.; Wieder, E.; Rafie, C. I.; Dosch, A. R.; Zhou, Z.; Umland, O.; Amirian, H.; Ogobuiro, I. C.; Zhang, J.; Ban, Y.; Shiau, C.; Nagathihalli, N. S.; Montgomery, E. A.; Hwang, W. L.; Brambilla, R.; Komanduri, K.; Villarino, A. V.; Toska, E.; Stanger, B. Z.; Gabrilovich, D. I.; Merchant, N. B.; Datta, J. Cell-Autonomous Cxcl1 Sustains Tolerogenic Circuitries and Stromal Inflammation via Neutrophil-Derived TNF in Pancreatic Cancer. *Cancer Discov* **2023**, *13* (6), 1428–1453. https://doi.org/10.1158/2159-8290.CD-22-1046.

(255) Alam, M. S.; Gaida, M. M.; Witzel, H. R.; Otsuka, S.; Abbasi, A.; Guerin, T.; Abdelmaksoud, A.; Wong, N.; Cam, M. C.; Kozlov, S.; Ashwell, J. D. TNFR1 Signaling Promotes Pancreatic Tumor Growth by Limiting Dendritic Cell Number and Function. *Cell Rep Med* **2024**, *5* (9), 101696. https://doi.org/10.1016/j.xcrm.2024.101696.

(256) Ma, S.; Ming, Y.; Wu, J.; Cui, G. Cellular Metabolism Regulates the Differentiation and Function of T-Cell Subsets. *Cell Mol Immunol* **2024**, *21* (5), 419–435. https://doi.org/10.1038/s41423-024-01148-8.

(257) Dimeloe, S.; Burgener, A.-V.; Grählert, J.; Hess, C. T-Cell Metabolism Governing Activation, Proliferation and Differentiation; a Modular View. *Immunology* **2017**, *150* (1), 35–44. https://doi.org/10.1111/imm.12655.

(258) Kong, F.; Pan, Y.; Wu, D. Activation and Regulation of Pancreatic Stellate Cells in Chronic Pancreatic Fibrosis: A Potential Therapeutic Approach for Chronic Pancreatitis. *Biomedicines* **2024**, *12* (1), 108. https://doi.org/10.3390/biomedicines12010108.

(259) Tiyaboonchai, A.; Mac, H.; Shamsedeen, R.; Mills, J. A.; Kishore, S.; French, D. L.; Gadue, P. Utilization of the AAVS1 Safe Harbor Locus for Hematopoietic Specific

Transgene Expression and Gene Knockdown in Human ES Cells. *Stem Cell Res* **2014**, *12* (3), 630–637. https://doi.org/10.1016/j.scr.2014.02.004.

(260) Dost, A. F. M.; Moye, A. L.; Vedaie, M.; Tran, L. M.; Fung, E.; Heinze, D.; Villacorta-Martin, C.; Huang, J.; Hekman, R.; Kwan, J. H.; Blum, B. C.; Louie, S. M.; Rowbotham, S. P.; Aja, J. S. de; Piper, M. E.; Bhetariya, P. J.; Bronson, R. T.; Emili, A.; Mostoslavsky, G.; Fishbein, G. A.; Wallace, W. D.; Krysan, K.; Dubinett, S. M.; Yanagawa, J.; Kotton, D. N.; Kim, C. F. Organoids Model Transcriptional Hallmarks of Oncogenic KRAS Activation in Lung Epithelial Progenitor Cells. *Cell Stem Cell* **2020**, *27* (4), 663-678.e8. https://doi.org/10.1016/j.stem.2020.07.022.

7. Statutory declaration

I hereby declare that I wrote the present dissertation with the topic:

Characterizing early oncogenic KRAS signaling by employing human stem cell-derived pancreatic ductal organoids as a pre-cancer model

independently and used no other aids than those cited. In each individual case, I have clearly identified the source of the passages that are taken word for word or paraphrased from other works.

I also hereby declare that I have carried out my scientific work according to the principles of good scientific practice in accordance with the current „Satzung der Universität Ulm zur Sicherung guter wissenschaftlicher Praxis" [Rules of the University of Ulm for Assuring Good Scientific Practice].

Ulm, 13.12.25

_____

Chantal Allgöwer

8. List of publications

1. **Allgöwer, C.**, Mulaw, M. A., Nagai, J., Wiedenmann, S., Ringel, E. A., Ferrara, B., Piemonti, L., Maulana, T. I., Ferreira, L. T., Flinders, A., Teufel, C., Reichardt, L., Lopatta, P. B., Srinivasan, D., Lahusen, A., Gaisa, N. T., Beck, A., Lindenmayer, J., Melzer, M. K., Rodger, E., Heller, S., Löhr, M., Liebau, S., Loskill, P., Lin, Y.-N., Camisa, P. R., Jorgensen, C., Crippa, S., Meier, M., Hohwieler, Costa, I. G., Breunig, M., Kleger, A. An oncogenic KRAS-driven secretome involving TNFα promotes niche preparation prior to pancreatic cancer onset. *Molecular Cancer,* 2026, 25 (29). https://doi.org/10.1186/s12943-025-02541-1.

2. Srinivasan, D.; Roger, E.; Perkhofer, L.; Zimmer, E.; Barth, T. F. E.; Mosler, J. P.; Härle, A.; Weissinger, S. E.; Gaisa, N. T.; Möller, P.; Fischer, N.; **Allgöwer, C**.; Löhr, J.-M.; Grimm, D.; Seufferlein, T.; Liebau, S.; Azoitei, N.; Melzer, M. K.; Arnold, F.; Gout, J.; Kleger, A. DKK3 Initially Preserves Acinar Integrity Through MEK-Fos Signaling, but Later Switches to an Oncogenic Role in Pancreatic Cancer. *Advanced Science*, 2025, e17606. https://doi.org/10.1002/advs.202417606.

3. Merz, S.; Senée, V.; Philippi, A.; Oswald, F.; Shaigan, M.; Führer, M.; Drewes, C.; **Allgöwer, C**.; Öllinger, R.; Heni, M.; Boland, A.; Deleuze, J.-F.; Birkhofer, F.; Gusmao, E. G.; Wagner, M.; Hohwieler, M.; Breunig, M.; Rad, R.; Siebert, R.; Messerer, D. A. C.; Costa, I. G.; Alvarez, F.; Julier, C.; Kleger, A.; Heller, S. A ONECUT1 Regulatory, Non-Coding Region in Pancreatic Development and Diabetes. *Cell Reports* 2024, 43 (11). https://doi.org/10.1016/j.celrep.2024.114853.

4. Ruta, V.; Naro, C.; Pieraccioli, M.; Leccese, A.; Archibugi, L.; Cesari, E.; Panzeri, V.; **Allgöwer, C**.; Arcidiacono, P. G.; Falconi, M.; Carbone, C.; Tortora, G.; Borrelli, F.; Attili, F.; Spada, C.; Quero, G.; Alfieri, S.; Doglioni, C.; Kleger, A.; Capurso, G.; Sette, C. An Alternative Splicing Signature Defines the Basal-like Phenotype and Predicts Worse Clinical Outcome in Pancreatic Cancer. *CR Med* 2024, 5 (2). https://doi.org/10.1016/j.xcrm.2024.101411.

5. Krüger, J.; Fischer, A.; Breunig, M.; **Allgöwer, C**.; Schulte, L.; Merkle, J.; Mulaw, M. A.; Okeke, N.; Melzer, M. K.; Morgenstern, C.; Azoitei, N.; Seufferlein, T.; Barth, T. F.; Siebert, R.; Hohwieler, M.; Kleger, A. DNA Methylation-Associated Allelic Inactivation Regulates Keratin 19 Gene Expression during Pancreatic Development and Carcinogenesis. The *Journal of Pathology* 2023, 261 (2), 139–155. https://doi.org/10.1002/path.6156

6. Melzer, M. K.; Schirge, S.; Gout, J.; Arnold, F.; Srinivasan, D.; Burtscher, I.; **Allgöwer, C**.; Mulaw, M.; Zengerling, F.; Günes, C.; Lickert, H.; Christoffels, V. M.; Liebau, S.; Wagner, M.; Seufferlein, T.; Bolenz, C.; Moon, A. M.; Perkhofer, L.; Kleger, A. TBX3 Is Dynamically Expressed in Pancreatic Organogenesis and Fine-Tunes Regeneration. *BMC Biol* 2023, 21 (1), 55. https://doi.org/10.1186/s12915-023-01553-x

7. Merkle, J.; Breunig, M.; Schmid, M.; **Allgöwer, C**.; Krüger, J.; Melzer, M. K.; Bens, S.; Siebert, R.; Perkhofer, L.; Azoitei, N.; Seufferlein, T.; Heller, S.; Meier, M.; Müller, M.; Kleger, A.; Hohwieler, M. CDKN2A-Mutated Pancreatic Ductal Organoids from Induced Pluripotent Stem Cells to Model a Cancer Predisposition Syndrome. *Cancers (Basel)* 2021, 13 (20), 5139. https://doi.org/10.3390/cancers13205139

9. Acknowledgements

This section was removed from the public version of the dissertation due to data protection reasons.